Stability of Mechanical Systems with Varying Time Delays

Tamás Insperger

Dissertation for the Title Doctor of the Hungarian Academy of Sciences

May, 2014

Contents

Chapter 1

Introduction

Dynamical systems described with differential equations often come up in different field of science and engineering. A differential equation can serve as a model for how the rate of change of state depends on the present state of a system. However, the rate of change of state may depend on past states, too. It has been known for a long time that several problems can be described by models including past effects. One of the classical examples is the predator–prey model of Volterra [230], where the growth rate of predators depends not only on the present quality of food (say, prey), but also on past quantities (in the period of gestation, say). The first delay models in engineering appeared for wheel shimmy [190] and for ship stabilization [157] in the early 1940s. There are several other engineering applications in which time delay plays a crucial role. As recognized in the late 1940s with the development of control theory, time delay typically arises in feedback control systems due to the finite speed of information transmission and data processing [228, 204]. Another typical application is the stability of machining processes, where time delay appears due to the surface regeneration by the cutting edge [223, 226, 209, 5]. Similar equations describe the car-following traffic models involving the reaction time of drivers [173], or the active suspension of cars with a time delay in driver's response [176, 177, 68]. Time delay also plays important role in neural networks [35, 174], in human motion control [213, 155, 10] and in epidemiology models [186, 2].

Systems whose rate of change of state depends on states at deviating arguments are generally described by functional differential equations (FDEs). According to Myshkis [164], FDEs are equations involving the function $x(t)$ of one scalar argument t (called time) and its derivatives for several values of argument t. The literature on FDEs is quite extensive. Several books have appeared summarizing the most important theorems; see, for instance, the books by Myshkis [164], Bellman and Cooke [19], Èl'sgol'c [54], Halanay [77], Hale [78], Driver [51], Kolmanovskii and Nosov [127], Hale and Lunel [79], Diekmann et al. [44], just to mention a few. There are also several

books dealing with different applications and numerical techniques; see for instance, Stépán [206], Niculescu [168], Bellen and Zennaro [18], Gu et al. [71], Zhong [243], Michiels and Niculescu [152], Erneux [58], Balachandran et al. [15], Yi et al. [239], and Insperger and Stépán [115].

RFDE is a mathematical terminology. In the engineering literature, RFDEs are referred to as delay-differential equations (DDEs), or simply delay equations. In this dissertation, we follow the latter terminology, and use the term DDE rather than RFDE.

In this dissertation, different engineering problems are considered that are all described with DDEs with varying time delays. Chapter 2 gives a brief overview on some special cases of linear DDEs with time-periodic coefficients. Then each chapter is related to a thesis of the dissertation.

Chapter 3 presents an efficient numerical method, the so-called first-order semi-discretization, for the stability analysis of linear time-periodic DDEs. A basic version of the semi-discretization method (called zeroth-order semi-discretization) was presented by Insperger and Stépán [100, 104]. The point of the method is that the time-delayed terms are discretized, the time-periodic coefficients are approximated by piecewise constant ones, while the actual time-domain terms are left in their original form during the discretization process. The new result given in Thesis 1 is related to the convergence of the discretization method with respect to the order of the approximation of the delayed term. It is shown that if the periodic coefficients are approximated by piecewise constant ones then the zeroth-order approximation gives a discretization error proportional to the square of the discretization step, while the first- and any higher-order approximation gives a discretization error proportional to the cube of the discretization step. This result was published in Insperger et al. [110] and was also included into the book Insperger and Stépán [115].

In Chapter 4, a two-degrees-of-freedom model of turning processes is presented, where state-dependent regenerative delays arise in the model equations. DDEs with state-dependent delays are strongly nonlinear, since the state appears in its own argument through the time delay, i.e., the nonlinearity in the systems is defined by the solution. The new result given in Thesis 2 is the application of the linearization technique of Hartung and Turi [82] to the model equations. It is shown that the linear stability boundaries are slightly different from that of the constant delay model due to the dependence of the instantaneous chip thickness on the regenerative delay. This result was published by Insperger et al. [108].

Chapter 5 presents a single-degree-of-freedom model of milling processes with varying spindle speed. The corresponding mechanical model is a DDE with time-periodic delay. As a new result, the stability charts are determined for the model in the plane

of the spindle speed and the axial depth of cut using the first-order semi-discretization method. It is shown that multiple lobes appears at the location of the flip lobes of the constant-spindle-speed milling. These results are composed in Thesis 3, and were also published in the book Insperger and Stépán [115]. Experimental verification of suppressing period doubling chatter by spindle speed variation is also presented according to the joint papers Seguy et al. [193, 194] that were made in collaboration with French partners. The experiments were performed by Sebastien Seguy (École Nationale d'Ingénieurs de Tarbes, France), who made his PhD on this topic in 2008 [192]. The experimental results are not included into Thesis 3, but they are presented for the sake of completeness.

Chapter 6 presents the so called act-and-wait control technique for systems with feedback delays. The act-and-wait controller is a special case of periodic controllers where the feedback is periodically switched off and on. Control systems with feedback delays are described by DDEs associated with infinite-dimensional state spaces. Consequently, the stability of the control process is determined by infinitely many eigenvalues (poles) that all should be monitored during the adjustment of the control parameters. It is shown that if the act-and-wait control technique is applied such that the waiting (switch-off) period is larger than the feedback delay, then the system can be described by a finite-dimensional discrete map, and only finite number of eigenvalues should be considered during the stabilization process. This result is composed in Thesis 4 and was published in Insperger [106] and also in the book Insperger and Stépán [115].

Chapter 7 deals with a force control process in the presence of feedback delay. Here, the goal is to reduce the error of the contact force between the actuator and the environment. In order to achieve this goal, the proportional gain in the controller should be increased, but on the other hand, for large proportional gains, the system looses stability due to the feedback delay. It is shown that the proportional gain and, consequently, the accuracy of the contact force can be increased by the application of the act-and-wait control concept without loosing stability. The results are composed in Thesis 5 and were published in Insperger et al. [111] and also in the book Insperger and Stépán [115].

Chapter 2

Mathematical background

Since most of the theses in this dissertation are related to time-periodic DDEs, an overview is given in this chapter on the related mathematical theory. In the next sections, some basic properties of some special classes of differential equations, namely, linear autonomous ordinary differential equations (ODEs), linear time-periodic ODEs, linear autonomous DDEs, linear time-periodic DDEs and DDEs with state-dependent delays are summarized briefly.

2.1 Linear Autonomous ODEs

Linear autonomous ordinary differential equations (ODEs) have the general form

$$\dot{\mathbf{x}}(t) = \mathbf{A}\mathbf{x}(t) \,, \tag{2.1}$$

where $\mathbf{x}(t) \in \mathbb{R}^n$, $\mathbf{A}$ is an $n \times n$ matrix, and

$$\dot{\mathbf{x}} = \frac{\mathrm{d}\mathbf{x}}{\mathrm{d}t} = \mathrm{col}\left(\frac{\mathrm{d}x_1}{\mathrm{d}t} \; \frac{\mathrm{d}x_2}{\mathrm{d}t} \; \cdots \; \frac{\mathrm{d}x_n}{\mathrm{d}t}\right)$$

with $x_1, x_2, \ldots, x_n$ being the elements of vector $\mathbf{x}$. For a given initial value $\mathbf{x}(0)$, the solution of (2.1) can be written in the form

$$\mathbf{x}(t) = \mathrm{e}^{\mathbf{A}t}\mathbf{x}(0) \,, \tag{2.2}$$

where $\mathrm{e}^{\mathbf{A}t}$ is the exponential of matrix $\mathbf{A}t$, defined by the Taylor series of the exponential function (see Appendix A). For a general overview on matrix exponentials, see the book of Hirsch and Smale [90], or the book of Perko [179].

The stability of the trivial solution $\mathbf{x}(t) \equiv \mathbf{0}$ is determined by the eigenvalues λ_j, $j = 1, 2, \ldots, n$, of the coefficient matrix $\mathbf{A}$. These eigenvalues are the *characteristic exponents* of (2.1), but they are often called *characteristic roots* or *poles*, too. If each

λ_j is unique in the minimal polynomial of $\mathbf{A}$, then each solution of (2.1) can be written in the form

$$\mathbf{x}(t) = \sum_{j=1}^{n} \mathbf{C}_j \, \mathrm{e}^{\lambda_j t} \, , \tag{2.3}$$

with $\mathbf{C}_j \in \mathbb{C}^n$ being appropriate vectors depending on the initial condition. If the characteristic exponents have negative real parts, i.e., $\mathrm{Re}\, \lambda_j < 0$ for all $j = 1, 2, \ldots, n$, then the trivial solution of (2.1) is asymptotically stable. In the general case, the characteristic exponents can be determined by solving the characteristic equation

$$\det (\lambda \mathbf{I} - \mathbf{A}) = 0 \, , \tag{2.4}$$

where $\mathbf{I}$ stands for the $n \times n$ identity matrix. Development of (2.4) results in an nth-degree polynomial of λ, whose roots (i.e., the characteristic exponents) can be determined by a number of numerical methods. Stability analysis, however, does not require the exact calculation of the characteristic exponents; only the sign of the real part of the critical (i.e., rightmost) exponent must be determined. This analysis can be performed by the celebrated Routh–Hurwitz criterion [187, 95], which gives a necessary and sufficient condition for stability based on the coefficients of the characteristic polynomial.

Depending on the location of the critical characteristic exponents, there are two typical mechanisms for loss of stability of linear autonomous systems [72]:

1. The critical characteristic exponents form a complex conjugate pair moving from the left-hand side of the complex plane to the right-hand side; they cross the imaginary axis, as shown by case (a) in Figure 2.1. This case is an essential necessary condition for the so-called *Hopf* (or *Andronov–Hopf* or *Poincaré–Andronov–Hopf*) bifurcation of the corresponding nonlinear system, for which the equation under analysis is the variational system. The systematic study of the conditions and a proof of the corresponding bifurcation theorem have been done by Andronov and Leontovich [8] for the two-dimensional case, and by Hopf [92] for the n-dimensional case. According to the theory of nonlinear systems, either stable or unstable periodic motion may exist around the equilibrium of the corresponding nonlinear system, called supercritical and subcritical bifurcation, respectively.

2. The critical characteristic exponent is a real one moving from the left-hand side of the complex plane to the right-hand side through the origin, as shown by case (b) in Figure 2.1. This case is called *saddle-node* bifurcation of the corresponding nonlinear system.

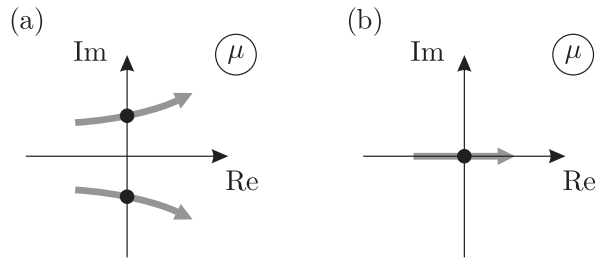

Figure 2.1: Critical characteristic exponents for linear autonomous ODEs: (a) Hopf bifurcation, (b) and saddle-node bifurcation.

2.2 Linear Periodic ODEs

The general form of linear periodic ODEs reads

$$\dot{\mathbf{x}}(t) = \mathbf{A}(t)\mathbf{x}(t) \,, \quad \mathbf{A}(t) = \mathbf{A}(t+T) \,, \tag{2.5}$$

with $\mathbf{x}(t) \in \mathbb{R}^n$. Here, the $n \times n$ coefficient matrix $\mathbf{A}(t)$ is time-periodic at period T, called the *principal period* in contrast to the constant-coefficient matrix of the autonomous system (2.1). The main theorems on general periodic systems are summarized in the book of Farkas [60].

For periodic ODEs, a stability condition is provided by the Floquet theory [61]. The solution of (2.5) with the initial condition $\mathbf{x}(0)$ is given by $\mathbf{x}(t) = \mathbf{\Phi}(t)\mathbf{x}(0)$, where $\mathbf{\Phi}(t)$ is a fundamental matrix of (2.5). According to the Floquet theory, the fundamental matrix can be written in the form $\mathbf{\Phi}(t) = \mathbf{P}(t)\,\mathrm{e}^{\mathbf{B}t}$, where $\mathbf{P}(t) = \mathbf{P}(t+T)$ is a periodic matrix with initial value $\mathbf{P}(0) = \mathbf{I}$, and $\mathbf{B}$ is a constant matrix. The matrix $\mathbf{\Phi}(T) = \mathrm{e}^{\mathbf{B}T}$ is called the *monodromy matrix* (or *principal matrix* or *Floquet transition matrix*) of (2.5). This matrix gives the connection between the initial state and the state one principal period later: $\mathbf{x}(T) = \mathbf{\Phi}(T)\mathbf{x}(0)$.

The eigenvalues of $\mathbf{\Phi}(T)$ are the *characteristic multipliers* (μ_j, $j = 1, 2, \ldots, n$) (also called *Floquet multipliers* or the *poles* of $\mathbf{\Phi}(T)$) calculated from

$$\det(\mu\mathbf{I} - \mathbf{\Phi}(T)) = 0 \,. \tag{2.6}$$

The eigenvalues of matrix $\mathbf{B}$ are the *characteristic exponents* (λ_j, $j = 1, 2, \ldots, n$) given by

$$\det(\lambda\mathbf{I} - \mathbf{B}) = 0 \,. \tag{2.7}$$

If μ is a characteristic multiplier, then there are characteristic exponents λ such that $\mu = \exp(\lambda T)$, and vice versa. Due to the periodicity of the complex exponential function, each characteristic multiplier is associated with infinitely many characteristic exponents of the form $\lambda_k = \gamma + \mathrm{i}\,(\omega + k2\pi/T)$, where $\gamma, \omega \in \mathbb{R}$, $k \in \mathbb{Z}$, and $T\omega \in (-\pi, \pi]$.

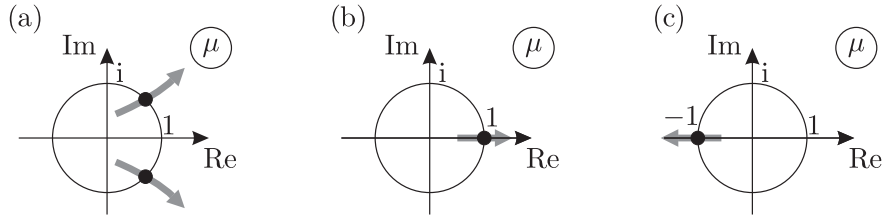

Figure 2.2: Critical characteristic multipliers for periodic systems: (a) secondary Hopf bifurcation, (b) cyclic-fold bifurcation, and (c) period-doubling bifurcation.

The trivial solution $\mathbf{x}(t) \equiv \mathbf{0}$ of (2.5) is asymptotically stable if and only if all the characteristic multipliers have modulus less than one, that is, all the characteristic exponents have negative real parts.

Similarly to autonomous systems, the basic types of loss of stability can be classified according to the location of the critical characteristic multipliers [72]. For periodic systems, there are three typical cases:

1. The critical characteristic multipliers form a complex conjugate pair crossing the unit circle, i.e., $|\mu| = 1$ and $|\bar{\mu}| = 1$, as shown by case (a) in Figure 2.2. This case is topologically equivalent to the Hopf bifurcation of autonomous systems and is called *secondary Hopf* (or *Neimark–Sacker*) bifurcation.

2. The critical characteristic multiplier is real and crosses the unit circle at $+1$, as shown by case (b) in Figure 2.2. The bifurcation that arises is topologically equivalent to the saddle-node bifurcation of autonomous systems and is called *cyclic-fold* (or *period-one*) bifurcation.

3. The critical characteristic multiplier is real and crosses the unit circle at -1, as shown by case (c) in Figure 2.2. There is no topologically equivalent type of bifurcation for autonomous systems. This case is called *period-doubling* (or *period-two* or *flip*) bifurcation.

Generally, the monodromy matrix cannot be determined in closed form, but there exist several numerical and semi-analytical techniques to approximate it, such as Hill's infinite determinant method and its generalizations [89, 215, 22, 166], the method of strained parameters [166], the method of multiple scales [166], and the Chebyshev polynomial approach [201, 202]. A simple numerical method is the piecewise constant approximation of the periodic matrix $\mathbf{A}(t)$ in the form

$$\mathbf{A}(t) \approx \mathbf{A}_i := \int_{(i-1)h}^{ih} \mathbf{A}(s)\,\mathrm{d}s\ , \quad t \in [t_i, t_{i+1})\ , \tag{2.8}$$

where $t_i = ih$ is the discrete time with $i \in \mathbb{Z}$, $h = T/p$ is the length of the discretization step, and p is an integer [94, 60]. The original system can be approximated by

$$\dot{\mathbf{y}}(t) = \mathbf{A}_i \mathbf{y}(t) \ , \quad t \in [t_i, t_{i+1}) \ , \tag{2.9}$$

for which the solution over a discretization interval is

$$\mathbf{y}(t_{i+1}) = \ \mathrm{e}^{\mathbf{A}_i h} \mathbf{y}(t_i) \ . \tag{2.10}$$

Application of (2.10) over p repeated discretization steps with initial state $\mathbf{y}(0)$ results in

$$\mathbf{y}(T) = \tilde{\mathbf{\Phi}}(T) \mathbf{y}(0) \ , \tag{2.11}$$

where

$$\tilde{\mathbf{\Phi}}(T) = \ \mathrm{e}^{\mathbf{A}_{p-1} h} \ \mathrm{e}^{\mathbf{A}_{p-2} h} \ \cdots \ \mathrm{e}^{\mathbf{A}_0 h} \tag{2.12}$$

is an approximation for the monodromy matrix $\mathbf{\Phi}(T)$. Eigenvalue analysis of $\tilde{\mathbf{\Phi}}(T)$ gives then an approximate description of the stability properties of (2.5). A higher-order generalization of this piecewise constant approximation technique is the method of Magnus expansion, which involves higher-order terms of the so-called Magnus series of the logarithm of the fundamental matrix $\mathbf{\Phi}(h)$ (see, e.g., [145, 116, 117, 32]). Approximation (2.8) corresponds to the first-order Magnus expansion of $\ln\big(\mathbf{\Phi}(h)\big)$.

2.3 Linear Autonomous DDEs

The general form of linear autonomous DDEs is

$$\dot{\mathbf{x}}(t) = \mathbf{L}(\mathbf{x}_t) \ , \tag{2.13}$$

where $\mathbf{L} : C \to \mathbb{R}^n$ is a continuous linear functional (C is the Banach space of continuous functions) and the continuous function $\mathbf{x}_t$ is defined by the shift

$$\mathbf{x}_t(\vartheta) = \mathbf{x}(t + \vartheta) \ , \quad \vartheta \in [-\sigma, 0] \ . \tag{2.14}$$

According to the Riesz representation theorem (see [78]), the linear functional $\mathbf{L}$ can be represented in the matrix form

$$\mathbf{L}(\mathbf{x}_t) = \int_{-\sigma}^{0} \mathrm{d}\boldsymbol{\eta}(\vartheta) \, \mathbf{x}(t + \vartheta) \ , \tag{2.15}$$

where $\boldsymbol{\eta} : [-\sigma, 0] \to \mathbb{R}^{n \times n}$ is a matrix function of bounded variation, and the integral is a Stieltjes one, i.e., (2.15) contains both point delays and distributed delays.

The characteristic equation can be obtained by substituting the nontrivial solution $\mathbf{x}(t) = \mathbf{C}\ \mathrm{e}^{\lambda t}$, $\mathbf{C} \in \mathbb{C}^n$, into (2.13), which gives

$$\underbrace{\det\left(\lambda\mathbf{I} - \int_{-\sigma}^{0} \mathrm{e}^{\lambda\vartheta}\,\mathrm{d}\boldsymbol{\eta}(\vartheta)\right)}_{:=\,D(\lambda)} = 0\ . \tag{2.16}$$

The left-hand side of this equation defines the characteristic function $D(\lambda)$ of (2.13). The characteristic exponents are the zeros of the characteristic function. As opposed to the characteristic polynomial of autonomous ODEs, the characteristic function $D(\lambda)$ has, in general, an infinite number of zeros in the complex plane, all of which should be considered during the stability analysis. Stability charts that present the stability properties as a function of the system parameters have therefore a rich and intricate structure even for the simplest DDEs.

Linear autonomous DDEs containing only point/discrete delays can be given in the form

$$\dot{\mathbf{x}}(t) = \mathbf{A}\mathbf{x}(t) + \sum_{j=1}^{g} \mathbf{B}_j\,\mathbf{x}(t-\tau_j)\ , \tag{2.17}$$

where $\mathbf{A}$ and the $\mathbf{B}_j$'s are $n \times n$ matrices, $\tau_j > 0$ for all j, and $g \in \mathbb{Z}^+$. In this case, only discrete values of the past have influence on the present rate of change of state.

An example of a DDE with distributed delay is

$$\dot{\mathbf{x}}(t) = \mathbf{A}\mathbf{x}(t) + \int_{-\sigma_1}^{-\sigma_2} \mathbf{K}(\vartheta)\,\mathbf{x}(t+\vartheta)\,\mathrm{d}\vartheta\ , \tag{2.18}$$

where $\mathbf{K}(\vartheta)$ is an $n \times n$ measurable kernel function, $\sigma_1, \sigma_2 \in \mathbb{R}$, and $\sigma_1 > \sigma_2 \geq 0$. The kernel function $\mathbf{K}(\vartheta)$ describes the weight of the past effects over the interval $[t-\sigma_1, t-\sigma_2]$. If the kernel is a constant matrix multiplied by the shifted Dirac delta distribution, i.e., $\mathbf{K}(\vartheta) = \mathbf{K}_0\,\delta(\vartheta+\tau)$ with $\sigma_1 \leq \tau \leq \sigma_2$, then the integral in (2.18) gives the point delay $\mathbf{K}_0\,\mathbf{x}(t-\tau)$.

Linear autonomous DDEs with distributed delay and with a finite number of point delays can be given in the general form

$$\dot{\mathbf{x}}(t) = \int_{-\sigma}^{0} \mathbf{K}(\vartheta)\mathbf{x}(t+\vartheta)\,\mathrm{d}\vartheta\ , \tag{2.19}$$

where $\mathbf{K}(\vartheta)$ is an $n \times n$ measurable kernel function that may comprise a measurable distribution and finitely many shifted Dirac delta distributions. That is, $\mathbf{K}(\vartheta)$ can also be given in the form

$$\mathbf{K}(\vartheta) = \mathbf{W}(\vartheta) + \sum_{j=1}^{g} \mathbf{B}_j\delta(\vartheta+\tau_j)\ , \tag{2.20}$$

where $\mathbf{W}(\vartheta)$ is an $n \times n$ measurable function (a weight function), the $\mathbf{B}_j$'s are $n \times n$ constant matrices, $\delta(\vartheta)$ denotes the Dirac delta distribution, $\tau_j \geq 0$ for all j, and $g \in \mathbb{N}$. Thus, (2.19) can be written as

$$\dot{\mathbf{x}}(t) = \int_{-\sigma}^{0} \mathbf{W}(\vartheta)\mathbf{x}(t+\vartheta)\mathrm{d}\vartheta + \sum_{j=1}^{g} \mathbf{B}_j \mathbf{x}(t-\tau_j) \; . \tag{2.21}$$

A necessary and sufficient condition for the asymptotic stability of DDE (2.13) with (2.15) is that all the infinite number of characteristic exponents have negative real parts and there exist a scalar $\nu > 0$ such that

$$\int_{-\infty}^{0} \mathrm{e}^{-\nu\vartheta} \left|\mathrm{d}\eta_{jk}(\vartheta)\right| < \infty \; , \quad j,k = 1,2,\ldots,n \; , \tag{2.22}$$

where $\eta_{jk}(\vartheta)$ are the elements of $\boldsymbol{\eta}(\vartheta)$. Condition (2.22) means that the past effect decays exponentially in the past. Obviously, this condition holds if σ in the lower limit of the integral in (2.15) is finite.

Although there are infinitely many characteristic exponents, it is not necessary to compute all of them, since stability analysis requires only the sign of the real part of the rightmost one(s). There exist several analytical and semi-analytical methods to derive the stability conditions for the system parameters. The first attempts for determining stability criteria for first- and second-order scalar DDEs were made by Bellmann and Cooke [19] and by Bhatt and Hsu [20]. They used the D-subdivision method of Neimark [167] combined with a theorem of Pontryagin [181]. The book of Kolmanovskii and Nosov [127] summarizes the main theorems on the stability of DDEs, and contains several examples as well. A sophisticated method was developed by Stépán [206] (generalized also by Hassard [86]) that can be applied even for a combination of multiple point delays and for distributed delays. There exist several efficient numerical methods to determine the rightmost exponents for a delayed system; see, for instance, the celebrated DDE-BIFTOOL developed by Engelborghs et al. [56, 57], the pseudospectral differencing method by Breda et al. [23, 24], the cluster treatment method by Olgac and Sipahi [171, 172], the Galerkin projection by Wahi and Chatterjee [231, 232], the mapping algorithm by Vyhlídal and Zítek [229], the harmonic balance by Liu and Kalmár-Nagy [143], or the Lambert W function approach by Ulsoy et al. [11, 238].

The stability properties of DDEs are often represented in the form of stability charts that show the stable and unstable domains, or alternatively, the number of unstable characteristic exponents (also called instability degree) in the space of system parameters. Stability charts for autonomous DDEs can be constructed by the *D-subdivision method*. The curves where changes in the number of unstable exponents

happen are given by the so-called *D-curves* (also called exponent-crossing curves or transition curves) given by

$$R(\omega) = 0 \,, \quad S(\omega) = 0 \,, \qquad \omega \in [0, \infty) \,, \tag{2.23}$$

where

$$R(\omega) := \operatorname{Re} D(\mathrm{i}\,\omega) \,, \quad S(\omega) := \operatorname{Im} D(\mathrm{i}\,\omega) \,, \tag{2.24}$$

with $D(\lambda)$ being the characteristic function defined in (2.16) and ω the parameter of the curves [209]. Due to the continuity of the characteristic exponents with respect to changes in the system parameters (see, for instance, [152]), the D-curves separate the parameter space into domains where the numbers of unstable characteristic exponents are constant. The determination of these numbers for the individual domains is not a trivial task. One technique is to calculate the *exponent-crossing direction* (also called root-crossing direction or root tendency) along the D-curves, which is the sign of the partial derivative of the real part of the characteristic exponent with respect to one of the system parameters. If the number of unstable exponents is known for at least one point in one domain, then it can be determined for all the other domains by considering the exponent-crossing direction along the D-curves. The *stability boundaries* are the D-curves bounded the domains with zero unstable characteristic exponent.

Alternatively, Stépán's formulas [206] can also be used to determine the number of unstable characteristic exponents in a simple and elegant way. This technique requires the analysis of the functions $R(\omega)$ and $S(\omega)$ defined in (2.24) only, without the analysis of the exponent-crossing direction. Assume that the characteristic function $D(\lambda)$ associated with (2.13) has no zeros on the imaginary axis and (2.22) holds. If the dimension n of (2.13) is even, i.e., $n = 2m$ with m being an integer, then the number of unstable exponents is

$$N = m + (-1)^m \sum_{k=1}^{r} (-1)^{k+1} \operatorname{sgn} S(\rho_k) \,, \tag{2.25}$$

where $\rho_1 \geq \cdots \geq \rho_r > 0$ are the positive real zeros of $R(\omega)$. If the dimension n of (2.13) is odd, i.e., $n = 2m + 1$ with m being an integer, then the number of unstable exponents is

$$N = m + \frac{1}{2} + (-1)^m \left(\frac{1}{2} (-1)^s \operatorname{sgn} R(0) + \sum_{k=1}^{s-1} (-1)^k \operatorname{sgn} R(\sigma_k) \right) \,, \tag{2.26}$$

where $\sigma_1 \geq \cdots \geq \sigma_s = 0$ are the nonnegative real zeros of $S(\omega)$. For further details and for an exact proof, see Theorems 2.15 and 2.16 in [206].

2.4 Linear Time-Periodic DDEs

Linear time-periodic DDEs have the general form

$$\dot{\mathbf{x}}(t) = \mathbf{L}(t, \mathbf{x}_t) \ , \quad \mathbf{L}(t+T) = \mathbf{L}(t) \ , \tag{2.27}$$

where $\mathbf{x}_t$ is a continuous function defined by (2.14), $\mathbf{L} : \mathbb{R} \times C \to \mathbb{R}^n$ is continuous and linear in $\mathbf{x}_t$. According to the Riesz representation theorem, the functional $\mathbf{L}$ can be written in the Stieltjes integral form

$$\mathbf{L}(t, \mathbf{x}_t) = \int_{-\sigma}^{0} \mathrm{d}_\vartheta \boldsymbol{\eta}(t, \vartheta) \mathbf{x}(t+\vartheta) \ , \tag{2.28}$$

where $\boldsymbol{\eta} : \mathbb{R} \times [-\sigma, 0] \to \mathbb{R}^{n \times n}$ is a matrix function of bounded variation in $\vartheta \in [-\sigma, 0]$.

Linear time-periodic DDEs with constant point delays can be defined as

$$\begin{aligned} \dot{\mathbf{x}}(t) &= \mathbf{A}(t)\mathbf{x}(t) + \sum_{j=1}^{g} \mathbf{B}_j(t)\, \mathbf{x}(t-\tau_j) \ , \\ \mathbf{A}(t+T) &= \mathbf{A}(t) \ , \quad \mathbf{B}_j(t+T) = \mathbf{B}_j(t) \ , \end{aligned} \tag{2.29}$$

where $\mathbf{A}(t)$ and the $\mathbf{B}_j(t)$'s are $n \times n$ matrices, $\tau_j > 0$ for all j, and $g \in \mathbb{Z}^+$. Linear time-periodic DDEs with distributed delay read

$$\begin{aligned} \dot{\mathbf{x}}(t) &= \mathbf{A}(t)\mathbf{x}(t) + \int_{-\sigma_1}^{-\sigma_2} \mathbf{K}(\vartheta, t)\, \mathbf{x}(t+\vartheta)\, \mathrm{d}\vartheta \ , \\ \mathbf{A}(t+T) &= \mathbf{A}(t) \ , \quad \mathbf{K}(\vartheta, t+T) = \mathbf{K}(\vartheta, t) \ , \end{aligned} \tag{2.30}$$

where $\mathbf{K}(\vartheta, t)$ is the time-periodic $n \times n$ kernel function, $\sigma_1, \sigma_2 \in \mathbb{R}$, and $\sigma_1 > \sigma_2 \geq 0$. A special case of (2.30) occurs when the kernel function is a constant matrix multiplied by a time-periodic Dirac delta distribution, i.e., $\mathbf{K}(\vartheta, t) = \mathbf{K}_0 \delta(\vartheta - \tau(t))$ with $\sigma_1 \leq \tau(t) \leq \sigma_2$ and $\tau(t+T) = \tau(t)$. In this case, the integral in (2.30) gives the time-periodic point delay $\mathbf{K}_0 \mathbf{x}(t - \tau(t))$. The general form of linear time-periodic DDEs with time-periodic point delays is

$$\begin{aligned} \dot{\mathbf{x}}(t) &= \mathbf{A}(t)\mathbf{x}(t) + \sum_{j=1}^{g} \mathbf{B}_j(t)\, \mathbf{x}(t-\tau_j(t)) \ , \\ \mathbf{A}(t+T) &= \mathbf{A}(t) \ , \quad \mathbf{B}_j(t+T) = \mathbf{B}_j(t) \ , \quad \tau_j(t+T) = \tau_j(t) \ . \end{aligned} \tag{2.31}$$

Linear time-periodic DDEs with distributed delay and with a finite number of point delays can be given in the general form

$$\dot{\mathbf{x}}(t) = \int_{-\sigma}^{0} \mathbf{K}(\vartheta, t)\mathbf{x}(t+\vartheta)\, \mathrm{d}\vartheta \ , \tag{2.32}$$

where $\mathbf{K}(\vartheta, t)$ is an $n \times n$ measurable kernel function that can be written in the form

$$\mathbf{K}(\vartheta, t) = \mathbf{W}(\vartheta, t) + \sum_{j=1}^{g} \mathbf{B}_j(t)\delta(\vartheta + \tau_j(t)) \,. \tag{2.33}$$

Here $\mathbf{W}(\vartheta, t+T) = \mathbf{W}(\vartheta, t)$ is a time-periodic $n \times n$ measurable function (a time-periodic weight function), $\mathbf{B}_j(t+T) = \mathbf{B}_j(t)$ are $n \times n$ time-periodic matrices, $\delta(\vartheta)$ denotes the Dirac delta distribution, $\tau_j(t) \geq 0$ for all j, and $g \in \mathbb{N}$. Thus, (2.32) can be written as

$$\dot{\mathbf{x}}(t) = \int_{-\sigma}^{0} \mathbf{W}(\vartheta, t)\mathbf{x}(t+\vartheta)\mathrm{d}\vartheta + \sum_{j=1}^{g} \mathbf{B}_j(t)\mathbf{x}(t-\tau_j(t)) \,. \tag{2.34}$$

According to the Floquet theory of DDEs [76, 79], the solution segment $\mathbf{x}_t$ for (2.27) associated with the initial function $\mathbf{x}_0$ can be given as $\mathbf{x}_t = \mathcal{U}(t)\mathbf{x}_0$, where $\mathcal{U}(t)$ is the solution operator (infinitesimal generator). The stability of the system is determined by the spectrum of the corresponding monodromy operator $\mathcal{U}(T)$. The nonzero elements of the spectrum of $\mathcal{U}(T)$ are called *characteristic multipliers* (also referred to as *Floquet multipliers* or *poles*) and are defined by

$$\mathrm{Ker}(\mu\mathcal{I} - \mathcal{U}(T)) \setminus \{\mathbf{0}\} \neq \emptyset \,, \quad \mu \neq 0 \,, \tag{2.35}$$

or

$$\mathrm{Ker}(\mu\mathcal{I} - \mathcal{U}(T)) \neq \{\mathbf{0}\} \,, \quad \mu \neq 0 \,, \tag{2.36}$$

with $\mathcal{I}$ denoting the identity operator. Generally, time-periodic DDEs have infinitely many characteristic multipliers. If μ is a characteristic multiplier, and $\mu = \mathrm{e}^{\lambda T}$, then λ is called the characteristic exponent. Similarly to linear periodic ODEs, each characteristic multiplier is associated with infinitely many characteristic exponents of the form $\lambda_k = \gamma + \mathrm{i}\,(\omega + k2\pi/T)$, where $\gamma, \omega \in \mathbb{R}$, $k \in \mathbb{Z}$, and $T\omega \in (-\pi, \pi]$.

A necessary and sufficient condition for the asymptotic stability of the time-periodic DDE (2.27) with (2.28) is that all the characteristic multipliers have modulus less than one (that is, all the characteristic exponents have negative real parts) and there exist a scalar $\nu > 0$ such that

$$\int_{-\infty}^{0} \mathrm{e}^{-\nu\vartheta} \left|\mathrm{d}_\vartheta \eta_{jk}(t, \vartheta)\right| < \infty \,, \quad j, k = 1, 2, \ldots, n \,, \tag{2.37}$$

for all $t \in \mathbb{R}$, where $\eta_{jk}(t, \vartheta)$ are the elements of $\boldsymbol{\eta}(t, \vartheta)$. Similarly to autonomous DDEs, condition (2.37) trivially holds if σ in the lower limit of the integral in (2.28) is finite. The difficulty in the stability analysis of periodic DDEs is that the monodromy operator $\mathcal{U}(T)$ has generally no closed form; consequently, the stability conditions cannot be derived in an analytic form.

There exist several numerical and semi-analytical techniques to determine the stability conditions for periodic DDEs. Most of them were developed with the aim of constructing stability charts for milling processes. Insperger and Stépán [100] introduced the semi-discretization method that is based on a special discretization of the individual terms in the DDE. Budak and Altintas [26, 27] and Merdol and Altintas [150] developed the multi-frequency solution method, which is a kind of alternative application of Hill's infinite determinant method. Butcher et al. [30, 33] used an expansion of the solution in terms of Chebyshev polynomials to obtain an approximate monodromy matrix. A temporal finite element method using Hermite polynomials was developed by Bayly et al. [17] for interrupted turning, and formulated to general periodic DDEs by Mann and Patel [147]. Szalai et al. [219] used the characteristic matrices of the system to derive stability charts (see also [200]). Recently, Khasawneh and Mann presented an effective numerical algorithm called the spectral element method that is a temporal finite element method involving highly accurate numerical quadratures for the integral terms [121, 122].

2.5 DDEs with state-dependent delays

If the delay depends not only on the time but also on the state, then the corresponding equation is called a DDE with state-dependent delay (SD-DDE). A simple example for SD-DDEs is

$$\dot{\mathbf{x}}(t) = \mathbf{A}\mathbf{x}(t) + \mathbf{B}\,\mathbf{x}(t - \tau(t, \mathbf{x}(t))) \tag{2.38}$$

with $\tau(t, \mathbf{x}(t)) \geq 0$. Here, the delay depends on the actual time t and on the actual state $\mathbf{x}(t)$. If the delay depends also on delayed values of the state, then it is usually written in the form $\tau(t, \mathbf{x}_t) \geq 0$, where $\mathbf{x}_t$ is defined as in equation (2.14).

State-dependent delays arose first in the two-body problem of classical electrodynamics [50], but they appear in many other fields, such as population models [169, 135], automatic position control [233], neural networks models [16], and machine tool vibration theory [108]. There are several papers dealing with some special classes of systems with state-dependent delays [80, 133, 134]. A survey about DDEs with state-dependent delays is given in [85].

SD-DDEs are always nonlinear, since the state appears in its own argument. Thus, the nonlinearity is defined by the solution of the system. The corresponding linear system is, however, a DDE with constant (or time-dependent) delay. Linearization of SD-DDEs is complicated by the fact that the solution of the system is not differentiable with respect to the state-dependent delay (see, e.g., [81] and the references therein). Consequently, "true" linearization is not possible, rather we are looking for a linear

DDE, which is associated to the original system in the sense that they have the same local stability properties. For example, consider the autonomous scalar SD-DDE

$$\dot{x}(t) = x(t - (\tau_0 + x(t))) \ . \tag{2.39}$$

This is a nonlinear equation due to the state-dependent time delay $\tau(x(t)) = \tau_0 + x(t)$. The DDE

$$\dot{y}(t) = y(t - \tau_0) \tag{2.40}$$

with constant time delay is a linear system that can be considered as a linear variational system corresponding to (2.39) around the equilibrium $x = 0$. In our terminology, linearization means that the trivial solutions $y(t) \equiv 0$ of (2.40) and $x(t) \equiv 0$ of (2.39) are asymptotically stable at the same time. Linearization techniques for general autonomous SD-DDEs were given by Hartung and Turi [82] and for time-periodic SD-DDEs by Hartung [83]. The mathematical background for the full-discretization of DDEs with state-dependent delays was presented by Győri et al. [73, 74].

In engineering practice, DDEs with state-dependent delay are rarely used since the appropriate mathematical tools, like linearization techniques, have just been developed recently (see [82, 83]), and these new results have not been adopted in engineering problems yet. Still, the effect of state-dependent delay becomes important in rotary cutting processes (e.g., in milling, or drilling) where the torsional vibrations of the tool are significant in the system's dynamics. Richard et al. [184] and Germay et al. [67] investigated drilling with drag bits and showed that state-dependent regenerative delay arises due to the torsional vibration of the tool. They investigated self-excited vibrations and periodic orbits of the tool numerically. Insperger et al. [105] showed that state-dependent delay arises in the governing equation of the milling process even when only the bending oscillation of the tool is considered and its torsional compliance is neglected. The stability analysis for the same system was performed by Bachrathy et al. [14]. The state-dependency of the regenerative delay due to the bending compliance of the milling tool was also derived by Long et al. [144].

Chapter 3

Higher-order semi-discretization method

The semi-discretization method was introduced by Insperger and Stepan [100] for general time-periodic DDEs. This method was later referred to as zeroth-order semi-discretization. Elbeyli and Sun [53] generalized the method to the so-called improved zeroth-order (see also [104]) and the first-order semi-discretization for second-order scalar systems. The general higher-order formalism was presented in [110]. The convergence of the method was established by Hartung et al. [84] for a large class of DDEs appearing in engineering applications. It was shown that semi-discretization preserves asymptotic stability of the original equation; therefore it can be used to construct approximate stability charts.

The merit of the semi-discretization method is that it can be used effectively to determine stability charts for time-periodic DDEs arising in different engineering problems while the numerical scheme itself is relatively simple. One of the main fields of application of semi-discretization is the stability prediction for machining processes. Different milling models were analyzed by Gradišek et al. [70], Henninger and Eberhard [87, 88], Sims et al. [203], Dombovari et al. [48], Bachrathy et al. [13], and Wan et al. [234] using the semi-discretization method. Ding et al. [45, 46] applied an alternative semi-discretization method for the milling problem using a slightly different concept in the discretization scheme (see also [112]). Sellmeier and Denkena [195] applied the method to milling processes with uneven tooth pitches and pointed out that the method can be considered an extension of the theory of sampled control systems with feedback delay according to Ackermann [1] (see also [137, 12, 170]).

A continuous-time approximation technique was introduced by Sun and Song [216, 217] based on the concept of semi-discretization that can handle multiple time delays for both linear and nonlinear dynamical systems. Models with time-periodic delays

were considered by Insperger and Stépán [103], Long et al. [144], Faassen et al. [59], Zatarain et al. [241], and Seguy et al. [193]. The method can also be used for other models, for instance, for the stability analysis of periodic control systems with delayed feedback, as was shown by Sheng et al. [197] and by Konishi and Hara [128].

In this chapter, first, the general formulas for the higher-order semi-discretization method are presented. Then the zeroth- and the first-order techniques are described in detail. After that, rate of convergence estimates are given. The new results are composed in Thesis 1 at the end of the chapter. The results presented here were published in Insperger et al. [110] and was also included into the book Insperger and Stépán [115].

3.1 General formulas

Consider the time-periodic DDE with multiple time-periodic point delays of the form

$$\dot{\mathbf{x}}(t) = \mathbf{A}(t)\mathbf{x}(t) + \sum_{j=1}^{g} \mathbf{B}_j(t)\mathbf{u}(t-\tau_j(t)) \,, \tag{3.1}$$

$$\mathbf{u}(t) = \mathbf{D}\mathbf{x}(t) \,, \tag{3.2}$$

where $\mathbf{x}(t) \in \mathbb{R}^n$ is the state, $\mathbf{u}(t) \in \mathbb{R}^m$ is the input, $\mathbf{A}(t+T) = \mathbf{A}(t)$ and $\mathbf{B}_j(t+T) = \mathbf{B}_j(t)$, $j = 1, 2, \ldots, g$, are $n \times n$ and $n \times m$ time-periodic matrices, respectively, $\mathbf{D}$ is an $m \times n$ constant matrix, and $\tau_j(t+T) = \tau_j(t) > 0$, $j = 1, 2, \ldots, g$. The principal period of the system is T. Note that (3.1)–(3.2) can also be written in the form

$$\dot{\mathbf{x}}(t) = \mathbf{A}(t)\mathbf{x}(t) + \sum_{j=1}^{g} \mathbf{B}_j(t)\mathbf{D}\mathbf{x}(t-\tau_j(t)) \,. \tag{3.3}$$

The main point of higher-order semi-discretization methods is that the time-periodic coefficients and the time-periodic delays are approximated by piecewise constant functions, the delayed terms are approximated by linear combinations of some discrete delayed values of the state variable $\mathbf{x}$, while the nondelayed terms are left in their original form. Consider the discrete time scale $t_i = ih$, $i \in \mathbb{Z}$, such that the time step is $h = T/p$ with p being an integer approximation parameter. The approximating semi-discrete system is formulated as

$$\dot{\mathbf{y}}(t) = \mathbf{A}_i\mathbf{y}(t) + \sum_{j=1}^{g} \mathbf{B}_{j,i}\mathbf{\Gamma}_{j,i}^{(q)}(t-\tau_{j,i}) \,, \quad t \in [t_i, t_{i+1}) \,, \tag{3.4}$$

$$\mathbf{\Gamma}_{j,i}^{(q)}(t-\tau_{j,i}) = \sum_{k=0}^{q} \left(\prod_{l=0, l\neq k}^{q} \frac{t-\tau_{j,i}-(i+l-r_{j,i})h}{(k-l)h} \right) \mathbf{v}(t_{i+k-r_{j,i}}) \,, \tag{3.5}$$

$$\mathbf{v}(t_i) = \mathbf{D}\mathbf{y}(t_i), \tag{3.6}$$

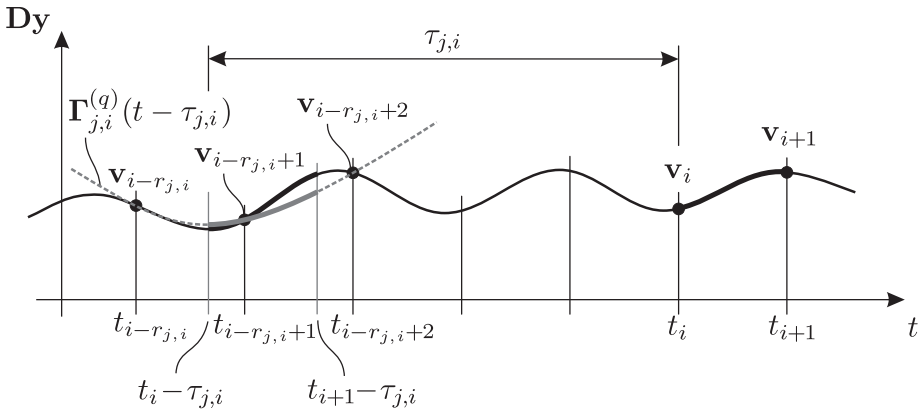

Figure 3.1: Approximation of the delayed term $\mathbf{Dy}(t-\tau_{j,i})$ by the polynomial $\mathbf{\Gamma}_{j,i}^{(q)}(t-\tau_{j,i})$, shown by a dashed line (in the depicted case, $q=2$).

where

$$\mathbf{A}_i = \frac{1}{h}\int_{t_i}^{t_{i+1}} \mathbf{A}(t)\,\mathrm{d}t\ , \tag{3.7}$$

$$\mathbf{B}_{j,i} = \frac{1}{h}\int_{t_i}^{t_{i+1}} \mathbf{B}_j(t)\,\mathrm{d}t\ , \qquad j=1,2,\ldots,g\ , \tag{3.8}$$

$$\tau_{j,i} = \frac{1}{h}\int_{t_i}^{t_{i+1}} \tau_j(t)\,\mathrm{d}t\ , \qquad j=1,2,\ldots,g\ , \tag{3.9}$$

are the piecewise constant approximations of $\mathbf{A}(t)$, $\mathbf{B}_j(t)$, and $\tau_j(t)$, $j=1,2,\ldots,g$, over the discretization interval $[t_i,t_{i+1})$. Use again the notation $\mathbf{y}_i := \mathbf{y}(t_i)$ and $\mathbf{v}_i := \mathbf{v}(t_i)$ for all $i\in\mathbb{Z}$. The delayed term $\mathbf{\Gamma}_{j,i}^{(q)}(t-\tau_{j,i})$ is a qth-order Lagrange polynomial interpolation of $\mathbf{D}(t)\mathbf{y}(t)$ in $t\in[t_{i-r_{j,i}},t_{i-r_{j,i}+q}]$ using the discrete values $\mathbf{v}_{i-r_{j,i}},\mathbf{v}_{i-r_{j,i}+1},\ldots,\mathbf{v}_{i-r_{j,i}+q}$. The integer $r_{j,i}$ is defined by

$$r_{j,i} = \mathrm{int}\left(\frac{\tau_{j,i}}{h}+\frac{q}{2}\right)\ , \qquad j=1,2,\ldots,g\ , \qquad i=1,2,\ldots,p\ , \tag{3.10}$$

where int denotes the integer-part function. The concept of the approximation scheme is illustrated in Figure 3.1, where the dashed curve indicates the approximating polynomial $\mathbf{\Gamma}_{j,i}^{(q)}(t-\tau_{j,i})$.

The key feature of the semi-discretization method is that the approximate system (3.4)–(3.6) can be solved analytically over the discretization interval $t\in[t_i,t_{i+1})$ for given initial values $\mathbf{y}_i$ and $\mathbf{v}_{i+k-r_{j,i}}$, $k=0,1,\ldots,q$, $j=1,2,\ldots,g$, in the form

$$\mathbf{y}_{i+1} = \mathbf{P}_i\mathbf{y}_i + \sum_{j=1}^{g}\sum_{k=0}^{q}\mathbf{R}_{j,i,k}\mathbf{v}_{i+k-r_{j,i}}\ , \tag{3.11}$$

where

$$\mathbf{P}_i = \mathrm{e}^{\mathbf{A}_i h}\,, \tag{3.12}$$

$$\mathbf{R}_{j,i,k} = \int_{t_i}^{t_{i+1}} \mathrm{e}^{\mathbf{A}_i(t_{i+1}-s)} \left(\prod_{l=0,\, l\neq k}^{q} \frac{s-\tau_{j,i}-(i+l-r_{j,i})h}{(k-l)h} \right) \mathbf{B}_{j,i}\, \mathrm{d}s$$

$$= \int_{0}^{h} \mathrm{e}^{\mathbf{A}_i(h-s)} \left(\prod_{l=0,\, l\neq k}^{q} \frac{s-\tau_{j,i}-(l-r_{j,i})h}{(k-l)h} \right) \mathbf{B}_{j,i}\, \mathrm{d}s \tag{3.13}$$

(see the variation of constants formula (A.15) in Appendix A). Equations (3.11) and (3.6) imply the discrete map

$$\mathbf{z}_{i+1} = \mathbf{G}_i \mathbf{z}_i, \tag{3.14}$$

where

$$\mathbf{z}_i = \begin{pmatrix} \mathbf{y}_i & \mathbf{v}_{i-1} & \mathbf{v}_{i-2} & \dots & \mathbf{v}_{i-r} \end{pmatrix}^T \tag{3.15}$$

is an augmented state vector and the coefficient matrix reads

$$\mathbf{G}_i = \left(\begin{array}{c|cccc} \mathbf{P}_i & \mathbf{0} & \cdots & \mathbf{0} & \mathbf{0} \\ \hline \mathbf{D} & \mathbf{0} & \cdots & \mathbf{0} & \mathbf{0} \\ \mathbf{0} & \mathbf{I} & \cdots & \mathbf{0} & \mathbf{0} \\ \vdots & & \ddots & & \vdots \\ \mathbf{0} & \mathbf{0} & \cdots & \mathbf{I} & \mathbf{0} \end{array}\right)$$

$$+ \sum_{j=1}^{g} \left(\begin{array}{c|ccccccccc} & \multicolumn{3}{c}{\scriptstyle 1} & & \scriptstyle r_{j,i}-q & & \scriptstyle r_{j,i} & & \scriptstyle r \\ \mathbf{0} & \mathbf{0} & \cdots & \mathbf{0} & \mathbf{R}_{j,i,q} & \cdots & \mathbf{R}_{j,i,0} & \mathbf{0} & \cdots & \mathbf{0} \\ \hline \mathbf{0} & \mathbf{0} & \cdots & \mathbf{0} & \mathbf{0} & \cdots & \mathbf{0} & \mathbf{0} & \cdots & \mathbf{0} \\ \mathbf{0} & \mathbf{0} & \cdots & \mathbf{0} & \mathbf{0} & \cdots & \mathbf{0} & \mathbf{0} & \cdots & \mathbf{0} \\ \vdots & \vdots & & \vdots & \vdots & & \vdots & \vdots & & \vdots \\ \mathbf{0} & \mathbf{0} & \cdots & \mathbf{0} & \mathbf{0} & \cdots & \mathbf{0} & \mathbf{0} & \cdots & \mathbf{0} \end{array}\right). \tag{3.16}$$

This is an $(n+rm)\times(n+rm)$ matrix, where $r = \max\left(r_{j,i}\right)$. Matrix $\mathbf{G}_i$ can be divided into four blocks, as shown by the lines in (3.16). The left upper block is the $n \times n$ matrix $\mathbf{P}_i$. The right upper block consists of r pieces of $n \times m$ matrices numbered in (3.16). Matrices $\mathbf{R}_{j,i,k}$, $k = 0, 1, \dots, q$, are located at the $(r_{j,i}-k)$th place within this block. The left lower block of $\mathbf{G}_i$ consists of r pieces of $m \times n$ matrices ($\mathbf{D}$ and zero matrices). The right lower block is an $rm \times rm$ block containing zero matrices and identity matrices $\mathbf{I}$ of size $m \times m$.

Utilizing that $T = ph$, p repeated applications of (3.14) with initial state $\mathbf{z}_0$ gives the monodromy mapping

$$\mathbf{z}_p = \mathbf{\Phi} \mathbf{z}_0\,, \tag{3.17}$$

where

$$\mathbf{\Phi} = \mathbf{G}_{p-1}\mathbf{G}_{p-2}\cdots\mathbf{G}_0 \tag{3.18}$$

is an $(n+rm)$-dimensional matrix representation of the monodromy operator of (3.4)–(3.6), which is at the same time a finite-dimensional approximation of the infinite-dimensional monodromy operator of the original system (3.1)–(3.2). If all the eigenvalues of $\mathbf{\Phi}$ are inside the unit circle of the complex plane, then the approximate system (3.4)–(3.6) is asymptotically stable. Since discretization techniques preserve asymptotic stability for DDEs (see [75, 63, 84]), the stability charts of the approximate system (3.4)–(3.6) give an approximation for the stability charts of the original time-periodic DDE (3.1)–(3.2).

The approximation parameter p is related to the resolution of the principal period such that $T = ph$; therefore, the integer p is called the *period resolution*. The integer r is related to the discretization of the state $\mathbf{x}_t$ over the delay interval $[-\tau_{\max}, 0]$, where $\tau_{\max} = \max\big(\tau_{j,i}\big)$, such that $\tau_{\max} \approx (r - q/2)h$. Therefore, the integer r is called the *delay resolution*. The number of matrices $\mathbf{G}_i$ to be multiplied to obtain the monodromy matrix $\mathbf{\Phi}$ in (3.18) is equal to the period resolution p. The size of the matrices $\mathbf{G}_i$ (and the size of the monodromy matrix $\mathbf{\Phi}$) is equal to $(n+rm)$. Recall that $r = \max\big(r_{j,i}\big)$, $j = 1, 2, \ldots, g$, $i = 1, 2, \ldots, p$, and $r_{j,i} = \mathrm{int}\big(\tau_{j,i}/h + q/2\big) = \mathrm{int}\big(p\tau_{j,i}/T + q/2\big)$. Here, $r_{j,i}$ is the *particular delay resolution* associated with the particular delay $\tau_{j,i}$. Thus, the larger the period resolution p, the larger the size of the approximate monodromy matrix. If p tends to infinity, then $\mathbf{\Phi}$ converges to the infinite-dimensional monodromy operator of the original system (3.1)–(3.2).

The convergence of the semi-discretization method can be visualized by plotting the characteristic multipliers in the complex plane. Let us denote the characteristic multipliers of the original system (3.1)–(3.2) by μ_k, $k = 1, 2, \ldots$, and the characteristic multipliers of the approximate semi-discrete system (3.4)–(3.6) by $\tilde{\mu}_k$, $k = 1, 2, \ldots, (n+rm)$. Let the circles of center $\tilde{\mu}_k$ and radius ε be denoted by $S_{\tilde{\mu}_k,\varepsilon}$. For any small $\varepsilon > 0$, there exists an integer $M(\varepsilon)$ such that for every $p > M(\varepsilon)$, the set $\bigcup_{k=1}^{n+rm} S_{\tilde{\mu}_k,\varepsilon}$ contains exactly $n + rm$ characteristic multipliers μ_k of (3.1)–(3.2), and all the other characteristic multipliers have modulus less than ε.

Thus, if all the characteristic multipliers of (3.4)–(3.6) have modulus less than 1, then by choosing $\varepsilon = \frac{1}{2}\big(1 - \max_j |\tilde{\mu}_j|\big)$, the finite approximation number $M(\varepsilon)$ exists, and if $p > M(\varepsilon)$, then the discretized system and the original system have the same stability properties (see Figure 3.2 with $n + rm = 5$).

During the construction of stability charts, the numerical efficiency of the method depends, of course, on the choice of the period resolution p. A lower estimate can be given based on the above derivation of $M(\varepsilon)$, but in practice, it is easier to use a trial-and-error technique and to check how the stability boundaries converge for increasing

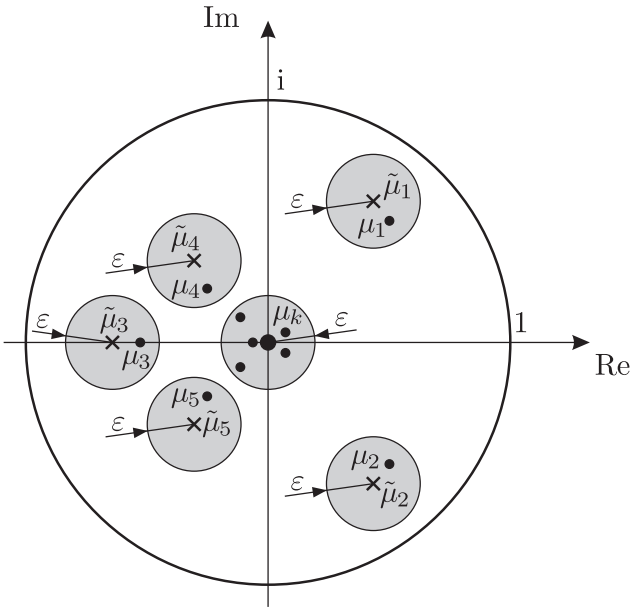

Figure 3.2: Locations of the exact (μ) and the approximate ($\tilde{\mu}$) characteristic multipliers.

p. The value of the required p depends on the system's parameters, which means that the construction of the stability charts can be optimized by choosing different values in different domains of the charts.

The formulas presented in this section give the steps of the semi-discretization method for arbitrary approximation order q. For the sake of completeness, some special cases of these formulas are presented for the zeroth- and the first-order approximations in the next sections.

3.2 Zeroth-Order Semi-Discretization

For the zeroth-order case ($q = 0$), (3.5) and (3.10) give $\mathbf{\Gamma}_{j,i}^{(q)}(t - \tau_{j,i}) \equiv \mathbf{v}(t_{i-r_{j,i}})$ and $r_{j,i} = \mathrm{int}\big(\tau_{j,i}/h\big)$, and the approximate system reads

$$\dot{\mathbf{y}}(t) = \mathbf{A}_i\mathbf{y}(t) + \sum_{j=1}^{g} \mathbf{B}_{j,i}\mathbf{v}(t_{i-r_{j,i}}) \,, \quad t \in [t_i, t_{i+1}) \,, \tag{3.19}$$

$$\mathbf{v}(t_i) = \mathbf{D}\mathbf{y}(t_i) \,. \tag{3.20}$$

This corresponds to a piecewise constant approximation of the delayed term according to Figure 3.3.

Using the notation $\mathbf{y}_i := \mathbf{y}(t_i)$ and $\mathbf{v}_i := \mathbf{v}(t_i)$, $i \in \mathbb{Z}$, the solution over one discrete

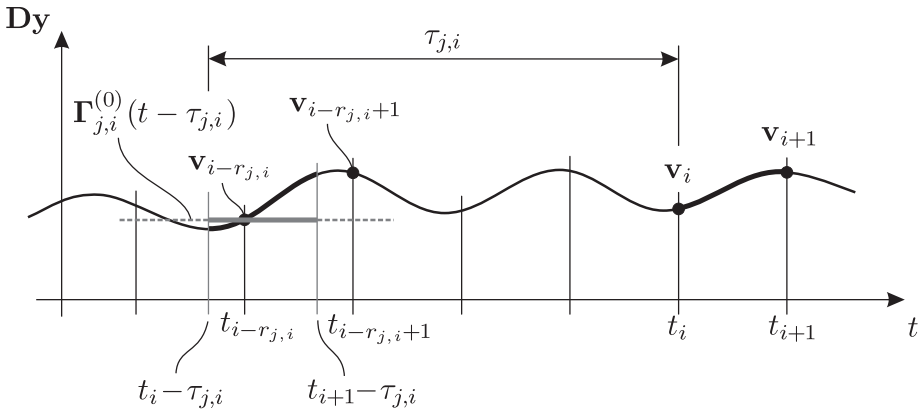

Figure 3.3: Zeroth-order approximation of the delayed term $\mathbf{Dy}(t-\tau_{j,i})$ by $\mathbf{\Gamma}^{(0)}_{j,i}(t-\tau_{j,i}) \equiv \mathbf{v}_{i-r_{j,i}}$, shown by the dashed line.

step can be formulated as

$$\mathbf{y}_{i+1} = \mathbf{P}_i \mathbf{y}_i + \sum_{j=1}^{g} \mathbf{R}_{j,i,0} \mathbf{v}_{i-r_{j,i}} \ , \tag{3.21}$$

where $\mathbf{P}_i$ is given by (3.12) and

$$\mathbf{R}_{j,i,0} = \int_0^h \mathrm{e}^{\mathbf{A}_i(h-s)} \, \mathrm{d}s \, \mathbf{B}_{j,i} \ . \tag{3.22}$$

If $\mathbf{A}_i^{-1}$ exists, then integration gives

$$\mathbf{R}_{j,i,0} = \left(\mathrm{e}^{\mathbf{A}_i h} - \mathbf{I} \right) \mathbf{A}_i^{-1} \mathbf{B}_{j,i} \ , \tag{3.23}$$

where $\mathbf{I}$ is the $n \times n$ identity matrix. In this case, the coefficient matrix $\mathbf{G}_i$ in (3.14) reads

$$\mathbf{G}_i = \left(\begin{array}{c|cccc} \mathbf{P}_i & \mathbf{0} & \cdots & \mathbf{0} & \mathbf{0} \\ \hline \mathbf{D} & \mathbf{0} & \cdots & \mathbf{0} & \mathbf{0} \\ \mathbf{0} & \mathbf{I} & \cdots & \mathbf{0} & \mathbf{0} \\ \vdots & & \ddots & & \vdots \\ \mathbf{0} & \mathbf{0} & \cdots & \mathbf{I} & \mathbf{0} \end{array}\right) + \sum_{j=1}^{g} \left(\begin{array}{c|ccccccc} \mathbf{0} & \mathbf{0} & \cdots & \mathbf{0} & \mathbf{R}_{j,i,0} & \mathbf{0} & \cdots & \mathbf{0} \\ \hline \mathbf{0} & \mathbf{0} & \cdots & \mathbf{0} & \mathbf{0} & \mathbf{0} & \cdots & \mathbf{0} \\ \mathbf{0} & \mathbf{0} & \cdots & \mathbf{0} & \mathbf{0} & \mathbf{0} & \cdots & \mathbf{0} \\ \vdots & \vdots & & \vdots & \vdots & \vdots & & \vdots \\ \mathbf{0} & \mathbf{0} & \cdots & \mathbf{0} & \mathbf{0} & \mathbf{0} & \cdots & \mathbf{0} \end{array}\right) \begin{array}{c} \\ \hline \\ \\ \\ \\ \end{array} \begin{array}{c} \\ 1 \\ \hline \\ \\ \\ \\ \end{array} \begin{array}{c} \\ r_{j,i} \\ \hline \\ \\ \\ \\ \end{array} \begin{array}{c} \\ r \\ \hline \\ \\ \\ \\ \end{array} \ . \tag{3.24}$$

Here, matrix $\mathbf{R}_{j,i,0}$ is located at the $r_{j,i}$th place within the right upper block of $\mathbf{G}_i$. The approximate monodromy matrix is given by (3.18).

3.3 First-Order Semi-Discretization

For the first-order case ($q = 1$), (3.5) and (3.10) give

$$\mathbf{\Gamma}_{j,i}^{(1)}(t-\tau_{j,i}) = \beta_{j,i,0}(t)\mathbf{v}(t_{i-r_{j,i}}) + \beta_{j,i,1}(t)\mathbf{v}(t_{i-r_{j,i}+1}) \tag{3.25}$$

with

$$\beta_{j,i,0}(t) = \frac{\tau_{j,i} + (i - r_{j,i} + 1)h - t}{h}\,, \qquad \beta_{j,i,1}(t) = \frac{t - (i - r_{j,i})h - \tau_{j,i}}{h}\,, \tag{3.26}$$

and $r_{j,i} = \operatorname{int}\big(\tau_{j,i}/h + 1/2\big)$. In this case, the approximate system reads

$$\dot{\mathbf{y}}(t) = \mathbf{A}_i\mathbf{y}(t) + \sum_{j=1}^{g} \mathbf{B}_{j,i}\left(\beta_{j,i,0}(t)\mathbf{v}(t_{i-r_{j,i}}) + \beta_{j,i,1}(t)\mathbf{v}(t_{i-r_{j,i}+1})\right)\,, \quad t \in [t_i, t_{i+1})\,, \tag{3.27}$$

$$\mathbf{v}(t_i) = \mathbf{D}\mathbf{y}(t_i)\,. \tag{3.28}$$

The scheme of the first-order approximation is shown in Figure 3.4. Using the notation $\mathbf{y}_i := \mathbf{y}(t_i)$ and $\mathbf{v}_i := \mathbf{v}(t_i)$, $i \in \mathbb{Z}$, the solution over one discrete step can be formulated as

$$\mathbf{y}_{i+1} = \mathbf{P}_i\mathbf{y}_i + \sum_{j=1}^{g}\left(\mathbf{R}_{j,i,0}\mathbf{v}_{i-r_{j,i}} + \mathbf{R}_{j,i,1}\mathbf{v}_{i-r_{j,i}+1}\right)\,, \tag{3.29}$$

where $\mathbf{P}_i$ is given by (3.12) and

$$\mathbf{R}_{j,i,0} = \int_0^h \frac{\tau_{j,i} - (r_{j,i}-1)h - s}{h}\,\mathrm{e}^{\mathbf{A}_i(h-s)}\,\mathrm{d}s\,\mathbf{B}_{j,i}\,, \tag{3.30}$$

$$\mathbf{R}_{j,i,1} = \int_0^h \frac{s - \tau_{j,i} + r_{j,i}h}{h}\,\mathrm{e}^{\mathbf{A}_i(h-s)}\,\mathrm{d}s\,\mathbf{B}_{j,i}\,. \tag{3.31}$$

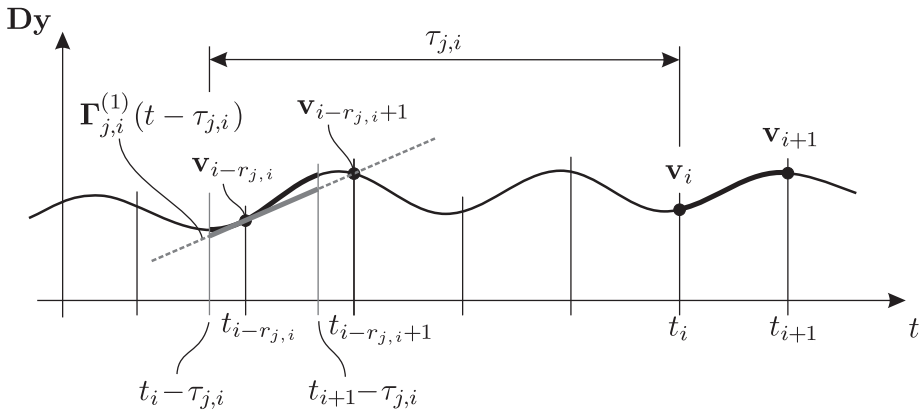

Figure 3.4: First-order approximation of the delayed term $\mathbf{D}\mathbf{y}(t-\tau_{j,i})$ by $\mathbf{\Gamma}_{j,i}^{(1)}(t-\tau_{j,i})$, shown by the dashed line.

If $\mathbf{A}_i^{-1}$ exists, then integration gives

$$\mathbf{R}_{j,i,0} = \left(\mathbf{A}_i^{-1} + \frac{1}{h} \left(\mathbf{A}_i^{-2} - (\tau_{j,i} - (r_{j,i} - 1)h)\, \mathbf{A}_i^{-1} \right) \left(\mathbf{I} - \mathrm{e}^{\mathbf{A}_i h} \right) \right) \mathbf{B}_{j,i} \,, \tag{3.32}$$

$$\mathbf{R}_{j,i,1} = \left(-\mathbf{A}_i^{-1} + \frac{1}{h} \left(-\mathbf{A}_i^{-2} + (\tau_{j,i} - r_{j,i}h)\, \mathbf{A}_i^{-1} \right) \left(\mathbf{I} - \mathrm{e}^{\mathbf{A}_i h} \right) \right) \mathbf{B}_{j,i} \,. \tag{3.33}$$

In this case, the coefficient matrix $\mathbf{G}_i$ in (3.14) reads

$$\mathbf{G}_i = \left(\begin{array}{c|ccc|c} \mathbf{P}_i & \mathbf{0} & \cdots & \mathbf{0} & \mathbf{0} \\ \hline \mathbf{D} & \mathbf{0} & \cdots & \mathbf{0} & \mathbf{0} \\ \mathbf{0} & \mathbf{I} & \cdots & \mathbf{0} & \mathbf{0} \\ \vdots & & \ddots & & \vdots \\ \mathbf{0} & \mathbf{0} & \cdots & \mathbf{I} & \mathbf{0} \end{array} \right) + \sum_{j=1}^{g} \left(\begin{array}{c|\overbrace{ccc}^{1}\overbrace{c}^{r_{j,i}-1}\overbrace{cc}^{r_{j,i}}\overbrace{ccc}^{r} } \mathbf{0} & \mathbf{0} & \cdots & \mathbf{0} & \mathbf{R}_{j,i,1} & \mathbf{R}_{j,i,0} & \mathbf{0} & \cdots & \mathbf{0} \\ \hline \mathbf{0} & \mathbf{0} & \cdots & \mathbf{0} & \mathbf{0} & \mathbf{0} & \mathbf{0} & \cdots & \mathbf{0} \\ \mathbf{0} & \mathbf{0} & \cdots & \mathbf{0} & \mathbf{0} & \mathbf{0} & \mathbf{0} & \cdots & \mathbf{0} \\ \vdots & \vdots & & \vdots & \vdots & \vdots & \vdots & & \vdots \\ \mathbf{0} & \mathbf{0} & \cdots & \mathbf{0} & \mathbf{0} & \mathbf{0} & \mathbf{0} & \cdots & \mathbf{0} \end{array} \right) . \tag{3.34}$$

Here, matrices $\mathbf{R}_{j,i,1}$ and $\mathbf{R}_{j,i,0}$ are located at the $(r_{j,i}-1)$th and $r_{j,i}$th places within the right upper block of $\mathbf{G}_i$, respectively. The approximate monodromy matrix is given by (3.18).

3.4 Rate of Convergence Estimates

In this section, rate of convergence estimates are given for the zeroth- and the first-order semi-discretization methods. A system with multiple point delays is considered in the form given by (3.1) and (3.2). The corresponding semi-discrete system is given by (3.4) and (3.6) with (3.5). In order to compare the methods of different order, local discretization errors are determined as a function of the discretization step h.

The state spaces of (3.1)–(3.2) and (3.4)–(3.6) are described by the functions $\mathbf{x}_t(\vartheta)$ and $\mathbf{y}_t(\vartheta)$, respectively, where $\vartheta \in [-\sigma, 0]$ with $\sigma = \max\left(\tau_j(s)\right)$, $j = 1, 2, \ldots, g$, $s \in [0, T]$. The local discretization error over the discretization interval $[0, h]$ is defined as

$$E_{\text{local}} = ||\mathbf{x}_t(h) - \mathbf{y}_t(h)|| \,, \tag{3.35}$$

where it is assumed that the initial conditions satisfy $\mathbf{x}_t(0) \equiv \mathbf{y}_t(0)$. Here, $||\cdot||$ denotes the supremum norm, i.e.,

$$E_{\text{local}} = \sup_{t\in[-\sigma,0]} |\mathbf{x}_t(h) - \mathbf{y}_t(h)| \ , \tag{3.36}$$

where $|\cdot|$ denotes the Euclidean norm on $\mathbb{R}^n$. Assume that $h < \sigma$ (note that this is usually the case in practical problems). Utilizing that $\mathbf{x}_t(\vartheta) = \mathbf{x}(t+\vartheta)$, $\mathbf{y}_t(\vartheta) = \mathbf{y}(t+\vartheta)$ and $\mathbf{x}_t(0) \equiv \mathbf{y}_t(0)$, one obtains

$$E_{\text{local}} = \sup_{t\in(0,h]} |\mathbf{x}(t) - \mathbf{y}(t)| \ . \tag{3.37}$$

For $0 < t \le h$, the difference $\mathbf{x}(t) - \mathbf{y}(t)$ can be expanded as

$$\begin{aligned}
\mathbf{x}(t) - \mathbf{y}(t) &= \int_0^t \mathbf{A}(s)\mathbf{x}(s) - \mathbf{A}_0\mathbf{y}(s)\,\mathrm{d}s \\
&\quad + \sum_{j=1}^{g} \int_0^t \mathbf{B}_j(s)\mathbf{u}(s-\tau_j(s)) - \mathbf{B}_{j,0}\mathbf{\Gamma}_{j,0}^{(q)}(s-\tau_{j,0})\,\mathrm{d}s \\
&= \underbrace{\int_0^t \mathbf{A}(s)\mathbf{x}(s) - \mathbf{A}_0\mathbf{x}(s)\,\mathrm{d}s}_{=:\,\mathbf{J}_0(t)} + \int_0^t \mathbf{A}_0\mathbf{x}(s) - \mathbf{A}_0\mathbf{y}(s)\,\mathrm{d}s \\
&\quad + \sum_{j=1}^{g} \Bigg(\underbrace{\int_0^t \mathbf{B}_j(s)\mathbf{u}(s-\tau_j(s)) - \mathbf{B}_{j,0}\mathbf{u}(s-\tau_j(s))\,\mathrm{d}s}_{=:\,\mathbf{J}_{j,1}(t)} \\
&\qquad + \underbrace{\int_0^t \mathbf{B}_{j,0}\mathbf{u}(s-\tau_j(s)) - \mathbf{B}_{j,0}\mathbf{u}(s-\tau_{j,0})\,\mathrm{d}s}_{=:\,\mathbf{J}_{j,2}(t)} \\
&\qquad + \underbrace{\int_0^t \mathbf{B}_{j,0}\mathbf{D}\mathbf{x}(s-\tau_{j,0}) - \mathbf{B}_{j,0}\mathbf{D}\mathbf{y}(s-\tau_{j,0})\,\mathrm{d}s}_{=:\,\mathbf{J}_{j,3}(t)} \\
&\qquad + \underbrace{\int_0^t \mathbf{B}_{j,0}\mathbf{D}\mathbf{y}(s-\tau_{j,0}) - \mathbf{B}_{j,0}\mathbf{\Gamma}_{j,0}^{(q)}(s-\tau_{j,0})\,\mathrm{d}s}_{=:\,\mathbf{J}_{j,4}(t)} \Bigg) \ .
\end{aligned} \tag{3.38}$$

A measure for the difference $\mathbf{x}(t) - \mathbf{y}(t)$ can be given as

$$E(t) = ||\mathbf{x}(t) - \mathbf{y}(t)|| \le \left|\left| \mathbf{J}_0(t) + \sum_{j=1}^{g}\sum_{k=1}^{4} \mathbf{J}_{j,k}(t) \right|\right| + \int_0^t K||\mathbf{x}(s) - \mathbf{y}(s)||\,\mathrm{d}s \ , \tag{3.39}$$

where $K = ||\mathbf{A}_0||$. Due to the Gronwall inequality, (3.39) yields

$$E(t) = ||\mathbf{x}(t) - \mathbf{y}(t)|| \le \left|\left| \mathbf{J}_0(t) + \sum_{j=1}^{g}\sum_{k=1}^{4} \mathbf{J}_{j,k}(t) \right|\right| \mathrm{e}^{Kt} \ . \tag{3.40}$$

If $h < \tau_{j,i}$, then, due to the initial assumption $\mathbf{x}_t(0) \equiv \mathbf{y}_t(0)$, the term $\mathbf{J}_{j,3}(t)$ is equal to 0. For the analysis of the other terms $\mathbf{J}_0(t)$, $\mathbf{J}_{j,1}(t)$, $\mathbf{J}_{j,2}(t)$ and $\mathbf{J}_{j,4}(t)$, $j = 1, 2, \ldots, g$, the Taylor expansion of $\mathbf{x}(t)$, $\mathbf{y}(t)$, $\mathbf{A}(t)$, $\mathbf{B}(t)$ and $\tau_j(t)$ over the interval $t \in [0, h]$ should be analyzed.

A long but straightforward calculation (see Appendix B) gives that $\mathbf{J}_0(h) = \mathcal{O}(h^3)$, $\mathbf{J}_1(h) = \mathcal{O}(h^3)$ and $\mathbf{J}_2(h) = \mathcal{O}(h^3)$ and these terms do not depend on q. The term $\mathbf{J}_4(h)$, however, do depend on q, such that

$$\begin{aligned} &\text{if} \quad q = 0 \quad \text{then} \quad \mathbf{J}_{j,4}(h) = \mathcal{O}(h^2) \; ; \\ &\text{if} \quad q = 1 \quad \text{then} \quad \mathbf{J}_{j,4}(h) = \mathcal{O}(h^3) \; . \end{aligned}$$

Using (3.40) and (3.37), the local discretization error can be given as

$$\begin{aligned} &\text{if} \quad q = 0 \quad \text{then} \quad E_{\text{local}} = E(h) = \mathcal{O}(h^2) \; , \\ &\text{if} \quad q = 1 \quad \text{then} \quad E_{\text{local}} = E(h) = \mathcal{O}(h^3) \; . \end{aligned}$$

If $q > 1$, then the order of the term $\mathbf{J}_{j,4}(h)$ increases, but the terms $\mathbf{J}_0(h)$, $\mathbf{J}_{j,1}(h)$, and $\mathbf{J}_{j,2}(h)$ remain of order 3. Consequently, $E_{\text{local}} = \mathcal{O}(h^3)$ for all $q > 1$. In order to achieve higher-order convergence for $q > 1$, the approximation of the time-periodic terms should be improved. For this purpose, a higher-order Magnus expansion should be used for the approximation of the periodic terms $\mathbf{A}(t)$, $\mathbf{B}_j(t)$, and $\tau_j(t)$ instead of the piecewise constant approximations (3.7), (3.8), (3.9) (see, e.g., [145, 116, 117, 32]). Note that approximations (3.7), (3.8), (3.9) correspond to the first-order Magnus expansion.

3.5 Application to the delayed Mathieu equation

As an application, the stability diagrams for the delayed Mathieu equation are determined using both the first- and the second-order semi-discretization method. The delayed Mathieu equation reads

$$\ddot{x}(t) + (\delta + \varepsilon \cos(\omega t))\, x(t) = b_0 x(t - \tau) \; . \tag{3.41}$$

Here, the special case will be considered, when the principal period $T = 2\pi/\omega$ and the time delay τ are equal. For this special case, the stability boundaries are known in closed form (see [101]) and can be compared to the ones obtained by the semi-discretization method.

First, the system is transformed into the form

$$\dot{\mathbf{x}}(t) = \mathbf{A}(t)\mathbf{x}(t) + \mathbf{B}\mathbf{u}(t - \tau) \; , \tag{3.42}$$

$$\mathbf{u}(t) = \mathbf{D}\mathbf{x}(t) \; , \tag{3.43}$$

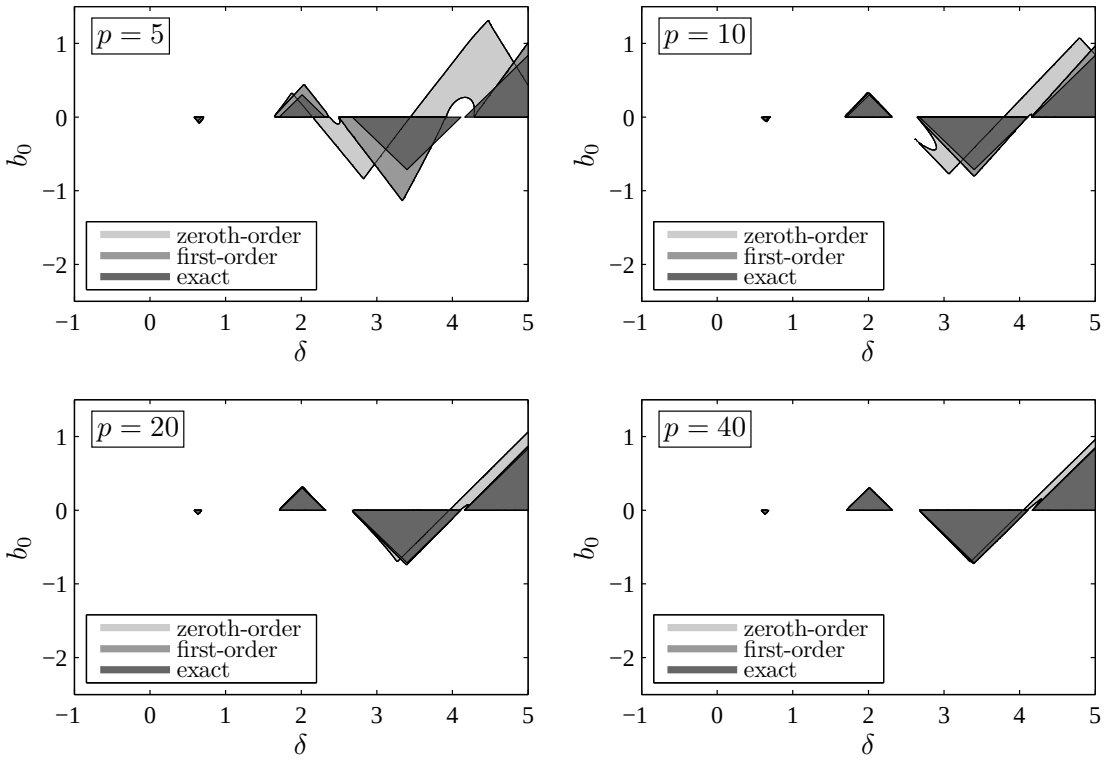

Figure 3.5: Exact and approximate stability charts for (3.41) with $\varepsilon = 2$, $\tau = T = 2\pi$ and for different period resolutions p. Stable domains are indicated by gray shading.

where

$$\mathbf{x}(t) = \begin{pmatrix} x(t) \\ \dot{x}(t) \end{pmatrix} , \qquad \mathbf{u}(t) = \begin{pmatrix} x(t) \end{pmatrix} , \tag{3.44}$$

$$\mathbf{A}(t) = \begin{pmatrix} 0 & 1 \\ -\left(\delta + \varepsilon \cos(\omega t)\right) & 0 \end{pmatrix} , \qquad \mathbf{B} = \begin{pmatrix} 0 \\ b_0 \end{pmatrix} , \qquad \mathbf{D} = \begin{pmatrix} 1 & 0 \end{pmatrix} . \tag{3.45}$$

Then, the system can be analyzed by the semi-discretization method as was shown in the previous sections.

Figure 3.5 presents the stability charts for (3.41) with $\varepsilon = 2$ and $\tau = T = 2\pi$ obtained by the zeroth-, the improved zeroth-, and the first-order semi-discretization methods with different period resolutions p. The diagrams were constructed by point-by-point numerical evaluation of the critical eigenvalues over a 400×200 grid of parameters δ and b_0. Stable domains associated with different approximation types are indicated by different shades of gray. The exact stability boundaries (see [101]) are also given for reference. The figure shows how the boundaries for the different approximations approach the exact boundaries as the period resolution p is increasing. It can be seen that the stability boundaries obtained by the first-order semi-discretization

method practically coincide with the exact boundaries already for period resolution $p = 20$. Note that in this example, the principal period T is equal to the time delay τ; consequently, the delay resolution is $r = \text{int}\,(\tau/h) = p$ for the zeroth-order method and $r = \text{int}\,(\tau/h + 1/2) = p$ for the first-order method.

3.6 New results

Thesis 1 *Higher-order versions of the semi-discretization method was developed to the stability analysis of linear periodic delay-differential equations such that the periodic coefficients and the periodic time delays are approximated by piecewise constant functions, the delayed terms are approximated by higher-order polynomials while the other terms are unchanged.*

It was shown that the rate of convergence of the approximation error over a single discretization step is proportional to the square of the discretization step for the zeroth-order approximation, and it is proportional to the cube of the discretization step for the first-order method. For any higher-order approximations, the rate of convergence is proportional to the cube of the discretization step if the periodic coefficients and the periodic time delays are approximated by piecewise constant functions.

The results composed in the thesis were published in Insperger et al. [110] and Insperger and Stépán [115] for general systems, and in Insperger [112] for an application to the computation of the stability chart of milling processes.

Chapter 4

State-dependent delay model for turning processes

One of the most important fields of engineering where time delays appear in the model equations is the theory of regenerative machine tool vibrations. The history of machine tool chatter goes back to a century, when Taylor [222] described machine tool chatter as the "most obscure and delicate of all problems facing the machinist." After the extensive work of Tobias [225, 226], Tlusty et al. [223], and Kudinov [136], the so-called regenerative effect became the most commonly accepted explanation for machine tool chatter [5, 224, 191]. This effect is related to the cutting-force variation due to the wavy workpiece surface cut one revolution ago. The phenomenon can be described by involving time delay in the model equations. Stability properties of the machining process are depicted by the so-called stability lobe diagrams, which plot the maximum stable axial depths of cut versus the spindle speed. These diagrams provide a guide to the machinist to select the optimal technological parameters in order to achieve maximum material removal rate without chatter. Although there exist many sophisticated methods to optimize manufacturing processes [93, 160, 52, 161, 138], machine tool chatter is still an existing problem in manufacturing centers [6, 182].

The basis of regenerative cutting model is that either the tool, or the workpiece or both are flexible and the chip thickness varies due the relative vibrations of the tool and the workpiece. The tool cuts the surface that was formed in the precious cut, and the chip thickness is determined by the current and a previous position of the tool/workpiece. In standard models appearing in the literature, the time delay between two succeeding cuts is considered to be constant, which is equal to the period of the workpiece rotation for turning or the tooth-passing period for milling. The corresponding mathematical model of the turning process in that case is an autonomous DDE.

Models with constant time delay capture the main character of regenerative dynamics, and can be used to describe linear stability properties in good agreement with experiments. However, some phenomena can only be explained using more sophisticated models that incorporate varying time delays. If the regeneration process is modeled accurately, then the vibrations of the tool should also be included in the regeneration model. In turning processes, the time delay is basically determined by the rotation of the workpiece but it is also affected by the current and the delayed position of the tool. This results in a DDE with state-dependent delay (SD-DDE), where the delay depends on the present state and also on a delayed state.

In this chapter, a two-degrees-of-freedom model of turning process is considered. First, it is shown that an accurate modeling of the regenerative effect results in a state-dependent delay, and the governing equation is an SD-DDE. Then, the linearized equation corresponding to the steady state motion of the tool is determined using the technique of Hartung and Turi [82]. It is shown that the associated linear equation differs from the DDE with constant delay used in the standard turning models. After that, the stability analysis of the constant-delay model and the state-dependent-delay model is performed. It is shown that the incorporation of the state-dependent delay into the model slightly affects linear stability properties of the system. The new results are composed in Thesis 2 at the end of the chapter. The results presented here were published in Insperger et al. [108].

4.1 Mechanical model

Figure 4.1 shows the chip removal process in an orthogonal turning operation for an ideally rigid tool and for a compliant tool. In the latter case, the tool experiences bending vibrations in directions x and y and leaves a wavy surface behind. The system can be modeled as a two-degrees-of-freedom oscillator excited by the cutting force, as shown in Figure 4.2. If there is no dynamic coupling between the x and y directions, then the governing equation can be given as

$$m\ddot{x}(t) + c_x\dot{x}(t) + k_x x(t) = F_x(t) \,, \tag{4.1}$$

$$m\ddot{y}(t) + c_y\dot{y}(t) + k_y y(t) = F_y(t) \,, \tag{4.2}$$

where m, c_x, c_y, k_x, and k_y are the modal mass and the damping and stiffness parameters in the x and y directions, respectively. The cutting force is given in the form

$$F_x(t) = K_x\, w\, h^q(t) \,, \tag{4.3}$$

$$F_y(t) = K_y\, w\, h^q(t) \,, \tag{4.4}$$

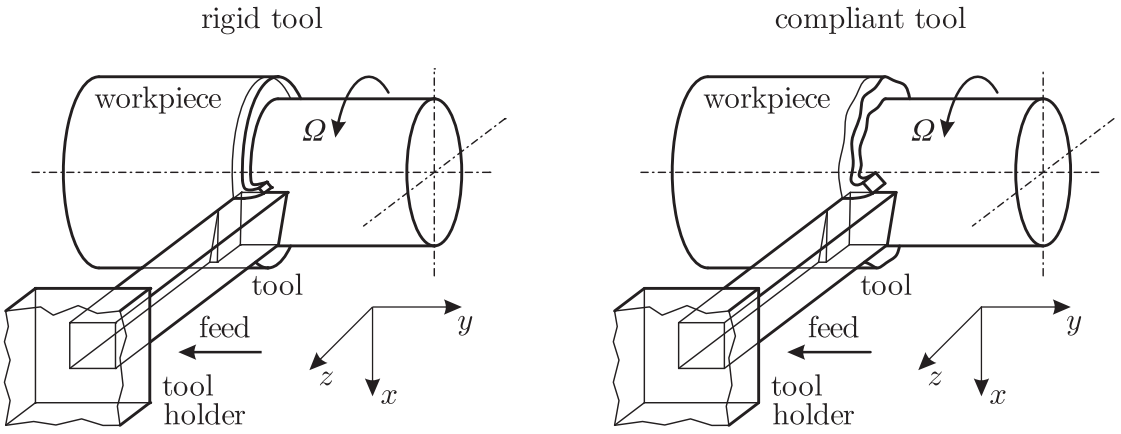

Figure 4.1: Chip removal in orthogonal turning processes in the case of an ideally rigid tool and real compliant tool.

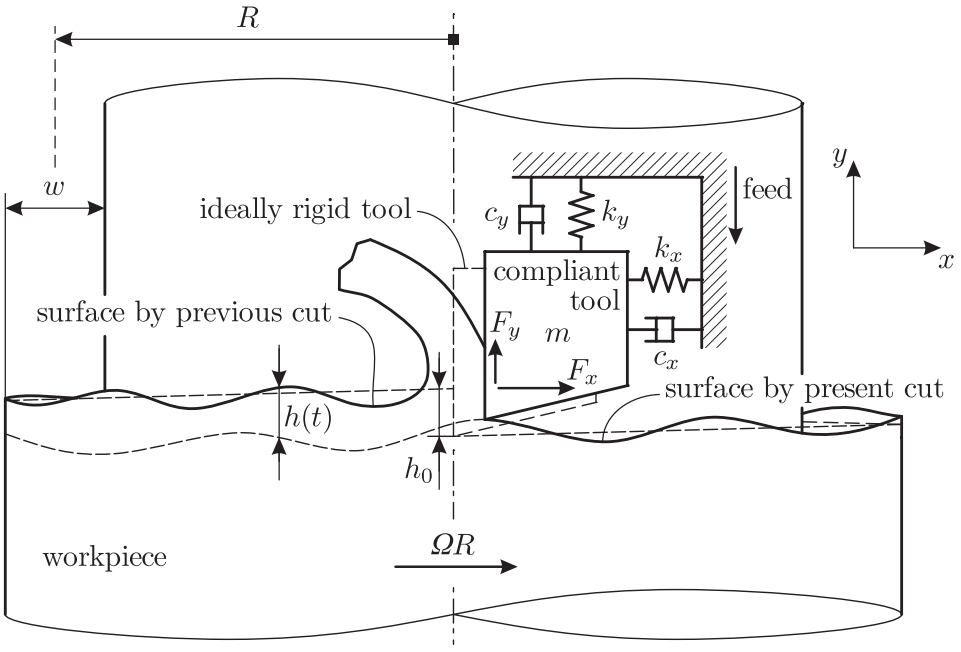

Figure 4.2: Surface regeneration in an orthogonal turning process.

where K_x and K_y are the cutting-force coefficients in the tangential (x) and the normal (y) directions, w is the depth of cut (also known as the width of cut or the chip width in cases of orthogonal cutting), $h(t)$ is the instantaneous chip thickness, and q is the cutting-force exponent. Note that other formulas for the cutting force are also used in the literature; see, e.g., [125, 198, 47]. In this model, it is assumed that the tool never leaves the workpiece, that is, $h(t) > 0$ during the cutting process.

If the tool were rigid, then the chip thickness would be constant $h(t) \equiv h_0$, which is just equal to the feed per revolution. However, in reality, the tool experiences vibrations that are recorded on the workpiece, and after one revolution, the tool cuts this wavy surface. The chip thickness h is determined by the feed motion, by the current tool position and by an earlier position of the tool. The time delay τ between the present and the previous cut is determined by the equation

$$\frac{R2\pi\Omega\tau}{60} = 2R\pi + x(t) - x(t-\tau) \,, \tag{4.5}$$

where Ω is the spindle speed given in [rpm] and R is the radius of the workpiece. Equation (4.5) is in fact an implicit equation for the time delay. It can be seen that the delay actually depends on the current state $x(t)$ and on a delayed state $x(t-\tau)$, that is, the time delay is state-dependent: $\tau(x_t)$, where $x_t(\vartheta) = x(t+\vartheta)$, $\vartheta \in [-\sigma, 0]$, with $\sigma \in \mathbb{R}^+$ describing the maximum length of the past effect.

The chip thickness can be given as the combination of the feed and the present and the delayed positions of the tool in the form

$$h(t) = v_{\mathrm{f}}\tau(x_t) + y(t-\tau(x_t)) - y(t) \,, \tag{4.6}$$

where v_{f} is the feed velocity.

Thus, the governing equation can be written as

$$m\ddot{x}(t) + c_x\dot{x}(t) + k_x x(t) = K_x w\Big(v_{\mathrm{f}}\tau(x_t) + y(t-\tau(x_t)) - y(t)\Big)^q \,, \tag{4.7}$$

$$m\ddot{y}(t) + c_y\dot{y}(t) + k_y y(t) = K_y w\Big(v_{\mathrm{f}}\tau(x_t) + y(t-\tau(x_t)) - y(t)\Big)^q \,. \tag{4.8}$$

This is a system of SD-DDEs, where the state-dependent delay $\tau(x_t)$ is given by the implicit equation (4.5).

Equations (4.7) and (4.8) can be written in the compact form

$$\dot{\mathbf{z}}(t) = \mathbf{f}(\mathbf{z}(t), \mathbf{z}(t-\tau(\mathbf{z}_t)), \tau(\mathbf{z}_t)) \,, \tag{4.9}$$

where

$$\mathbf{z} = \begin{pmatrix} x \\ y \\ \dot{x} \\ \dot{y} \end{pmatrix} \,, \qquad \mathbf{f} = \begin{pmatrix} \dot{x} \\ \dot{y} \\ -\frac{c_x}{m}\dot{x} - \frac{k_x}{m}x + \frac{K_x w}{m}\Big(v_{\mathrm{f}}\tau(x_t) + y(t-\tau(x_t)) - y(t)\Big)^q \\ -\frac{c_y}{m}\dot{y} - \frac{k_y}{m}y + \frac{K_y w}{m}\Big(v_{\mathrm{f}}\tau(x_t) + y(t-\tau(x_t)) - y(t)\Big)^q \end{pmatrix} \tag{4.10}$$

and $\mathbf{z}_t(s) = \mathbf{z}(t+s)$, $s \in [-r, 0]$, $r \in \mathbb{R}^+$. Note that $\mathbf{f}$ depends also explicitly on the delay $\tau(\mathbf{z}_t) = \tau(x_t)$.

4.2 Construction of the associated linear system

For nonlinear systems, a standard way for stability analysis consists of two steps: linearization of the nonlinear system and investigation of the characteristic exponents or characteristic multipliers of the linearized system.

In Hartung and Turi [82] (see Theorem 3.3 on page 423), under very non-restrictive conditions on the SD-DDE, it was shown that the asymptotic stability of the trivial solution of the associated linearized equation implies the asymptotic stability of a constant steady-state solution of the original equation. In particular, the linearized system associated to the constant solution $\mathbf{z}(t) \equiv \bar{\mathbf{z}}$ of SD-DDE (4.9) is given as

$$\dot{\mathbf{u}} = \mathrm{d}_1\mathbf{f}(\bar{\mathbf{z}}, \bar{\mathbf{z}}, \tau(\bar{\mathbf{z}}_t))\mathbf{u}(t) + \mathrm{d}_2\mathbf{f}(\bar{\mathbf{z}}, \bar{\mathbf{z}}, \tau(\bar{\mathbf{z}}_t))\mathbf{u}(t-\tau(\bar{\mathbf{z}})) + \mathrm{d}_3\mathbf{f}(\bar{\mathbf{z}}, \bar{\mathbf{z}}, \tau(\bar{\mathbf{z}}_t))\mathrm{d}\tau(\bar{\mathbf{z}}_t)\mathbf{u}_t \ , \quad (4.11)$$

where $\mathrm{d}_1\mathbf{f}$, $\mathrm{d}_2\mathbf{f}$, $\mathrm{d}_3\mathbf{f}$ denotes the derivatives with respect to the 1^{st}, 2^{nd} and 3^{rd} argument of $\mathbf{f}$, respectively, and $\mathrm{d}\tau$ denotes the Frechét derivative (the infinite dimensional gradient) of the time delay τ with respect to $\mathbf{z}_t$. The vector $\mathbf{u}$ reads

$$\mathbf{u} = (\xi \ \ \eta \ \ \dot{\xi} \ \ \dot{\eta})^{\mathrm{T}} \ , \quad (4.12)$$

where ξ and η denote the perturbations around the constant solution $x(t) \equiv \bar{x}$ and $y(t) \equiv \bar{y}$.

First, the constant solution

$$\bar{\mathbf{z}} = (\bar{x} \ \ \bar{y} \ \ 0 \ \ 0)^{\mathrm{T}} \quad (4.13)$$

of the SD-DDE (4.9) is determined. This solution corresponds to the stationary cutting process with a constant deflection of the tool. Substitution of $x(t) \equiv \bar{x}$ into (4.5) gives the constant delay

$$\tau(\bar{x}_t) = \bar{\tau} = \frac{60}{\Omega} + \frac{60(\bar{x} - \bar{x})}{R2\pi\Omega} = \frac{60}{\Omega} \ . \quad (4.14)$$

This constant time delay is used by the standard models of turning processes where the delay is assumed to be determined only by the workpiece rotation.

The substitution of $x(t) \equiv \bar{x}$ and $y(t) \equiv \bar{y}$ into (4.7) and (4.8) (or the substitution of $\mathbf{z}(t) \equiv \bar{\mathbf{z}}$ into (4.9)) gives the solution

$$\bar{x} = \frac{K_x w (v_{\mathrm{f}} \bar{\tau})^q}{k_x} \ , \quad (4.15)$$

$$\bar{y} = \frac{K_y w (v_{\mathrm{f}} \bar{\tau})^q}{k_y} \ . \quad (4.16)$$

This constant steady-state solution is equal to the deflection of the tool for a stationary case, when the tool does not vibrate during the cutting process, but it has a constant deflection.

Now, the terms in (4.11) are given as

$$\mathrm{d}_1\mathbf{f}(\bar{\mathbf{z}},\bar{\mathbf{z}},\tau(\bar{\mathbf{z}}_t)) = \begin{pmatrix} 0 & 0 & 1 & 0 \\ 0 & 0 & 0 & 1 \\ -\frac{k_x}{m} & -\frac{K_x w}{m} q (v_\mathrm{f}\bar{\tau})^{q-1} & -\frac{c_x}{m} & 0 \\ 0 & -\frac{k_y}{m} - \frac{K_y w}{m} q (v_\mathrm{f}\bar{\tau})^{q-1} & 0 & -\frac{c_y}{m} \end{pmatrix}, \tag{4.17}$$

$$\mathrm{d}_2\mathbf{f}(\bar{\mathbf{z}},\bar{\mathbf{z}},\tau(\bar{\mathbf{z}}_t)) = \begin{pmatrix} 0 & 0 & 0 & 0 \\ 0 & 0 & 0 & 0 \\ 0 & \frac{K_x w}{m} q (v_\mathrm{f}\bar{\tau})^{q-1} & 0 & 0 \\ 0 & \frac{K_y w}{m} q (v_\mathrm{f}\bar{\tau})^{q-1} & 0 & 0 \end{pmatrix} \tag{4.18}$$

and

$$\mathrm{d}_3\mathbf{f}(\bar{\mathbf{z}},\bar{\mathbf{z}},\tau(\bar{\mathbf{z}}_t)) = \begin{pmatrix} 0 \\ 0 \\ \frac{K_x w}{m} q (v_\mathrm{f}\bar{\tau})^{q-1} v_\mathrm{f} \\ \frac{K_y w}{m} q (v_\mathrm{f}\bar{\tau})^{q-1} v_\mathrm{f} \end{pmatrix}. \tag{4.19}$$

The term $\mathrm{d}\tau(\bar{\mathbf{z}}_t)\mathbf{u}_t$ is determined in the following way:

$$\mathrm{d}\tau(\bar{\mathbf{z}}_t)\mathbf{u}_t = \begin{pmatrix} \mathrm{d}_{x_t}\tau(\bar{\mathbf{z}}_t) \\ \mathrm{d}_{y_t}\tau(\bar{\mathbf{z}}_t) \\ \mathrm{d}_{\dot{x}_t}\tau(\bar{\mathbf{z}}_t) \\ \mathrm{d}_{\dot{y}_t}\tau(\bar{\mathbf{z}}_t) \end{pmatrix}^{\mathrm{T}} \begin{pmatrix} \xi_t \\ \eta_t \\ \dot{\xi}_t \\ \dot{\eta}_t \end{pmatrix} = \mathrm{d}_{x_t}\tau(\bar{\mathbf{z}}_t)\xi_t + \mathrm{d}_{y_t}\tau(\bar{\mathbf{z}}_t)\eta_t + \mathrm{d}_{\dot{x}_t}\tau(\bar{\mathbf{z}}_t)\dot{\xi}_t + \mathrm{d}_{\dot{y}_t}\tau(\bar{\mathbf{z}}_t)\dot{\eta}_t \,, \tag{4.20}$$

where $\mathrm{d}_{x_t}\tau$, $\mathrm{d}_{y_t}\tau$, $\mathrm{d}_{\dot{x}_t}\tau$ and $\mathrm{d}_{\dot{y}_t}\tau$ denote the Frechét derivatives of τ with respect to the 1^{st}, 2^{nd}, 3^{rd} and 4^{th} elements of vector $\mathbf{z}_t$. As it can be seen in equation (4.5), the time delay depends only on the first element x_t of vector $\mathbf{z}_t$, consequently, $\mathrm{d}_{y_t}\tau = 0$, $\mathrm{d}_{\dot{x}_t}\tau = 0$, $\mathrm{d}_{\dot{y}_t}\tau = 0$ and

$$\mathrm{d}\tau(\bar{\mathbf{z}}_t)\mathbf{u}_t = \mathrm{d}_{x_t}\tau(\bar{\mathbf{z}}_t)\xi_t \,. \tag{4.21}$$

Take the Frechét derivative of both sides of equation (4.5) with respect to x_t:

$$\frac{2\pi}{60} R\Omega \, \mathrm{d}\tau(\bar{x}_t)\xi_t = \xi(t) - \xi(t - \tau(\bar{x}_t)) \,. \tag{4.22}$$

From here, using the notation $\bar{\tau} = \tau(\bar{x}_t)$, we get

$$\mathrm{d}\tau(\bar{x}_t)\xi_t = \frac{60(\xi(t) - \xi(t-\bar{\tau}))}{2\pi R\Omega} \,. \tag{4.23}$$

Substitution of equations (4.17), (4.18), (4.19), (4.21) and (4.23) into equation (4.11) gives the linearized equation

$$\frac{\mathrm{d}}{\mathrm{d}t}\begin{pmatrix} \xi \\ \eta \\ \dot{\xi} \\ \dot{\eta} \end{pmatrix} = \begin{pmatrix} \dot{\xi} \\ \dot{\eta} \\ -\frac{k_x}{m}\xi - \frac{c_x}{m}\dot{\xi} + \frac{K_x w}{m} q (v_\mathrm{f}\bar{\tau})^{q-1} \left(\Delta\eta - \frac{60 v_\mathrm{f}}{2\pi R\Omega}\Delta\xi\right) \\ -\frac{k_x}{m}\eta - \frac{c_x}{m}\dot{\eta} + \frac{K_y w}{m} q (v_\mathrm{f}\bar{\tau})^{q-1} \left(\Delta\eta - \frac{60 v_\mathrm{f}}{2\pi R\Omega}\Delta\xi\right) \end{pmatrix}, \tag{4.24}$$

where $\Delta\eta = \eta(t-\bar{\tau}) - \eta(t)$ and $\Delta\xi = \xi(t-\bar{\tau}) - \xi(t)$.

Transformation of equation (4.24) results in the linear system of DDEs

$$m\ddot{\xi}(t) + c_x\dot{\xi}(t) + k_x\xi(t) = K_x w q (v_\mathrm{f}\bar{\tau})^{q-1}\Big((\eta(t-\bar{\tau}) - \eta(t)) - \frac{60 v_\mathrm{f}}{2\pi R\Omega}(\xi(t-\bar{\tau}) - \xi(t))\Big)\ , \quad (4.25)$$

$$m\ddot{\eta}(t) + c_y\dot{\eta}(t) + k_y\eta(t) = K_y w q (v_\mathrm{f}\bar{\tau})^{q-1}\Big((\eta(t-\bar{\tau}) - \eta(t)) - \frac{60 v_\mathrm{f}}{2\pi R\Omega}(\xi(t-\bar{\tau}) - \xi(t))\Big)\ , \quad (4.26)$$

with constant time delay $\bar{\tau} = 60/\Omega$.

It can easily be seen that if the state-dependency of the delay is not modeled, i.e., $\tau \equiv \bar{\tau}$ is used in the model, then the linearized equations of motion read

$$m\ddot{\xi}(t) + c_x\dot{\xi}(t) + k_x\xi(t) = K_x w q (v_\mathrm{f}\bar{\tau})^{q-1}(\eta(t-\bar{\tau}) - \eta(t))\ , \quad (4.27)$$

$$m\ddot{\eta}(t) + c_y\dot{\eta}(t) + k_y\eta(t) = K_y w q (v_\mathrm{f}\bar{\tau})^{q-1}(\eta(t-\bar{\tau}) - \eta(t))\ . \quad (4.28)$$

Note that equation (4.27) is an ordinary differential equation forced by η, while equation (4.28) is identical to the standard linear single-degree-of-freedom model of turning processes with constant regenerative delay. Consequently, the stability of the constant-delay model is determined only by equation (4.28).

Comparison of equations (4.25)–(4.26) and (4.27)–(4.28) shows that the only difference between the state-dependent-delay model and the standard constant-delay model is the term $-\frac{60 v_\mathrm{f}}{2\pi R\Omega}(\xi(t-\bar{\tau}) - \xi(t))$. Actually, the appearance of this additional term is related to the fact that the chip thickness and, consequently, the cutting force explicitly depend on the state-dependent time delay as it can be seen in equation (4.6) and as it was noted after equation (4.10).

4.3 Stability analysis for the constant-delay model

If the state-dependency of the delay is not modeled then the regenerative delay reads $\tau \equiv \bar{\tau} = 60/\Omega$ and the stability of the process is determined by equation (4.28). In this case, equation (4.28) can be written in the form

$$\ddot{\eta}(t) + 2\zeta\omega_\mathrm{n}\dot{\eta}(t) + \omega_\mathrm{n}^2\eta(t) = H\left(\eta(t-\bar{\tau}) - \eta(t)\right)\ , \quad (4.29)$$

where $\omega_\mathrm{n} = \sqrt{k_y/m}$ is the natural angular frequency, $\zeta = c_y/(2m\omega_\mathrm{n})$ is the damping ratio of the tool in the y direction, and $H = K_y w q (v_\mathrm{f}\bar{\tau})^{q-1}/m$ is the specific cutting-force coefficient. Note that H is linearly proportional to the depth of cut w, which is an important technological parameter for the machinist. Equation (4.29) is the simplest mathematical model that describes regenerative machine tool chatter.

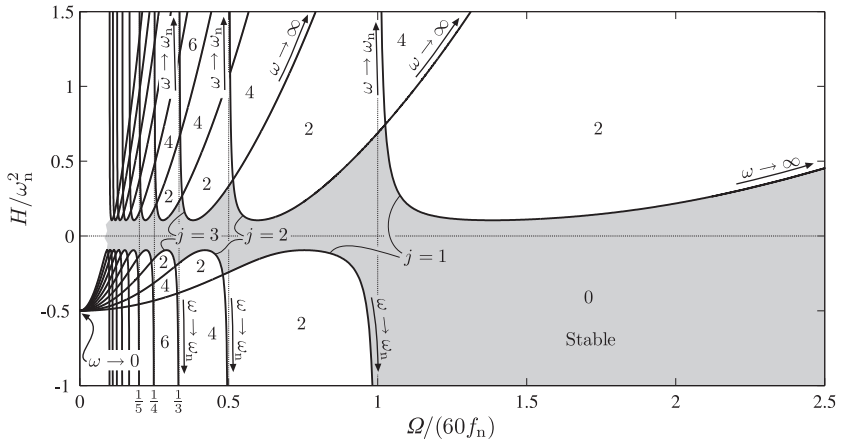

Figure 4.3: Stability chart and the number of unstable characteristic exponents for (4.29) with $\zeta = 0.05$.

The stability of the system can be determined by the D-subdivision method (see [167], [206]). The characteristic equation reads

$$\lambda^2 + 2\zeta\omega_n\lambda + \omega_n^2 + H\left(1 - \mathrm{e}^{-\lambda\bar{\tau}}\right) = 0\,. \tag{4.30}$$

Substitution of $\lambda = \pm \mathrm{i}\,\omega$ and decomposition into real and imaginary parts gives

$$\mathrm{Re}: \quad -\omega^2 + \omega_n^2 + H - H\cos(\omega\bar{\tau}) = 0\,, \tag{4.31}$$

$$\mathrm{Im}: \quad 2\zeta\omega_n\omega + H\sin(\omega\bar{\tau}) = 0\,. \tag{4.32}$$

Solving this system of equations for H and $\Omega = 60/\bar{\tau}$ gives the D-curves in the parametric form

$$\Omega = \frac{30\omega}{j\pi - \arctan\left(\dfrac{\omega^2 - \omega_n^2}{2\zeta\omega_n\omega}\right)}\,, \quad j = 1, 2, \dots\,, \tag{4.33}$$

$$H = \frac{(\omega^2 - \omega_n^2)^2 + 4\zeta^2\omega_n^2\omega^2}{2\,(\omega^2 - \omega_n^2)}\,, \tag{4.34}$$

where the parameter ω is the frequency of the arising vibrations in [rad/s].

Figure 4.3 shows the D-curves and the number of unstable characteristic exponents in the plane of the dimensionless specific cutting-force coefficient

$$\frac{H}{\omega_n^2} = \frac{\left(\left(\frac{\omega}{\omega_n}\right)^2 - 1\right)^2 + 4\zeta^2\left(\frac{\omega}{\omega_n}\right)^2}{2\left(\left(\frac{\omega}{\omega_n}\right)^2 - 1\right)} \tag{4.35}$$

and the dimensionless spindle speed $\Omega/(60f_n)$, where $f_n = \omega_n/2\pi$ is the natural frequency of the tool in [Hz]. As can be seen, (4.33) and (4.34) give a pair of D-curves

for each integer j, one in the domain $H > 0$ associated with $\omega > \omega_n$ and one in the domain $H < 0$ associated with $\omega < \omega_n$. In the literature, these D-curves are called lobes or stability lobes. The lobes of index $j = 1$ are the rightmost ones; all the other lobes with $j \geq 2$ are located at lower spindle speeds. Each pair of lobes has a vertical asymptote at $\Omega = 60 f_n/j$ indicated by dotted lines in Figure 4.3. The limits for the frequency parameter ω along the stability lobes are also presented. Frequency parameters $\omega < 0$ give D-curves in the negative spindle speed domain (not presented here). The number of unstable characteristic exponents can be determined by the analysis of the exponent-crossing direction along the D-curves (see [115]). The domain indicated by 0 in Figure 4.3 corresponds to asymptotic stability. Note that from a practical point of view, only the domains $H > 0$ are relevant, since these correspond to positive depth of cut values.

The stability boundaries in Figure 4.3 represent Hopf bifurcation, since the characteristic exponents cross the imaginary axis with a nonzero imaginary part (i.e. $\omega \neq 0$) as we cross the stability boundaries. If the state-dependency of the system is neglected, and the cutting forces are described by equations (4.3) and (4.4), then the stability boundaries represent subcritical Hopf bifurcations, as was shown by Stépán and Kalmár-Nagy [208, 120]. In case of subcritical Hopf bifurcation, an attractor (either a stable periodic or quasi-periodic orbit, or a chaotic attractor) coexists with the stable stationary cutting state that may lead to chatter even within the linear stability boundaries.

Figure 4.4 shows the practical region of the stability chart (i.e., for positive depths of cut) and the associated frequency ratio diagram, where $f = \omega/2\pi$ is the frequency of the arising self-excited vibrations at the stability boundaries in [Hz]. The stability lobes are usually characterized by their index: the lobe of index j is called the jth lobe. The minimum points of the lobes can be determined by differentiating (4.34) with respect to ω, giving

$$\frac{\mathrm{d}H}{\mathrm{d}\omega}(\omega^*) = 0 \quad \Rightarrow \quad \omega^* = \omega_n \sqrt{2\zeta + 1}\,, \quad H_{\min} = H(\omega^*) = 2\zeta\omega_n^2(1+\zeta)\,. \tag{4.36}$$

For $\zeta = 0.05$ in Figure 4.4, (4.36) gives $H_{\min}/\omega_n^2 = 2\zeta(1+\zeta) = 0.105$.

In the above model, machine tool chatter is related directly to the regenerative effect. It should be mentioned, however, that other types of self-excited vibrations may also occur in machining operations. For instance, the chip formation itself can produce oscillations in the cutting force for certain cutting speeds, as was shown by Burns and Davies [28, 29] and by Csernák and Pálmai [41, 178] for different models.

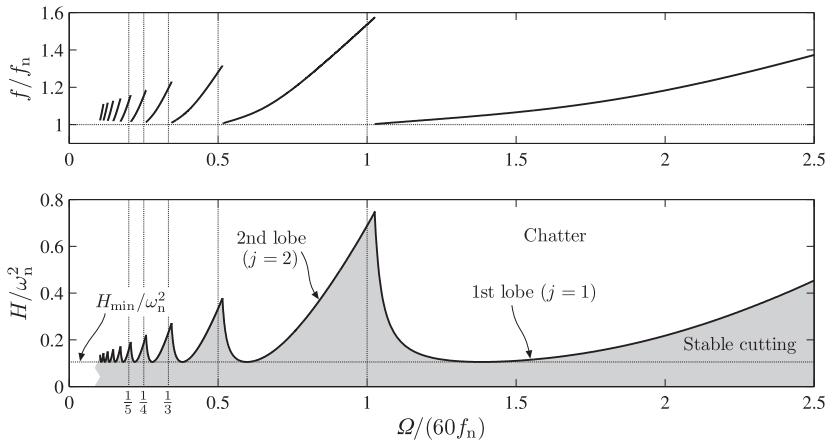

Figure 4.4: Stability lobe diagram and frequency diagram for (4.29) with $\zeta = 0.05$.

4.4 Stability analysis for the state-dependent-delay model

In the following investigations, it is assumed that the tool is symmetric: $c_x = c_y = c$, $k_x = k_y = k$. The corresponding natural angular frequency is $\omega_n = \sqrt{k/m}$ and the damping ratio is $\zeta = c/(2m\omega_n)$. The equations of motion (4.25) and (4.26) can be written in the form

$$\ddot{\xi}(t) + 2\zeta\omega_n\dot{\xi}(t) + \omega_n^2\xi(t) = \frac{1}{r_c}H^*\rho^{q-1}\Big(\eta(t-\bar{\tau}) - \eta(t)\Big) - \frac{1}{r_c}H^*\rho^q\Big(\xi(t-\bar{\tau}) - \xi(t)\Big)\,, \tag{4.37}$$

$$\ddot{\eta}(t) + 2\zeta\omega_n\dot{\eta}(t) + \omega_n^2\eta(t) = H^*\rho^{q-1}\Big(\eta(t-\bar{\tau}) - \eta(t)\Big) - H^*\rho^q\Big(\xi(t-\bar{\tau}) - \xi(t)\Big)\,, \tag{4.38}$$

where $r_c = K_y/K_x$ is the cutting force ratio, $\rho = 60v_f/(2\pi R\Omega)$ is the dimensionless feed per revolution. Here, $H^* = (K_y w q(2\pi R)^{q-1})/m$ is used as a dimensionless depth of cut (or chip width) instead of H defined in equation (4.29) for the constant-speed turning. Note that $H = H^*\rho^{q-1}$. The reason for using H^* instead of H is that while H depends on the feed velocity v_f, H^* is independent of v_f. This feature will be useful in later comparisons. Note that the dimensionless feed can be given as $\rho = f_z/(2\pi R)$, where $f_z = v_f\bar{\tau}$ is the feed per revolution and $2\pi R$ is the circumference of the workpiece. Since typically $f_z \ll 2\pi R$, practically, $\rho \ll 1$.

Stability analysis of the linear autonomous system of DDEs (4.37)–(4.38) is performed following the developments in Stépán [206]. First, the characteristic equation is determined, then the stability boundaries in the parameter plane $(\Omega/(60f_n), H^*)$ are given, where $\Omega/(60f_n)$ is the dimensionless spindle speed.

Equation (4.37) and (4.38) can be written in the form

$$\underbrace{\begin{pmatrix}1 & 0\\ 0 & 1\end{pmatrix}}_{:=\mathbf{A}_1}\begin{pmatrix}\ddot{\xi}(t)\\ \ddot{\eta}(t)\end{pmatrix}+\underbrace{\begin{pmatrix}2\zeta\omega_\mathrm{n} & 0\\ 0 & 2\zeta\omega_\mathrm{n}\end{pmatrix}}_{:=\mathbf{A}_2}\begin{pmatrix}\dot{\xi}(t)\\ \dot{\eta}(t)\end{pmatrix}+\underbrace{\begin{pmatrix}\omega_\mathrm{n}^2-\frac{1}{r_\mathrm{c}}H^*\rho^q & \frac{1}{r_\mathrm{c}}H^*\rho^{q-1}\\ -H^*\rho^q & \omega_\mathrm{n}^2+H^*\rho^{q-1}\end{pmatrix}}_{:=\mathbf{A}_3}\begin{pmatrix}\xi(t)\\ \eta(t)\end{pmatrix}$$
$$+\underbrace{\begin{pmatrix}\frac{1}{r_\mathrm{c}}H^*\rho^q & -\frac{1}{r_\mathrm{c}}H^*\rho^{q-1}\\ H^*\rho^q & -H^*\rho^{q-1}\end{pmatrix}}_{:=\mathbf{A}_4}\begin{pmatrix}\xi(t-\bar{\tau})\\ \eta(t-\bar{\tau})\end{pmatrix}=\begin{pmatrix}0\\ 0\end{pmatrix}\ . \quad (4.39)$$

According to the D-subdivision method, the characteristic equation is given by the determinant

$$\det\left(\mathbf{A}_1\lambda^2+\mathbf{A}_2\lambda+\mathbf{A}_3+\mathbf{A}_4\,\mathrm{e}^{-\lambda\bar{\tau}}\right)=0\ , \quad (4.40)$$

which gives

$$\det\begin{pmatrix}\lambda^2+2\zeta\omega_\mathrm{n}\lambda+\omega_\mathrm{n}^2-\frac{1}{r_\mathrm{c}}H^*\rho^q(1-\,\mathrm{e}^{-\lambda\bar{\tau}}) & \frac{1}{r_\mathrm{c}}H^*\rho^{q-1}(1-\,\mathrm{e}^{-\lambda\bar{\tau}})\\ -H^*\rho^q(1-\,\mathrm{e}^{-\lambda\bar{\tau}}) & \lambda^2+2\zeta\omega_\mathrm{n}\lambda+\omega_\mathrm{n}^2+H^*\rho^{q-1}(1-\,\mathrm{e}^{-\lambda\bar{\tau}})\end{pmatrix}=0\ . \quad (4.41)$$

Expanding the determinant gives the characteristic equation in the form

$$\left(\lambda^2+2\zeta\omega_\mathrm{n}\lambda+\omega_\mathrm{n}^2\right)\left(\lambda^2+2\zeta\omega_\mathrm{n}\lambda+\omega_\mathrm{n}^2+H^*\rho^{q-1}\left(1-\frac{\rho}{r_\mathrm{c}}\right)\left(1-\,\mathrm{e}^{-\lambda\bar{\tau}}\right)\right)=0\ . \quad (4.42)$$

There are two roots with negative real parts determined by $\lambda^2+2\zeta\omega_\mathrm{n}\lambda+\omega_\mathrm{n}^2=0$, and the remaining roots are determined by the transcendental equation

$$\lambda^2+2\zeta\omega_\mathrm{n}\lambda+\omega_\mathrm{n}^2+H^*\rho^{q-1}\left(1-\frac{\rho}{r_\mathrm{c}}\right)\left(1-\,\mathrm{e}^{-\lambda\bar{\tau}}\right)=0\ . \quad (4.43)$$

This equation is very similar to (4.30), the only difference is the appearance of the multiplicative term $(1-\rho/r_\mathrm{c})$. (Note that H^* was introduced such that $H=H^*\rho^{q-1}$.) Substitution of $\lambda=\pm\mathrm{i}\,\omega$ and decomposition into real and imaginary parts gives

$$\Omega=\frac{30\omega}{j\pi-\arctan\left(\dfrac{\omega^2-\omega_\mathrm{n}^2}{2\zeta\omega_\mathrm{n}\omega}\right)}\ , \quad j=1,2,\ldots\ , \quad (4.44)$$

$$H^*_\mathrm{SDD}=\frac{r_\mathrm{c}}{r_\mathrm{c}-\rho}\,\rho^{1-q}\,\frac{\left(\omega^2-\omega_\mathrm{n}^2\right)^2+4\zeta^2\omega_\mathrm{n}^2\omega^2}{2\left(\omega^2-\omega_\mathrm{n}^2\right)}\ , \quad (4.45)$$

where the parameter ω is the angular frequency of the arising vibrations in [rad/s] and the subscript SDD refers to state-dependent delay.

The stability boundaries corresponding to the model with constant delay is determined by

$$H^*_\mathrm{CD}=\rho^{1-q}\,\frac{\left(\omega^2-\omega_\mathrm{n}^2\right)^2+4\zeta^2\omega_\mathrm{n}^2\omega^2}{2\left(\omega^2-\omega_\mathrm{n}^2\right)}\ , \quad (4.46)$$

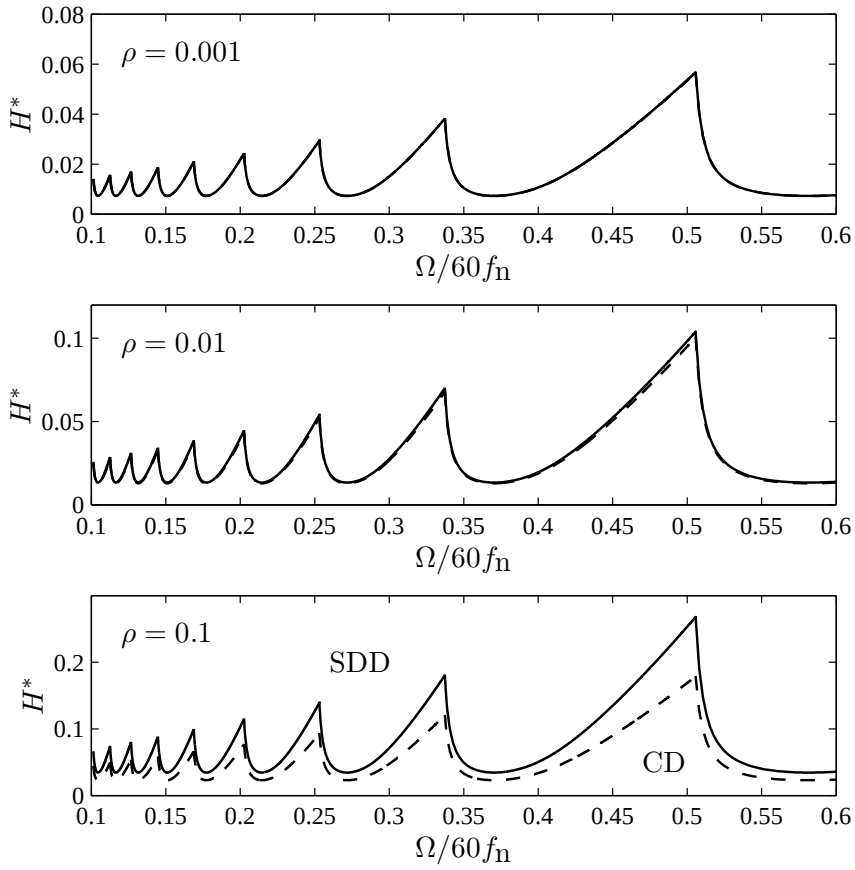

Figure 4.5: Stability charts for different dimensionless feeds ρ per revolution. Continuous and dashed lines correspond to state-dependent-delay and constant-delay models, respectively. The parameters are $\zeta = 0.02$, $q = 0.75$ and $r_\mathrm{c} = 0.3$.

while the expression for Ω is identical to equation (4.44). Here, the subscript CD refers to constant delay.

It can be seen that if the state dependency of the time delay is included into the model, then the resulting stability boundaries are shifted upwards by the ratio

$$\frac{H^*_\mathrm{SDD}}{H^*_\mathrm{CD}} = \frac{r_\mathrm{c}}{r_\mathrm{c} - \rho} \,. \tag{4.47}$$

Practically, this ratio is close to 1, since $\rho \ll 1$ as it was noted after equation (4.38), and a typical value of the cutting force ratio is $r_\mathrm{c} = 0.3$. This shows that the state-dependency of the time delay is important if ρ is large, i.e, large feed is applied for a workpiece with small diameter.

Figure 4.5 shows the stability diagrams in the space of the dimensionless spindle speed $\Omega/(60f_\mathrm{n})$ and the dimensionless specific cutting-force coefficient H^*/ω_n^2. Here, again, $f_\mathrm{n} = \omega_\mathrm{n}/2\pi$ is the natural frequency of the tool in [Hz]. The stability lobes

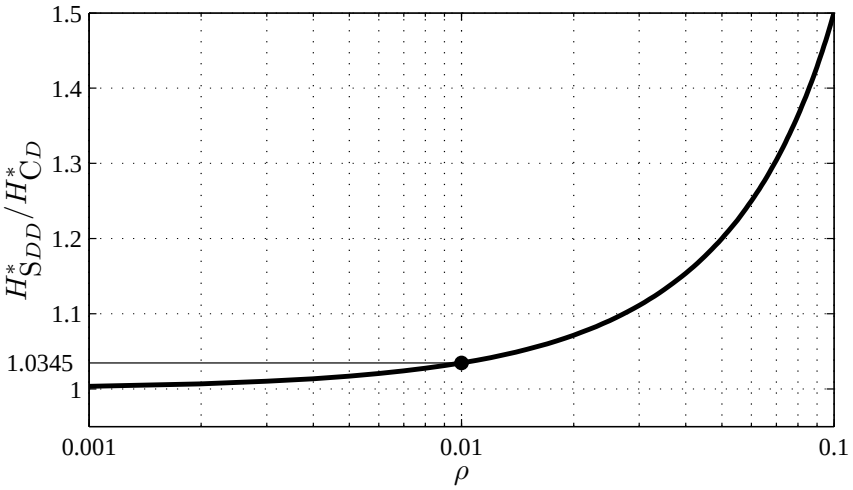

Figure 4.6: Ratio of the critical depths of cut for state-dependent-delay and constant-delay models as the function of the dimensionless feed ρ per revolution ($r_c = 0.3$).

are presented for different dimensionless feeds ρ per revolution both for the state-dependent-delay and for the constant-delay models. It can be seen that stability boundaries are higher for the state-dependent-delay model than those of the constant-delay model. This can also be seen from equation (4.47), since $H^*_{\mathrm{SDD}}/H^*_{\mathrm{CD}} > 1$ for positive r_c and ρ. The difference between the two models increases with increasing ρ.

In Figure 4.6, the ratio $H^*_{\mathrm{SDD}}/H^*_{\mathrm{CD}}$ is shown as a function of ρ. The case $\rho = 0.01$ can be considered as a limit case in practice for turning: when a 6.4 mm diameter workpiece is cut with 0.2 mm feed per revolution, the stability boundary is shifted upwards by 3.45% relative to the constant delay model.

In this chapter, only the linear behavior of the turning process was analyzed, but it should be mentioned that the state-dependency of the regenerative delay also affects the nonlinear behavior of the system. While the constant-delay model is associated with subcritical Hopf bifurcation, the state-dependent-delay model is associated with supercritical Hopf bifurcation for large feed rates (see Insperger et al. [109]). In the case of supercritical Hopf bifurcation, stable periodic orbits coexist with the linearly unstable stationary cutting state, and no attractors coexist with the stable stationary cutting state. This means that the system cannot experience chatter within the linear stability boundaries (as opposed to the subcritical Hopf bifurcation). From practical point of view, the supercritical Hopf bifurcation is more favorable than the subcritical one.

4.5 New results

Thesis 2 *The equations of motion for a two-degrees-of-freedom model of orthogonal turning process were analyzed. It was shown that if the relative vibrations between the tool and the workpiece are included into the model then the governing equation is a delay-differential equation with state-dependent delay.*

The linear equation corresponding to the stationary cutting with constant deflection of the tool was derived. It was shown that the resulting linearized equation is different from the delay-differential equation with constant time delay used in standard turning models: an additional term arises due to the explicit dependence of the cutting force on the state-dependent delay.

The stability chart for the state-dependent-delay model was determined in the plane of the spindle speed and the depth of cut. It was shown that the stability boundaries for the state-dependent-delay model are located slightly higher than those of the constant-delay model.

The results composed in the thesis were published in Insperger et al. [108].

Chapter 5

Milling processes with varying spindle speed

As it was mentioned in Chapter 4, machine tool chatter is one of the most important problems in machining operations. One technique to suppress machine tool chatter is the application of varying spindle speeds. The main idea behind this technique is that spindle speed variation disturbs the regenerative effect, which may reduce the self-excited vibrations for certain spindle speeds. The idea of suppressing chatter by spindle speed variation came up first in the 1970s, when a great deal of effort was focused in this area [96, 221, 196].

For turning processes with varying spindle speed, the governing equation is a DDE with time-varying delay. The variation of the spindle speed is typically periodic in time, consequently, the governing equation for turning processes is a periodic DDE. There are several approaches to determining the stability properties of these processes. Sexton et al. [196] approximated the quasiperiodic solutions of the system by periodic ones and applied the harmonic balance method to derive stability boundaries. Pakdemirli and Ulsoy [175] used angle coordinate as an independent variable instead of time, following Tsao et al. [227], and obtained a DDE with constant time delay and with periodic coefficients. They used the perturbation technique called the method of strained parameters for stability analysis. Jayaram et al. [118] used quasiperiodic trial solutions for the system, combined the Fourier expansion with an expansion with respect to Bessel functions, and determined stability boundaries by the harmonic balance method. Namachchivaya and Beddini [165] transformed the time dependency from the delay term to the coefficients, and also carried out some nonlinear analysis using the small-perturbations technique. The full-discretization technique was used by Sastry et al. [188] and by Wu et al. [237] for sinusoidal speed modulation and by Yilmaz et al. [240] for random spindle speed modulation. The semi-discretization method was ap-

plied to the problem by Insperger and Stépán [103] and by Insperger [99] for sinusoidal and for piecewise linear (sawtooth-like) spindle speed modulations.

Regenerative machine tool chatter is a challenging problem for milling operations, too. In the case of milling, surface regeneration is coupled with parametric excitation of the cutting teeth, resulting in a DDE with time-periodic coefficients. The first results regarding the stability properties of milling processes appeared in Tobias's and Tlusty's works [225, 226, 223]. They considered the time-averaged cutting force instead of the time-periodic one, and thus their models were equivalent to a DDE with constant coefficients. These models can be used for processes with large radial immersion and large number of cutting teeth when the parametric excitation of the teeth is negligible. For small radial immersion, however, the intermittent nature of the cutting process cannot be neglected. Minis and Yanushevsky [156] applied a Fourier expansion and Hill's infinite determinant technique in the frequency domain to derive stability charts for a two-degrees-of-freedom milling model. Budak and Altintas [4, 26, 27] used a similar approach for a multiple-degrees-of-freedom milling model. Their methods are often referred to as single-frequency (or zero-order) solution and multi-frequency solution, depending on the number of harmonics taken into account during the Fourier expansion. All these publications dealt with milling operations with large radial depth of cut and multiple cutting teeth such that the time-periodicity of the cutting force was not significant. In these models, the loss of stability is represented by a Hopf bifurcation similar to that of turning processes, i.e., a complex conjugate pair of characteristic exponents crosses the imaginary axis from left to right.

In the last decade, extended investigation of the high-speed milling process and the corresponding time-periodic DDE has led to the realization of a new bifurcation phenomenon. In addition to the stability lobes associated with Hopf bifurcation, new stability boundaries may appear representing a period-doubling (flip) bifurcation. Davies et al. [42, 43] modeled small radial immersion milling as an impact-like cutting process and obtained analytical formulas for the flip stability boundaries. Insperger and Stépán [97, 98] investigated a single-degree-of-freedom model of the milling process and demonstrated the appearance of flip stability lobes. They approximated the point delay in the model equations by a distributed delay with kernel function the gamma function. Zhao and Balachandran [242] determined stability charts by numerical simulations and showed period-doubling behavior at the stability boundaries. These results were confirmed by several other techniques: Bayly et al. [17] used the temporal finite element method; Merdol and Altintas [150] used the multi-frequency solution; Szalai and Stépán [218] determined the characteristic functions of the system and obtained stability criteria using the argument principle; Corpus and Endres [38] reduced the problem to the flip boundaries where time-periodic ODEs describe the system instead

of time-periodic DDEs; Butcher et al. [31] used an expansion of the solution in terms of Chebyshev polynomials. The semi-discretization method itself was developed in order to derive stability diagrams for the milling process [100, 102]. The existence of the period-doubling phenomenon was also confirmed by experiments in [42, 43, 17, 39, 70].

Varying spindle speeds are also applied in milling operations in order to avoid chatter and thus to increase productivity. The idea behind is the same as for turning processes: the regenerative effect is disturbed since each flute experiences a different regenerative delay.

Mathematical models for milling processes with spindle speed variation are more complex than those of turning operations, since the speed-variation frequency and tooth-passing frequency interact and the resulting system is typically quasiperiodic. However, if the ratio of the mean period of the spindle speed and the speed modulation period is a rational number, then the system is purely time-periodic, and the Floquet theory can be applied to determine stability properties. Sastry et al. [189] used Fourier expansion and applied the Floquet theory to derive stability lobe diagrams for face milling. They obtained some improvements for low spindle speeds. Zatarain et al. [241] presented a general method in the frequency domain for the problem, and showed that variable spindle speed can effectively be used for chatter suppression for low cutting speeds. They validated their model using the semi-discretization method and time-domain simulations, and confirmed their results also by experiments. Seguy et al. [193, 194] used the semi-discretization method to analyze the stability properties around the first flip lobe.

In this chapter a single-degree-of-freedom model of milling process with varying spindle speed is analyzed. First the governing equations are derived considering the time-varying regenerative delay. Then, the stability analysis is performed for the constant-speed model and the differences compared to the stability charts of turning process are highlighted. After that, the stability charts for the varying-spindle-speed case are presented and compared to that of constant-speed milling. Finally, experimental verification of suppressing period doubling chatter by spindle speed variation is presented based on the joint papers Seguy et al. [193, 194] made in collaboration with French partners. The new results, composed in Thesis 3 at the end of the chapter, are related to the mechanical model and the computation of the stability charts. These results were published in Insperger and Stépán [115]. The experimental verification is not included into the thesis, since all the experiments were performed by French partners, namely, by Sebastien Seguy (École Nationale d'Ingénieurs de Tarbes, France) who made his PhD about milling processes with varying spindle speed in 2008 [192]. The results of the experiments are presented here for the sake of completeness.

5.1 Mechanical model

A single-degree-of-freedom model of end milling is shown in Figure 5.1. The workpiece is assumed to be flexible in the feed direction (direction x) with modal mass m, damping coefficient c, and spring stiffness k, while the tool is assumed to be rigid. The tool has N equally distributed cutting teeth with zero helix angles. The spindle speed is modulated periodically in the form

$$\Omega(t) = \Omega_0 + \Omega_1 S(t) \,, \qquad S(t+T) = S(t) \,, \tag{5.1}$$

where Ω_0 is the mean value, Ω_1 is the amplitude, and the time-periodic bounded function $S : \mathbb{R} \to [-1, 1]$ presents the shape of the variation. It is assumed that $\Omega(t+T) = \Omega(t) > 0$.

According to Newton's law, the equation of motion reads

$$m\ddot{x}(t) + c\dot{x}(t) + kx(t) = -F_x(t) \,, \tag{5.2}$$

where $F_x(t)$ is the x component of the cutting force vector acting on the tool. Let the teeth of the tool be indexed by $j = 1, 2, \ldots, N$. The geometry of the milling process and the cutting forces are shown in Figure 5.2. The tangential and radial components of the cutting force acting on tooth j read

$$F_{j,\mathrm{t}}(t) = g_j(t) K_\mathrm{t} a_\mathrm{p} h_j^q(t) \,, \tag{5.3}$$

$$F_{j,\mathrm{r}}(t) = g_j(t) K_\mathrm{r} a_\mathrm{p} h_j^q(t) \,, \tag{5.4}$$

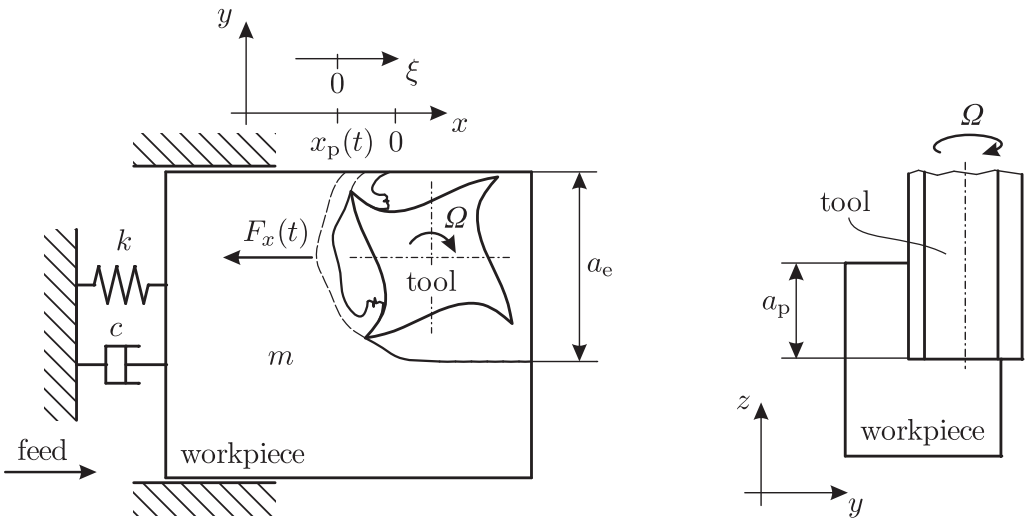

Figure 5.1: Single-degree-of-freedom mechanical model of end milling process with a straight fluted tool.

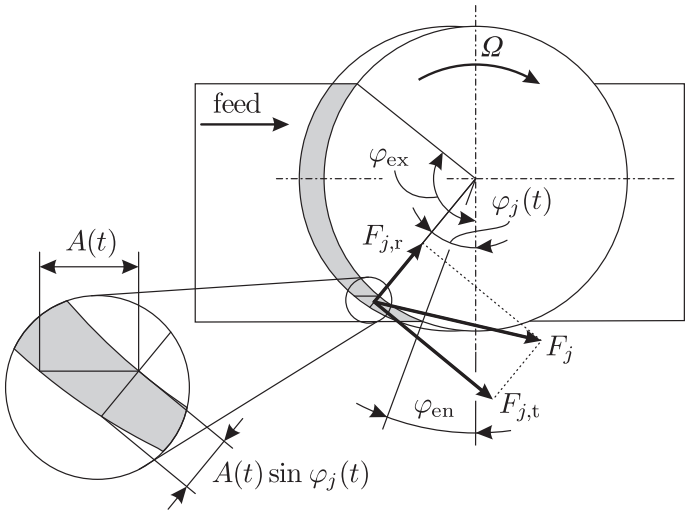

Figure 5.2: Cutting-force components and chip thickness model in the milling process.

where K_t and K_r are the tangential and radial cutting-force coefficients, respectively, a_p is the axial depth of cut, $h_j(t)$ is the chip thickness cut by tooth j, and q is the cutting-force exponent. Function $g_j(t)$ is a screen function; it is equal to 1 if tooth j is in the cut, and 0 if it is not. If φ_en and φ_ex denote the angular locations where the cutting teeth enter and exit the cut, then the screen function reads

$$g_j(t) = \begin{cases} 1 & \text{if } \varphi_\mathrm{en} < (\varphi_j(t) \bmod 2\pi) < \varphi_\mathrm{ex} \,, \\ 0 & \text{otherwise,} \end{cases} \tag{5.5}$$

where

$$\varphi_j(t) = \int_0^t \frac{2\pi\,\Omega(s)}{60}\mathrm{d}s + j\,\frac{2\pi}{N} \tag{5.6}$$

is the angular position of tooth j and mod is the modulo function. In the case of up-milling,

$$\varphi_\mathrm{en} = 0 \,, \qquad \varphi_\mathrm{ex} = \arccos\left(1 - \frac{2a_\mathrm{e}}{D}\right) \,, \tag{5.7}$$

while in the case of down-milling,

$$\varphi_\mathrm{en} = \arccos\left(\frac{2a_\mathrm{e}}{D} - 1\right) \,, \qquad \varphi_\mathrm{ex} = \pi \,, \tag{5.8}$$

where a_e is the radial immersion and D is the diameter of the tool (see Figure 5.3).

Although a constant feed velocity v_f is prescribed, the actual feed $A(t)$ per tooth is not constant, since it is affected by the spindle speed variation and by the present and a delayed position of the workpiece in the form

$$A(t) = v_\mathrm{f}\tau(t) + x(t) - x(t - \tau(t)) \,, \tag{5.9}$$

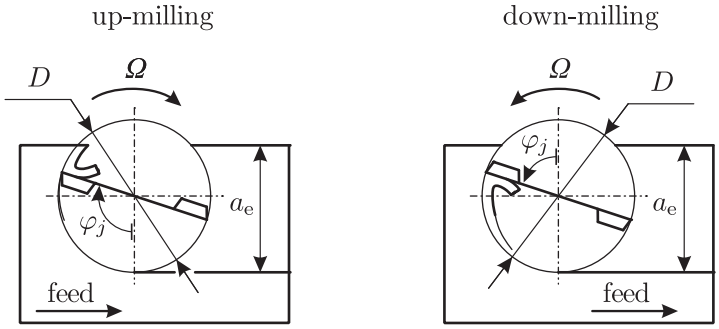

Figure 5.3: Sketch of up-milling and down-milling operations.

where $\tau(t)$ [s] is the tooth-passing period, which coincides with the regenerative delay. The variation of the regenerative delay $\tau(t)$ can approximately be given in the implicit form

$$\int_{t-\tau(t)}^{t} \frac{\Omega(s)}{60}\,\mathrm{d}s = \frac{1}{N}\,. \tag{5.10}$$

In general, the time delay $\tau(t)$ cannot be expressed in closed form, however, if Ω_1 is small enough compared to Ω_0, then it can be approximated by

$$\tau(t) \approx \tau_0 - \tau_1 S(t) \tag{5.11}$$

with $\tau_0 = 60/(N\Omega_0)$ and $\tau_1/\tau_0 = \Omega_1/\Omega_0$.

The instantaneous chip thickness $h_j(t)$ is determined by the actual feed per tooth and the angular position of the cutting teeth. A circular approximation of the tooth path gives

$$h_j(t) = A(t)\sin\varphi_j(t) = (v_\mathrm{f}\tau(t) + x(t) - x(t-\tau(t)))\sin\varphi_j(t)\,. \tag{5.12}$$

Note that there exist more complex models for the chip thickness calculation, such as the trochoidal tooth path model, which results in time-dependent delays [59, 144] and models including the vibrations of the tool–workpiece system that results in state-dependent delays in the model equations [105, 14].

The x component of the cutting force acting on tooth j is obtained as the projection of $F_{j,\mathrm{t}}$ and $F_{j,\mathrm{r}}$ in the x direction, i.e.,

$$F_{j,x}(t) = F_{j,\mathrm{t}}(t)\cos\varphi_j(t) + F_{j,\mathrm{r}}(t)\sin\varphi_j(t)\,. \tag{5.13}$$

The x component of the resultant cutting force acting on the tool reads

$$F_x(t) = Q(t)\,(v_\mathrm{f}\tau(t) + x(t) - x(t-\tau(t)))^q\ , \tag{5.14}$$

where

$$Q(t) = \sum_{j=1}^{N} a_{\mathrm{p}} g_j(t) \sin^q \varphi_j(t) \left(K_{\mathrm{t}} \cos\varphi_j(t) + K_{\mathrm{r}} \sin\varphi_j(t)\right) \ . \tag{5.15}$$

Thus, the equation of motion is the following nonlinear DDE:

$$m\ddot{x}(t) + c\dot{x}(t) + kx(t) = -Q(t) \left(v_{\mathrm{f}}\tau(t) + x(t) - x(t-\tau(t))\right)^q \ . \tag{5.16}$$

We assume that the ratio of the modulation period T and the mean time delay $\tau_0 = 60/(N\Omega_0)$ is a rational number, i.e., $q_1 T = q_2 \tau_0$ with q_1 and q_2 being relatively prime. In this case, equation (5.16) is a periodic DDE with principal period $q_1 T$. If the ratio T/τ_0 is not rational, then the system is quasiperiodic.

It is assumed that there is a periodic steady-state solution $x_{\mathrm{p}}(t) = x_{\mathrm{p}}(t + q_1 T)$ that satisfies (5.16). The general solution can be written as

$$x(t) = x_{\mathrm{p}}(t) + \xi(t) \ , \tag{5.17}$$

where $\xi(t)$ is the perturbation around $x_{\mathrm{p}}(t)$. Substitution of (5.17) into (5.16) yields

$$\begin{aligned} &m\ddot{x}_{\mathrm{p}}p(t) + c\dot{x}_{\mathrm{p}}(t) + kx_{\mathrm{p}}(t) + m\ddot{\xi}(t) + c\dot{\xi}(t) + k\xi(t) \\ &\qquad = -Q(t) \left(v_{\mathrm{f}}\tau(t) + x_{\mathrm{p}}(t) + \xi(t) - x_{\mathrm{p}}(t-\tau) - \xi(t-\tau)\right)^q \ . \end{aligned} \tag{5.18}$$

Taylor expansion with respect to ξ and neglecting the higher-order terms gives the variational system in the form

$$m\ddot{\xi}(t) + c\dot{\xi}(t) + k\xi(t) = -q(v_{\mathrm{f}}\tau(t) + x_{\mathrm{p}}(t) - x_{\mathrm{p}}(t-\tau))^{q-1} Q(t) \left(\xi(t) - \xi(t-\tau)\right) \ . \tag{5.19}$$

Now, we assume that the tool experiences only small forced oscillations such that the term $x_{\mathrm{p}}(t)$ can be neglected compared to the term $v_{\mathrm{f}}\tau(t)$. Utilizing this assumption, the stability of the system is determined by the equation

$$m\ddot{\xi}(t) + c\dot{\xi}(t) + k\xi(t) = -q(v_{\mathrm{f}}\tau(t))^{q-1} Q(t) \left(\xi(t) - \xi(t-\tau)\right) \ . \tag{5.20}$$

Introducing the natural angular frequency $\omega_{\mathrm{n}} = \sqrt{k/m}$ and the damping ratio $\zeta = c/(2m\omega_{\mathrm{n}})$, equation (5.20) can be written in the form

$$\ddot{\xi}(t) + 2\zeta\omega_{\mathrm{n}}\dot{\xi}(t) + \omega_{\mathrm{n}}^2 \xi(t) = -\tilde{G}(t) \left(\xi(t) - \xi(t-\tau(t))\right) \ , \tag{5.21}$$

where

$$\tilde{G}(t) = a_{\mathrm{p}} \frac{q(v_{\mathrm{f}}\tau(t))^{q-1}}{m} \sum_{j=1}^{N} g_j(t) \sin^q \varphi_j(t) \left(K_{\mathrm{t}} \cos\varphi_j(t) + K_{\mathrm{r}} \sin\varphi_j(t)\right) \tag{5.22}$$

is the specific directional dynamic cutting-force coefficient, or simply the specific directional factor. Since $q_1 T = q_2 \tau_0$ with q_1 and q_2 being relatively prime, the specific

directional factor $\tilde{G}(t)$ is periodic with period $q_1 T$. Consequently, equation (5.21) is a linear periodic DDE with principal period $q_1 T$, for which the Floquet theory of DDEs applies. Note that if the ratio T/τ_0 is not rational, then the system is quasiperiodic and the Floquet theory does not apply. The system is written in the first-order form

$$\dot{\mathbf{x}}(t) = \mathbf{A}(t)\mathbf{x}(t) + \mathbf{B}(t)\mathbf{u}(t-\tau(t)) \,, \tag{5.23}$$

$$\mathbf{u}(t) = \mathbf{D}\mathbf{x}(t) \,, \tag{5.24}$$

with

$$\mathbf{x}(t) = \begin{pmatrix} \xi(t) \\ \dot{\xi}(t) \end{pmatrix} \,, \qquad \mathbf{D} = \begin{pmatrix} 1 & 0 \end{pmatrix} \,, \tag{5.25}$$

$$\mathbf{A}(t) = \begin{pmatrix} 0 & 1 \\ -\left(\omega_{\mathrm{n}}^2 + \tilde{G}(t)\right) & -2\zeta\omega_{\mathrm{n}} \end{pmatrix} \,, \qquad \mathbf{B}(t) = \begin{pmatrix} 0 \\ \tilde{G}(t) \end{pmatrix} \,. \tag{5.26}$$

This system is a special case of system (3.1)-(3.2) with a single delay. The stability properties can be determined by the semi-discretization method, as shown in Chapter 3.

5.2 Stability charts for constant spindle speed

In order to give some insight into the structure of stability charts for milling processes, first, the constant-spindle-speed case is considered when $\Omega_1 = 0$ and $\Omega(t) = \Omega_0$. In this case, the tooth passing period (i.e., the regenerative time delay) is constant and can be given in the form $\tau(t) \equiv \tau_0 = 60/(N\Omega_0)\,[\mathrm{s}]$, where the spindle speed Ω_0 is given in [rpm]. The linearized equation of motion (5.21) reads

$$\ddot{\xi}(t) + 2\zeta\omega_{\mathrm{n}}\dot{\xi}(t) + \omega_{\mathrm{n}}^2\xi(t) = -\tilde{G}(t)\left(\xi(t) - \xi(t-\tau_0)\right) \,, \tag{5.27}$$

where the specific directional factor

$$\tilde{G}(t) = a_{\mathrm{p}}\frac{q(v_{\mathrm{f}}\tau_0)^{\,q-1}}{m}\sum_{j=1}^{N} g_j(t)\sin^q\varphi_j(t)\left(K_{\mathrm{t}}\cos\varphi_j(t) + K_{\mathrm{r}}\sin\varphi_j(t)\right) \tag{5.28}$$

is now a purely τ-periodic function, because the angular position of tooth j is now given by

$$\varphi_j(t) = \frac{2\pi\,\Omega_0}{60}t + j\,\frac{2\pi}{N} \,. \tag{5.29}$$

Equation (5.27) can also be written in the form

$$\ddot{\xi}(t) + 2\zeta\omega_{\mathrm{n}}\dot{\xi}(t) + \omega_{\mathrm{n}}^2\xi(t) = -HG(t)\left(\xi(t) - \xi(t-\tau_0)\right) \,, \tag{5.30}$$

where $H = a_{\mathrm{p}} q (v_{\mathrm{f}} \tau_0)^{q-1} K_{\mathrm{r}}/m$ is the specific cutting-force coefficient and

$$G(t) = \sum_{j=1}^{N} g_j(t) \sin^q \varphi_j(t) \left(\frac{K_{\mathrm{t}}}{K_{\mathrm{r}}} \cos \varphi_j(t) + \sin \varphi_j(t) \right) \tag{5.31}$$

is a τ-periodic function called the directional dynamic cutting-force coefficient, or simply the directional factor. If $c = c_x$, $k = k_x$, $K_{\mathrm{r}} = K_y$, $a_{\mathrm{p}} = w$, $v_{\mathrm{f}} \tau_0 = v_{\mathrm{f}} \hat{\tau}$, and $G(t) \equiv 1$, then (5.30) gives the governing equation (4.29) of turning without state-dependent delay.

The system can be written in the first-order form

$$\dot{\mathbf{x}}(t) = \mathbf{A}(t)\mathbf{x}(t) + \mathbf{B}(t)\mathbf{u}(t - \tau_0) \,, \tag{5.32}$$

$$\mathbf{u}(t) = \mathbf{D}\mathbf{x}(t) \,, \tag{5.33}$$

where

$$\mathbf{x}(t) = \begin{pmatrix} \xi(t) \\ \dot{\xi}(t) \end{pmatrix} \,, \qquad \mathbf{D} = \begin{pmatrix} 1 & 0 \end{pmatrix} \,, \tag{5.34}$$

$$\mathbf{A}(t) = \begin{pmatrix} 0 & 1 \\ -(\omega_{\mathrm{n}}^2 + HG(t)) & -2\zeta\omega_{\mathrm{n}} \end{pmatrix} \,, \qquad \mathbf{B}(t) = \begin{pmatrix} 0 \\ HG(t) \end{pmatrix} \,. \tag{5.35}$$

Then, the stability analysis can be performed using the semi-discretization method as shown in Chapter 3.

Figure 5.4 shows a series of stability lobe diagrams in the plane of the dimensionless spindle speed $N\Omega/(60 f_{\mathrm{n}})$ and the dimensionless specific cutting-force coefficient H/ω_{n}^2 for different milling operations. (Note that H is linearly proportional to the axial depth of cut a_{p}.) The diagrams were determined by the first-order semi-discretization method with period resolution $p = 50$. The corresponding frequency diagrams and the directional factor $G(t)$ are also presented. The damping ratio is $\zeta = 0.02$, the cutting-force ratio is $K_{\mathrm{t}}/K_{\mathrm{r}} = 0.3$, and the cutting-force exponent is $q = 0.75$. The same diagrams are also shown for turning as the special limiting case when $G(t) \equiv 1$. The technological parameters for the milling operations were determined such that the time-dependency of the directional factor $G(t)$ becomes stronger and stronger. The first case is a full-immersion milling with a 4-fluted tool. In this case the tool is always in contact with the workpiece, since two of its cutting edges are always in the cut, and the directional factor $G(t)$ is a continuous function. The other cases are all up-milling operations by a 4-fluted tool with smaller and smaller radial immersion, resulting in more and more interrupted machining. As was shown by Davies et al. [42, 43], highly interrupted machining operations can be modeled approximately by a finite-dimensional discrete map instead of infinite-dimensional DDEs such that the cutting process is considered as an impact with the cutting force impulse being proportional

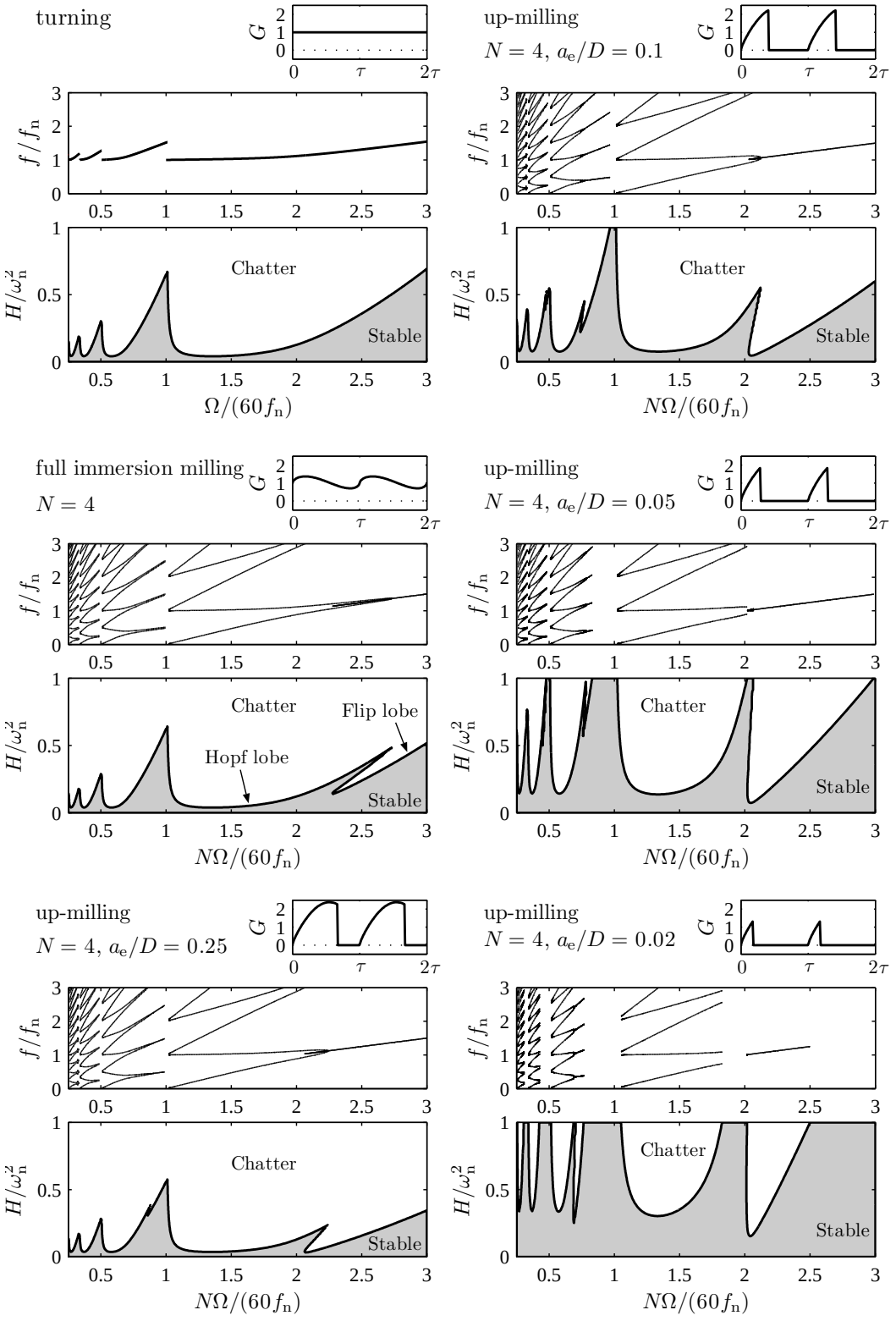

Figure 5.4: Stability charts and frequency diagrams with the corresponding directional factor $G(t)$ for turning and different milling operations.

to the chip thickness. In this sense, Figure 5.4 presents a transition between two special models of machining: the traditional time-independent DDE model of turning operation and the discrete map model of highly interrupted machining. Figure 5.4 shows that a series of extra stability lobes arises in addition to the Hopf lobes of turning as the process becomes more and more interrupted. Numerical calculation shows that along these additional lobes, a single characteristic multiplier crosses the unit circle at -1, i.e., these lobes are associated with period-doubling (flip) bifurcation. As the radial immersion decreases, the orientation of the flip lobes become vertical, and the stability diagrams tend to those of the highly interrupted model obtained by Davies et al. [42, 43].

As was mentioned in Chapter 2, the critical characteristic multipliers can be located in three ways:

1. $|\mu_{1,2}| = 1$ with $\mathrm{Im}\,\mu_{1,2} \neq 0$ (secondary Hopf bifurcation);
2. $\mu_1 = 1$ (cyclic-fold bifurcation);
3. and $\mu_1 = -1$ (period-doubling or flip bifurcation).

It can easily be seen that the case $\mu_1 = 1$ cannot occur for (5.30). It is known that in the critical subspace, $\xi(t+\tau) = \mu_1 \xi(t)$ is satisfied. If $\mu_1 = 1$, then $\xi(t-\tau) = \xi(t)$, and substitution into (5.30) gives the damped oscillator

$$\ddot{\xi}(t) + 2\zeta\omega_{\mathrm{n}}\dot{\xi}(t) + \omega_{\mathrm{n}}^2\xi(t) = 0\,. \tag{5.36}$$

Since ζ and ω_{n} are positive, (5.36) is asymptotically stable; consequently, it cannot have a characteristic exponent equal to zero, i.e., it cannot have a characteristic multiplier equal to 1. This proves that cyclic-fold bifurcation cannot arise for (5.30).

With a different conclusion, the same idea can be applied in the case $\mu_1 = -1$. Here, $\xi(t-\tau) = -\xi(t)$, and substitution into (5.30) gives

$$\ddot{\xi}(t) + 2\zeta\omega_{\mathrm{n}}\dot{\xi}(t) + \left(\omega_{\mathrm{n}}^2 + 2HG(t)\right)\xi(t) = 0\,. \tag{5.37}$$

This is an ODE with time-periodic coefficient, for which the characteristic multiplier $\mu_1 = -1$ typically arises for some parameter combination. As a matter of fact, the stability boundaries of (5.37) give the flip stability boundaries of the original equation (5.30). This means that the flip lobes can be determined by the analysis of the time-periodic ODE (5.37) instead of the time-periodic DDE (5.30). This was the basic idea of the analysis by Corpus and Endres [38] to determine the flip lobes for milling processes.

Figure 5.4 also shows the frequencies of the resulting vibrations in separate frequency diagrams. These frequencies can be determined using the critical characteristic

multipliers obtained by the semi-discretization method. Vibrations arise when the system loses stability, i.e., when the critical characteristic multiplier satisfies $|\mu_1| = 1$. Equation (5.30) is periodic at the tooth-passing period τ. According to the Floquet theory, the solution corresponding to the critical characteristic multiplier μ_1 reads

$$\xi(t) = a(t)\,\mathrm{e}^{\lambda_1 t} + \bar{a}(t)\,\mathrm{e}^{\bar{\lambda}_1 t}\,, \tag{5.38}$$

where $a(t)$ is a τ-periodic function, bar denotes complex conjugate, and λ_1 is the critical characteristic exponent, i.e., $\mu_1 = \mathrm{e}^{\lambda_1 \tau}$. Fourier expansion of $a(t)$ and substitution of $\lambda_1 = \mathrm{i}\,\omega_1$ results in

$$\xi(t) = \sum_{j=-\infty}^{\infty} \left(C_j\,\mathrm{e}^{\mathrm{i}\,(\omega_1 + j2\pi/\tau)t} + \bar{C}_j\,\mathrm{e}^{-\mathrm{i}\,(\omega_1 + j2\pi/\tau)t}\right)\,, \tag{5.39}$$

where C_j and $\bar{C}_j$ are some complex coefficients. Note that $\omega_1\tau$ is equal to the phase angle describing the direction of μ_1 in the complex plane, so that $-\pi < \omega_1\tau \leq \pi$. The exponents in (5.39) give the angular frequency content of the vibrations. The corresponding vibration frequencies are

$$f = \pm\frac{\omega_1}{2\pi} + \frac{j}{\tau}\ [\mathrm{Hz}]\,, \qquad j = 0, \pm1, \pm2, \ldots\,. \tag{5.40}$$

Of course, only the positive frequencies have physical meaning.

For the secondary Hopf lobes, the critical characteristic multipliers are a complex conjugate pair in the form $\mu = \mathrm{e}^{\pm\mathrm{i}\,\omega\tau}$, and the chatter frequencies are given by

$$f_{\mathrm{H}} = \pm\frac{\omega_1}{2\pi} + j\frac{N\Omega}{60}\ [\mathrm{Hz}]\,, \quad j = 0, \pm1, \pm2, \ldots\,. \tag{5.41}$$

According to (5.38), the solution is given as the product of the τ-periodic function $a(t)$ and the $(2\pi/\omega_1)$-periodic function $\mathrm{e}^{\lambda_1 t} = \mathrm{e}^{\mathrm{i}\omega_1 t}$. Consequently, the resulting vibrations are quasiperiodic. In the literature, vibrations due to secondary Hopf bifurcations are often referred to as quasiperiodic chatter.

For the flip lobes, the critical characteristic multiplier is $\mu_1 = -1$, i.e., $\omega_1\tau = \pi$. The corresponding chatter frequencies are

$$f_{\mathrm{F}} = \frac{N\Omega}{120} + j\frac{N\Omega}{60}\ [\mathrm{Hz}]\,, \quad j = 0, \pm1, \pm2, \ldots\,. \tag{5.42}$$

In this case, the period of the function $\mathrm{e}^{\lambda_1 t} = \mathrm{e}^{\mathrm{i}\omega_1 t} = \mathrm{e}^{\mathrm{i}\pi t/\tau}$ is 2τ. Consequently, the solution according to (5.38) is a 2τ-periodic function that explains the terminology period doubling: the period of the vibration is double the tooth-passing period.

The frequency diagrams in Figure 5.4 were obtained using (5.41) and (5.42). While turning operations are characterized by a well-defined single chatter frequency according to the Hopf bifurcation of autonomous systems, milling operations, being parametrically excited systems, present multiple vibration frequencies. Along the flip lobes, the

basic frequency of the vibrations is equal to half of tooth-passing frequency. Along the Hopf lobes, quasiperiodic vibrations arise. It should be mentioned that flip instability is directly related to the time-periodic nature of the milling process. It occurs mostly for operations with small radial immersion when the directional factor $G(t)$ is strongly time-dependent.

Note that the frequency diagrams in Figure 5.4 do not distinguish the dominant vibration frequencies. Generally, only one or two of these frequencies characterize the chatter signal, and the other harmonics are associated with negligible amplitudes. A technique to show the strength of the different frequency components in complex milling models using the semi-discretization method was presented by Dombovari et al. [49].

5.3 Stability charts for varying spindle speed

In this section, system (5.23)-(5.24) is analyzed such that $q_1 T = q_2 \tau_0$ satisfies with q_1 and q_2 being relatively prime, i.e., the system is periodic with principal period $q_1 T$. The variation of the spindle speed is described by the amplitude ratio RVA $= \Omega_1/\Omega_0$ and the frequency ratio RVF $= 60/(\Omega_0 T)$. Figure 5.5 shows some sample stability charts for RVA $= 0.1$ and for different RVF values in the high-speed domain. The parameters are as follows. A half-immersion up-milling process is considered (i.e., $a_e/D = 0.5$) by a 4-fluted tool ($N = 4$) with zero helix angle. The cutting-force coefficients are $K_t = 107 \times 10^6\,\mathrm{N/m^{1+q}}$ and $K_r = 40 \times 10^6\,\mathrm{N/m^{1+q}}$, the cutting-force exponent is $q = 0.75$. The feed per tooth is $f_z = 0.1\,\mathrm{mm}$, for which the linearized cutting-force coefficients are $K_t q f_z^{q-1} = 800{\times}10^6\,\mathrm{N/m^2}$ and $K_r q f_z^{q-1} = 300{\times}10^6\,\mathrm{N/m^2}$. The stiffness is $k = 20 \times 10^6\,\mathrm{N/m}$, the natural frequency is $f_n = \omega_n/2\pi = 400\,\mathrm{Hz}$, and the damping ratio is $\zeta = 0.02$. Using the assumption $q_1 T = q_2 \tau_0$, one obtains $q_1/q_2 = \mathrm{RVF}/N$. For the frequency ratios RVF $= 0.5, 0.2, 0.1$, and 0.05 in Figure 5.5, these relatively prime numbers are $q_1 = 1$ and $q_2 = 8, 20, 40$, and 80, respectively. The corresponding principal periods are $q_1 T = 8\tau_0, 20\tau_0, 40\tau_0$, and $80\tau_0$. The diagrams were determined by the first-order semi-discretization method such that the delay resolution was $r = 44$ for all cases. The period resolutions corresponding to the frequency ratios RVF $= 0.5, 0.2, 0.1$, and 0.05 were $p = 320, 800, 1600$, and 3200, respectively. (Note that the principal period of the system is $q_1 T = q_1 N \tau_0/\mathrm{RVF}$.)

In Figure 5.5, dashed lines indicate the stability boundaries corresponding to constant-spindle-speed machining. As can be seen, spindle speed modulation results in some improvements in the stability around the first flip lobe (13-20 krpm). While for constant-spindle-speed milling, a single flip lobe appears at 13-20 krpm (the so-called first flip lobe), for varying-spindle-speed milling, a series of new lobes show up. As

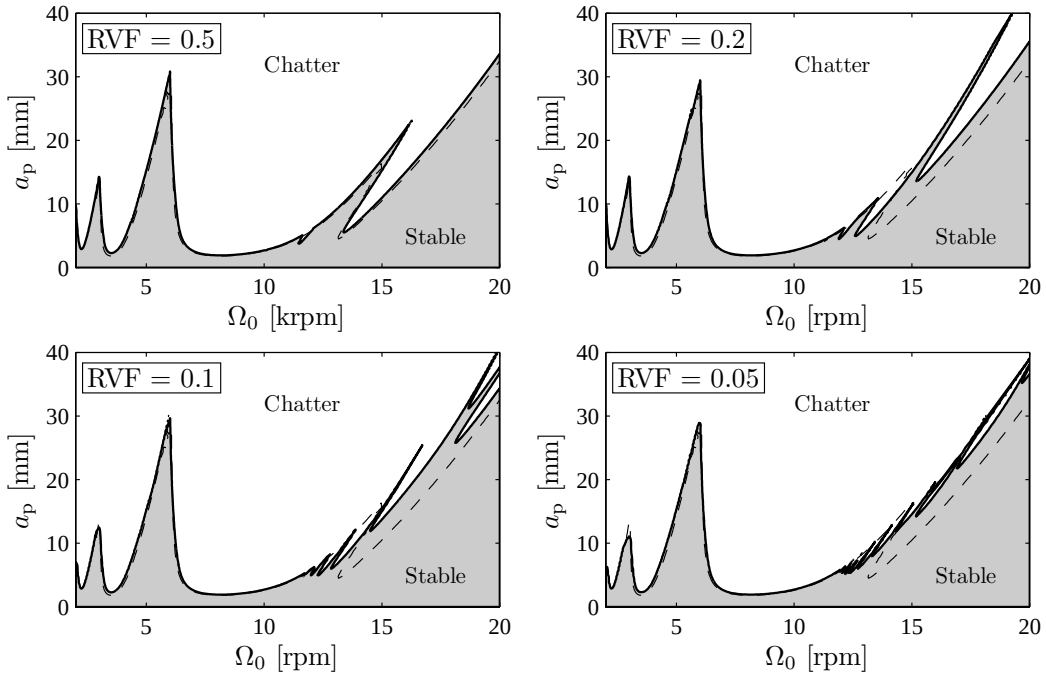

Figure 5.5: Stability charts for milling processes with sinusoidal spindle speed modulation with RVA = 0.1 in the high-speed domain. Dashed lines indicate the stability boundaries associated with constant-spindle-speed milling.

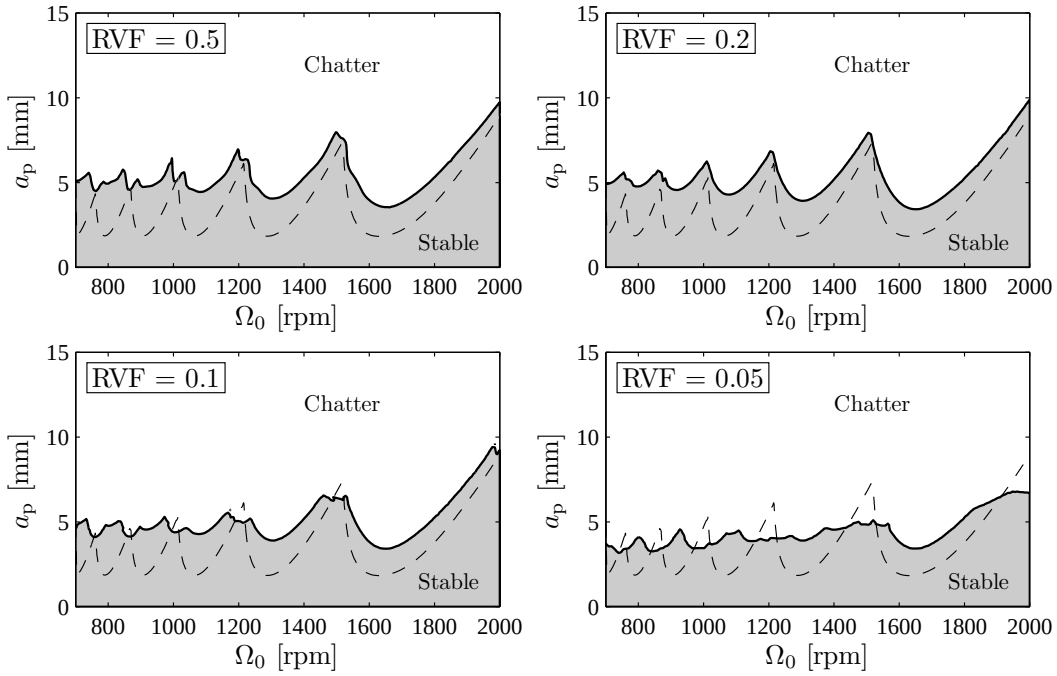

Figure 5.6: Stability charts for milling processes with sinusoidal spindle speed modulation with RVA = 0.1 in the low-speed domain. Dashed lines indicate the stability boundaries associated with constant-spindle-speed milling.

the frequency ratio RVF is decreased, more and more new lobes appear resulting in a kind of serration on the stability boundary (see the case RVF = 0.05). Although these new lobes are located around the first flip lobe of constant-speed milling, they are not associated to period doubling bifurcation in the strict mathematical sense, since the principal period of the system is $q_1 T = q_2 \tau_0$ and not τ_0.

Figure 5.6 shows the same stability charts for lower spindle speeds. Here, the first-order semi-discretization method was used with delay resolution $r = 110$. The period resolutions corresponding to the frequency ratios RVF $= 0.5, 0.2, 0.1$, and 0.05 were $p = 800, 2000, 4000$, and 8000, respectively. In this case, spindle speed modulation results in an increase of the stability lobes in general. For small RVF values (i.e., for small modulation frequencies), the peaks of the stability boundaries are flattened, but their minima become larger by 50–60% than those of constant-spindle-speed milling.

5.4 Experimental validation of chatter suppression by spindle-speed variation

The possibility of suppressing period doubling chatter by spindle speed variation were verified experimentally in collaboration with French partners. The experiments were performed by Sebastien Seguy at École Nationale d'Ingénieurs de Tarbes in France, who made his PhD about milling processes with varying spindle speed in 2008 [192]. The results presented in this section are based on the joint papers Seguy et al. [193, 194].

The machining tests were performed on a 3-axis high-speed milling center (Huron, KX10). The tool was an inserted mill with three teeth, $D = 25\,\text{mm}$ diameter without helix angle. The average feed per tooth was $v_\text{f}\tau_0 = 0.1\,\text{mm/tooth}$. Triangular spindle speed variation was implemented by a subprogram using a synchronous function (Siemens, 840D). Thus, the shape function in equation (5.1) is

$$S(t) = \begin{cases} 1 - 4(t \bmod T)/T & \text{if } \ 0 < (t \bmod T) \le T/2\ , \\ -3 + 4(t \bmod T)/T & \text{if } \ T/2 < (t \bmod T) \le T\ , \end{cases} \tag{5.43}$$

This gives a function varying linearly between -1 and 1 with period T. In compliance with the dynamics of the spindle, the difference between the input and the measured spindle speeds was less than 0.5% (see Figure 5.7).

The setup of the milling tests can be seen in Figure 5.8. A flexure was used to provide a single-degree-of-freedom system that is compliant in the x direction (perpendicular to the feed). The tool is considered to be rigid relative to the flexure. An aluminum (2017A) part was down-milled with a radial depth of cut $a_\text{e} = 2\,\text{mm}$, thus, the radial immersion ratio was $a_\text{e}/D = 0.08$. The length of the workpiece was 90 mm, and the

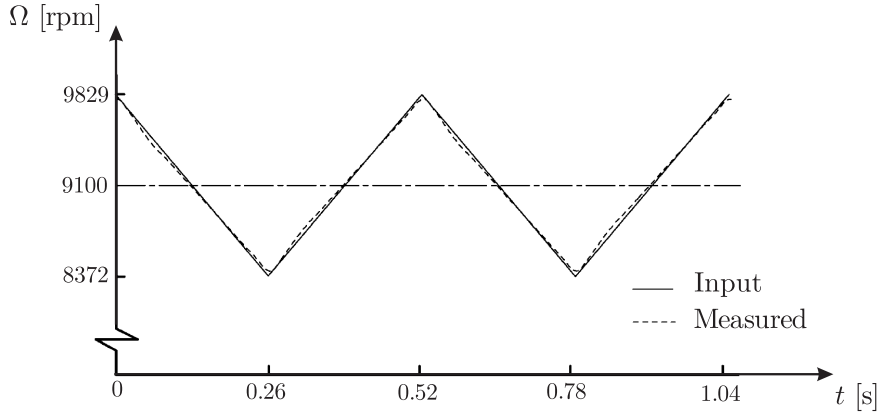

Figure 5.7: Comparison of the input and the measured spindle speeds for $\Omega_0 = 9100\,\text{rpm}$, RVA $= 0.08$ and RVF $= 0.0125$ ($T = 1.9$ Hz).

Figure 5.8: Experimental setup (see [193]).

operation time was approximately 2 s at a spindle speed of $\Omega_0 = 9100$ rpm. The vibrations of the part were measured by a laser velocimeter (Ometron, VH300+). Filtering followed by a numerical integration was used to extract the displacement of the part. The dynamic characteristics of the system were determined by hammer impact test. The modal mass was $m = 1.637\,\text{kg}$, the natural frequency was $f_\text{n} = 222.5\,\text{Hz}$, the damping ratio was $\zeta = 0.005$. The linearized cutting force coefficients in the tangential and the radial directions were $K_\text{t} q f_\text{z}^{q-1} = 700 \times 10^6\,\text{N/m}^2$ and $K_\text{r} q f_\text{z}^{q-1} = 140 \times 10^6\,\text{N/m}^2$, respectively.

The corresponding mechanical model can be seen in Figure 5.9. The linearized equation of motion reads

$$\ddot{\xi}(t) + 2\zeta\omega_\text{n}\dot{\xi}(t) + \omega_\text{n}^2\xi(t) = -\tilde{G}_y(t)\left(\xi(t) - \xi(t-\tau(t))\right)\ , \tag{5.44}$$

where the angular natural frequency is $\omega_\text{n} = \sqrt{k/m} = 2\pi f_\text{n} = 1398\,\text{rad/s}$ and the

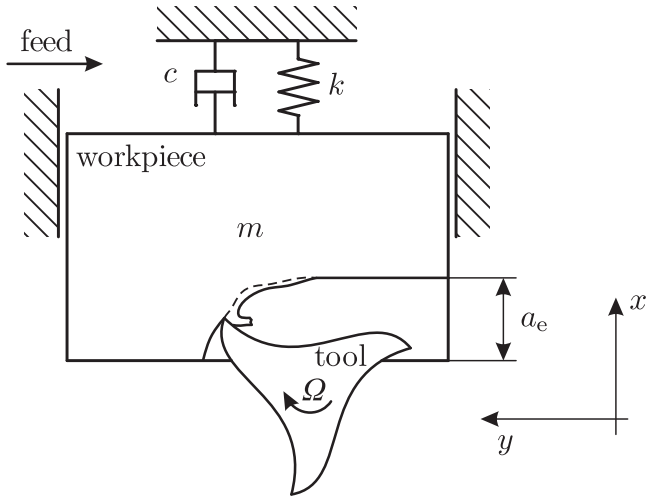

Figure 5.9: Mechanical model. The compliant direction of the workpiece is perpendicular to the feed direction.

specific directional factor is

$$\tilde{G}_y(t) = a_p \frac{q(v_f \tau(t))^{q-1}}{m} \sum_{j=1}^{N} g_j(t) \sin^{q-1} \varphi_j(t) \cos \varphi_j(t) \left(K_r \cos \varphi_j(t) - K_t \sin \varphi_j(t)\right) \ . \tag{5.45}$$

Note that here the compliant direction of the workpiece is perpendicular to the feed direction, therefore $\tilde{G}_y(t)$ in equation (5.45) is not identical to $\tilde{G}(t)$ in (5.28). As a simplification for the experiments, a linear cutting force characteristic was assumed, i.e., $q = 1$, for which equation (5.45) gives

$$\tilde{G}_y(t) = \frac{a_p}{m} \sum_{j=1}^{N} g_j(t) \cos \varphi_j(t) \left(K_r \cos \varphi_j(t) - K_t \sin \varphi_j(t)\right) \ . \tag{5.46}$$

Stability analysis of equation (5.44) is performed using the first-order semi-discretization method. Stability diagrams for constant-speed milling and for varying-speed milling with amplitude ratio RVA = 0.2 and with frequency ratio RVF = 0.0046875 can be seen in Figure 5.10. The parameter region under investigation is around the first flip lobe. For varying-speed milling, the stability boundary is strongly serrated by the small stability lobes that were also shown in Figure 5.5. Note that in Figure 5.5, the frequency ratio was RVF = 0.5, 0.2, 0.1 and 0.05, while in Figure 5.10, it is RVF = 0.0046875. It can be seen that for $\Omega_0 > 9000\,\text{rpm}$, spindle speed variation has a stabilizing effect, while for $8000\,\text{rpm} < \Omega_0 < 9000\,\text{rpm}$, it has a destabilizing effect.

During the experiments, machining processes with spindle speed $\Omega_0 = 9100$ rpm and depth of cut $a_p = 1\,\text{mm}$ were analyzed for constant and varying spindle speeds. This machining operation is denoted by point B in Figure 5.10. The measured spindle

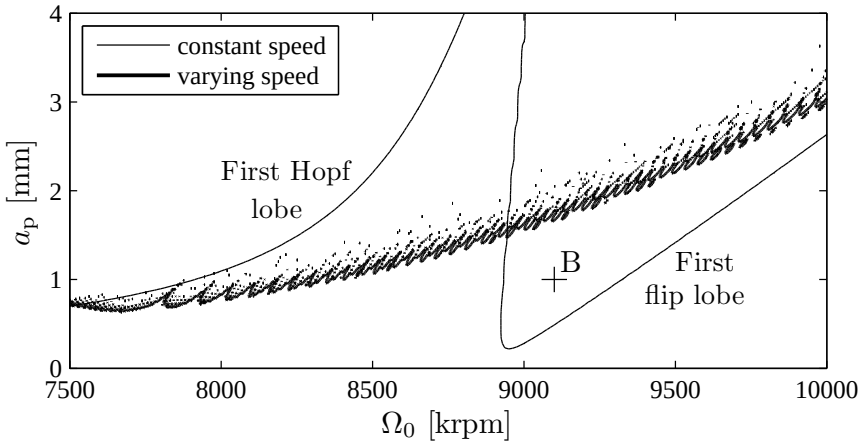

Figure 5.10: Stability chart for constant-spindle-speed milling and for varying-spindle-speed milling with RVA = 0.2 and RVF = 0.0046875.

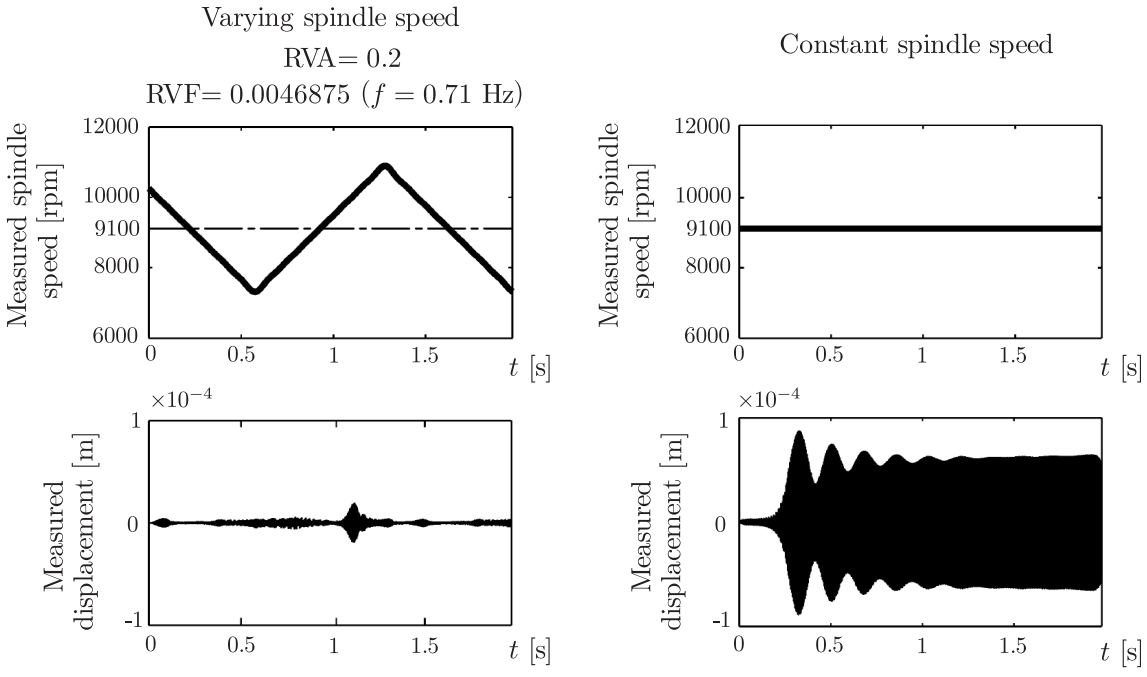

Figure 5.11: Time history for for constant-spindle-speed and for varying-spindle-speed machining for $\Omega_0 = 9100$ rpm and $a_p = 1\,\mathrm{mm}$.

speed variation and the resulted displacement is presented in Figure 5.11. As can be seen, for the constant-speed machining, chatter was clearly identified with vibration amplitude around 0.07 mm. When varying-spindle-speed was applied, then no chatter was observed. In this case the amplitude of the vibrations was less than 0.01 mm. Thus, the experiments confirmed the theoretical predictions: spindle speed modulation can be used to stabilize unstable machining processes.

5.5 New results

Thesis 3 *The linearized equation of motion was determined for single-degree-of-freedom model of milling processes with spindle speed modulation under the assumptions that (1) the ratio of the spindle speed modulation period and the mean regenerative delay is rational, and (2) the tool experiences only small forced oscillations relative to the average feed per tooth.*

The stability charts were determined by the first-order semi-discretization method in the plane of the mean spindle speed and the axial depth of cut. It was shown that for the high-speed domain, no significant improvements can be obtained by spindle speed variation except for the slight increase in the stability boundaries at the first flip lobe, where series of new stability lobes show up. For the low-speed domain, spindle speed modulation results in an increase of the stability lobes in general.

The results composed in the thesis were published in the book Insperger and Stépán [115].

Chapter 6

The act-and-wait control concept for continuous-time systems with feedback delay

The main problem in the stabilization of control systems in the presence of feedback delay is that infinitely many characteristic exponents (poles) should be controlled, while the number of control parameters is finite. One technique to deal with the problem is to assign the place of the rightmost poles only while monitoring the other uncontrolled poles with large (negative) real part (see, e.g., Michiels et al. [151, 153]). This technique requires the numerical calculation of some relevant poles for different control parameters. In this case, the infinitely many poles are controlled by a finite number of control parameters.

An alternative approach is to increase the number of control parameters with the application of distributed delays in the controller, where the kernel function of the distributed delay serves as a kind of infinite-dimensional vector of control gains. Another way is the application of time-periodic controllers, where the time-dependency of the gains can be assumed to be a set of infinitely many control parameters.

A special case for distributed-delay applications is that in which the feedback is based on a prediction of the state. This method is called finite spectrum assignment, since the resulting closed-loop system has only a finite number of poles that can be assigned arbitrarily, provided that there is no uncertainty in the system and in the control parameters (for details, see Manitius and Olbrot [146], Wang et al. [235]). If the open-loop system is unstable, then prediction by means of the solution of the differential equation cannot stabilize the system, since it involves an unstable pole–zero cancellation even for high-accuracy solutions (see Engelborghs et al. [55]). The conditions for stabilizing via distributed delays that approximates the solution of the system

were analyzed by Mondié et al. [158], and a safe implementation of finite spectrum assignment for unstable systems was provided in Mondié and Michiels [159].

For delay-free systems, stabilization by means of periodic control gains is a field of intensive research (see, for instance, [25, 142, 162, 3, 21]). However, the combined effect of feedback delay and time-periodic control gains results in time-periodic DDEs, for which the stability analysis requires the use of the infinite-dimensional Floquet theory.

Actually, sampling can also be considered a special case of periodic controllers, since it corresponds to a periodic variation of the feedback delay in time. Other, generalized, sampled-data hold functions can also effectively be used to improve control performance (see, e.g,. Kabamba [119]). A special case of generalized hold discrete-time control is the intermittent predictive control, where the sequence of open-loop trajectories is punctuated by intermittent feedback. This concept was introduced by Ronco et al. [185] and further developed by Gawthrop and Wang [64, 65].

In this chapter, a special case of periodic controllers, the act-and-wait controller, is analyzed, where the feedback term is switched on and off periodically in time. The technique was introduced by Insperger and Stépán [106, 212, 107] for both continuous-time and discrete-time systems. The merit of the technique is that if the switch-off (waiting) period is longer than the feedback delay, then the system can be transformed to a discrete map of finite dimension presenting a finite spectrum assignment problem. This feature may be useful during the controller design. Several examples show that a stable control process can be attained by the application of the act-and-wait concept for problems where the traditional controllers with continuous feedback cannot stabilize the system. Furthermore, the act-and-wait controller typically can be tuned to have dead-beat behavior (see, e.g., [106, 212, 129]). Due to its intermittent nature, the act-and-wait concept is relevant in biomechanical applications such as controlling biological networks [174] and human balancing [154, 10]. As was shown by Gawthrop [66], the act-and-wait controller is related to the intermittent controller in the sense that both techniques have a generalized hold interpretation.

In this chapter, first, some features of time-periodic controllers are summarized. Then, the act-and-wait controller is introduced in detail. After that, the stick balancing problem is presented with reflex delay as a case study. The new results are composed in Thesis 4 at the end of the chapter. The results presented here were published in Insperger [106] and also in the book Insperger and Stépán [115].

6.1 Time-invariant versus time-periodic controllers

Consider the linear multiple-input multiple-output system

$$\dot{\mathbf{x}}(t) = \mathbf{A}\mathbf{x}(t) + \mathbf{B}\mathbf{u}(t) \,, \tag{6.1}$$

$$\mathbf{y}(t) = \mathbf{C}\mathbf{x}(t) \,, \tag{6.2}$$

with state $\mathbf{x}(t) \in \mathbb{R}^n$, input $\mathbf{u}(t) \in \mathbb{R}^m$, and output $\mathbf{y}(t) \in \mathbb{R}^l$. Consider the delayed feedback controller

$$\mathbf{u}(t) = \mathbf{D}\mathbf{y}(t-\tau) \,, \tag{6.3}$$

with τ being the feedback delay. It is assumed that the delay is a fixed parameter of the control system and cannot be eliminated or tuned during the control design. There are several sources of such time delays, e.g., acquisition of response and excitation data, information transmission, on-line data processing, computation and application of control forces. It is assumed, furthermore, that the time delay is a known parameter during the control design. Note, however, that the time delay is often an uncertain parameter in feedback control processes that can lead to instabilities (see, e.g., [91, 124]) and affects also the robustness of the control process (see, e.g., [168, 123, 152]).

System (6.1)–(6.2) with (6.3) forms an autonomous DDE of the form

$$\dot{\mathbf{x}}(t) = \mathbf{A}\mathbf{x}(t) + \mathbf{B}\mathbf{D}\mathbf{C}\mathbf{x}(t-\tau) \,. \tag{6.4}$$

Stabilization of (6.4) brings the following pole placement problem: for given matrices $\mathbf{A}$, $\mathbf{B}$, and $\mathbf{C}$ and for given feedback delay τ, matrix $\mathbf{D}$ should be determined such that all the characteristic exponents (the poles) lie in the left half of the complex plane. The difficulty in this problem is that infinitely many characteristic exponents should be controlled by a finite number of control parameters, i.e., by the elements of matrix $\mathbf{D}$.

Consider now the periodic controller

$$\mathbf{u}(t) = \mathbf{G}(t)\mathbf{y}(t-\tau) \,, \tag{6.5}$$

where $\mathbf{G}(t)$ is a T-periodic function. System (6.1)–(6.2) with (6.5) implies the time-periodic DDE

$$\dot{\mathbf{x}}(t) = \mathbf{A}\mathbf{x}(t) + \mathbf{B}\mathbf{G}(t)\mathbf{C}\mathbf{x}(t-\tau) \,. \tag{6.6}$$

As was mentioned in Section 2.4, the general solution of (6.6) for the initial function $\mathbf{x}_0$ can be formulated as

$$\mathbf{x}_t = \mathcal{U}(t)\mathbf{x}_0 \,, \tag{6.7}$$

where $\mathcal{U}(t)$ is the solution operator (infinitesimal generator) of the system, and the function $\mathbf{x}_t$ is defined as

$$\mathbf{x}_t(\vartheta) = \mathbf{x}(t+\vartheta) \,, \quad \vartheta \in [-\tau, 0] \,. \tag{6.8}$$

The stability properties of the system are determined by the monodromy operator $\mathcal{U}(T)$. The nonzero elements of the spectrum of $\mathcal{U}(T)$ are called characteristic multipliers (or poles). The system is asymptotically stable if all the characteristic multipliers have modulus less than one. Like the time-independent system (6.4), stabilization of system (6.6) requires control over infinitely many poles, but now the control gains are functions of time over the period $[0, T]$, which corresponds to a kind of infinite-dimensional vector of control gains. The question is how to place all the infinitely many poles (i.e., infinitely many characteristic multipliers in this case) of the system inside the unit circle of the complex plane by tuning the control gain function $\mathbf{G}(t)$ over $[0, T]$. One possible approach to the problem is to decrease the dimension of the system using the act-and-wait control technique.

6.2 The act-and-wait control concept

The act-and-wait controller is a special case of the periodic controller (6.5) with the T-periodic matrix

$$\mathbf{G}(t) = \begin{cases} \mathbf{0} & \text{if } \ 0 \le (t \bmod T) < t_{\mathrm{w}} \ , \\ \mathbf{\Gamma}(t \bmod T) & \text{if } \ t_{\mathrm{w}} \le (t \bmod T) < t_{\mathrm{w}} + t_{\mathrm{a}} = T \ , \end{cases} \tag{6.9}$$

where $\mathbf{\Gamma} : [t_{\mathrm{w}}, T] \to \mathbb{R}^{m \times l}$ is an integrable matrix function. Here, t_{a} and t_{w} are the lengths of the acting and the waiting periods, respectively, and $t_{\mathrm{a}} + t_{\mathrm{w}} = T$ is the length of one act-and-wait period.

In what follows, it will be shown that if the waiting period is larger than the feedback delay (i.e., if $t_{\mathrm{w}} \ge \tau$), then the system can be described by an $n \times n$ monodromy matrix. Consequently, only n poles determine the stability instead of infinitely many.

Consider the general case $(k-1)\tau < t_{\mathrm{a}} \le k\tau$, where k is an arbitrary positive integer. According to the method of steps for DDEs, the solution can be constructed piecewise over the consecutive intervals $[0, t_{\mathrm{w}}]$, $[t_{\mathrm{w}}, t_{\mathrm{w}} + \tau]$, $\ldots$, $[t_{\mathrm{w}} + (k-1)\tau, T]$ step by step (see Figure 6.1 for $k = 3$).

Since the delayed term is switched off during the waiting period, the first section of the solution can be given as

$$\mathbf{x}^{(1)}(t) = \mathbf{\Phi}^{(1)}(t)\mathbf{x}(0) \ , \qquad 0 \le t \le t_{\mathrm{w}} \ , \tag{6.10}$$

with $\mathbf{\Phi}^{(1)}(t) = \mathrm{e}^{\mathbf{A}t}$. Here, superscript (1) refers to the number of the segment of the solution.

Now we utilize the facts that the waiting period is larger than (or equal to) the time delay and the solution over $0 \le t \le t_{\mathrm{w}}$ is already given by (6.10). Thus, in the

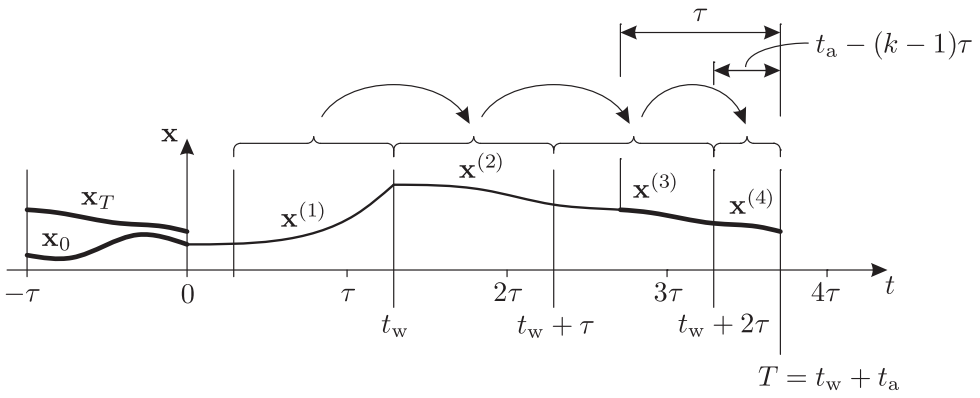

Figure 6.1: Sketch of the piecewise solution of (6.6) with (6.9) according to the method of steps for $t_w \geq \tau$ and $2\tau < t_a \leq 3\tau$ ($k = 3$).

interval $t_w < t \leq t_w + \tau$, (6.6) with (6.9) can be written as

$$\dot{\mathbf{x}}(t) = \mathbf{A}\mathbf{x}(t) + \mathbf{B}\boldsymbol{\Gamma}(t)\mathbf{C}\boldsymbol{\Phi}^{(1)}(t-\tau)\mathbf{x}(0) \,, \qquad t_w < t \leq t_w + \tau \,. \tag{6.11}$$

The solution for the initial condition $\mathbf{x}(t_w) = \mathbf{x}^{(1)}(t_w) = \boldsymbol{\Phi}^{(1)}(t_w)\mathbf{x}(0)$ can be given in the form

$$\mathbf{x}^{(2)}(t) = \boldsymbol{\Phi}^{(2)}(t)\mathbf{x}(0) \,, \qquad t_w < t \leq t_w + \tau \,, \tag{6.12}$$

with

$$\boldsymbol{\Phi}^{(2)}(t) = \mathrm{e}^{\mathbf{A}t} + \int_{t_w}^{t} \mathrm{e}^{\mathbf{A}(t-s)}\mathbf{B}\boldsymbol{\Gamma}(s)\mathbf{C}\boldsymbol{\Phi}^{(1)}(s-\tau)\,\mathrm{d}s \tag{6.13}$$

(see the variation of constants formula (A.15) in Appendix A). Provided that the solution in the hth interval is given as

$$\mathbf{x}^{(h)}(t) = \boldsymbol{\Phi}^{(h)}(t)\mathbf{x}(0) \,, \qquad t_w + (h-2)\tau < t \leq t_w + (h-1)\tau \,, \tag{6.14}$$

the solution in the next interval can be given by the recursive form

$$\mathbf{x}^{(h+1)}(t) = \boldsymbol{\Phi}^{(h+1)}(t)\mathbf{x}(0) \,, \qquad t_w + (h-1)\tau < t \leq t_w + h\tau \,, \tag{6.15}$$

with

$$\boldsymbol{\Phi}^{(h+1)}(t) = \mathrm{e}^{\mathbf{A}t} + \int_{t_w-(h-1)\tau}^{t} \mathrm{e}^{\mathbf{A}(t-s)}\mathbf{B}\boldsymbol{\Gamma}(s)\mathbf{C}\boldsymbol{\Phi}^{(h)}(s-\tau)\,\mathrm{d}s \,. \tag{6.16}$$

Finally, the solution at $t = T$ is given as

$$\mathbf{x}(T) = \mathbf{x}^{(k+1)}(T) = \boldsymbol{\Phi}^{(k+1)}(T)\mathbf{x}(0) \,. \tag{6.17}$$

As can be seen, the state $\mathbf{x}(T)$ depends only on the initial state $\mathbf{x}(0)$, and it does not depend on the initial function $\mathbf{x}_0$. Matrix $\boldsymbol{\Phi}^{(k+1)}(T)$ therefore serves as an $n \times n$ monodromy matrix for the system.

As a consequence, the infinite-dimensional monodromy mapping

$$\mathbf{x}_T = \mathcal{U}(T)\mathbf{x}_0 \tag{6.18}$$

can be written in the form

$$\begin{pmatrix} \mathbf{x}(T) \\ \tilde{\mathbf{x}}_T \end{pmatrix} = \begin{pmatrix} \mathbf{\Phi}^{(k+1)}(T) & \mathbf{O} \\ \tilde{\mathbf{f}}_{k+1} & \mathcal{O} \end{pmatrix} \begin{pmatrix} \mathbf{x}(0) \\ \tilde{\mathbf{x}}_0 \end{pmatrix} , \tag{6.19}$$

where the function $\tilde{\mathbf{x}}_t$ is defined by the shift

$$\tilde{\mathbf{x}}_t(\vartheta) = \mathbf{x}(t+\vartheta) , \qquad \vartheta \in [-\tau, 0) . \tag{6.20}$$

Note that $\vartheta = 0$ is excluded here as opposed to $\mathbf{x}_t$ in (6.8). In (6.19), $\mathbf{O}$ denotes the zero functional, $\mathcal{O}$ denotes the zero operator, and $\tilde{\mathbf{f}}_{k+1}$ is the function

$$\tilde{\mathbf{f}}_{k+1}(\vartheta) = \begin{cases} \mathbf{\Phi}^{(k)}(\vartheta + T) & \text{if } \ -\tau \le \vartheta < (k-1)\tau - t_{\mathrm{a}} , \\ \mathbf{\Phi}^{(k+1)}(\vartheta + T) & \text{if } \ (k-1)\tau - t_{\mathrm{a}} \le \vartheta < 0 . \end{cases} \tag{6.21}$$

Equation (6.19) shows that the function $\mathbf{x}_T$ can be determined using only the initial state $\mathbf{x}(0)$ and does not depend on the initial function $\tilde{\mathbf{x}}_0$. The stability properties are determined by the $n \times n$ matrix $\mathbf{\Phi}^{(k+1)}(T)$. The system is asymptotically stable if all the eigenvalues of $\mathbf{\Phi}^{(k+1)}(T)$ have modulus less than 1. Therefore, in this case, the stability analysis requires the calculation of the eigenvalues of the $n \times n$ matrix $\mathbf{\Phi}^{(k+1)}(T)$ only.

For instance, if $k = 1$, i.e., $0 < t_{\mathrm{a}} \le \tau$, then the monodromy matrix is given as

$$\mathbf{\Phi}^{(2)}(T) = \mathrm{e}^{\mathbf{A}T} + \int_{t_{\mathrm{w}}}^{T} \mathrm{e}^{\mathbf{A}(T-s)} \mathbf{B}\mathbf{\Gamma}(s)\mathbf{C}\, \mathrm{e}^{\mathbf{A}(s-\tau)}\, \mathrm{d}s . \tag{6.22}$$

If $k = 2$, i.e., $\tau < t_{\mathrm{a}} \le 2\tau$, then

$$\begin{aligned} \mathbf{\Phi}^{(3)}(T) = \ & \mathrm{e}^{\mathbf{A}T} + \int_{t_{\mathrm{w}}}^{T} \mathrm{e}^{\mathbf{A}(T-s)} \mathbf{B}\mathbf{\Gamma}(s)\mathbf{C}\, \mathrm{e}^{\mathbf{A}(s-\tau)}\, \mathrm{d}s \\ & + \int_{t_{\mathrm{w}}+\tau}^{T} \mathrm{e}^{\mathbf{A}(T-s_1)} \mathbf{B}\mathbf{\Gamma}(s_1)\mathbf{C} \int_{t_{\mathrm{w}}}^{s_1-\tau} \mathrm{e}^{\mathbf{A}(s_1-s_2-\tau)} \mathbf{B}\mathbf{\Gamma}(s_2) C\, \mathrm{e}^{\mathbf{A}(s_2-\tau)}\, \mathrm{d}s_2\, \mathrm{d}s_1 . \end{aligned} \tag{6.23}$$

Note that if the waiting period is less then the feedback delay, i.e., $t_{\mathrm{w}} < \tau$, then the above derivation is not valid, and the monodromy operator cannot be represented in the $n \times n$ matrix form as in (6.22) or (6.23). Still, if the waiting and the acting periods t_{w} and t_{a} satisfy certain conditions, then a finite-dimensional monodromy matrix can be constructed for the case $t_{\mathrm{w}} < \tau$, too (for details, see [113]).

6.3 Case study: stick-balancing with reflex delay

Balancing an inverted pendulum in the presence of feedback delay is a frequently cited example in dynamics and control theory [206, 199, 141], and it is also a relevant issue to human motion control [213, 155, 10]. It is known that conventional proportional-derivative (PD) controllers cannot stabilize the upward position if the time delay is larger than a critical value. As was shown by Stépán [214], this critical delay for a continuous PD feedback can be given in the simple form $\tau_{\rm crit} = T_{\rm p}/\left(\pi\sqrt{2}\right)$, where $T_{\rm p}$ is the period of the small oscillations of the pendulum hanging at its downward position. The same phenomenon is often communicated such that for a given feedback delay, there is a critical minimum length of the pendulum: if the pendulum is shorter than this critical length, then the upward position is unstable for any PD controller [34].

Here, it will be shown that the application of the act-and-wait control concept helps in the stabilization of the upper equilibrium of the pendulum. The mechanical model of the system can be seen in Figure 6.2. The pendulum of length l and mass m is attached to the horizontal slide. The mass m_0 of the slide is assumed to be negligible relative to the mass of the pendulum. The general coordinates are the angular position φ of the stick and the position x of the pivot point. A control force Q is applied on the slide in order to balance the stick at $\varphi = 0$. The equation of motion for this system takes the form

$$\begin{pmatrix} \frac{1}{3}ml^2 & \frac{1}{2}ml\cos\varphi \\ \frac{1}{2}ml\cos\varphi & m \end{pmatrix} \begin{pmatrix} \ddot{\varphi} \\ \ddot{x} \end{pmatrix} + \begin{pmatrix} -\frac{1}{2}mgl\sin\varphi \\ -\frac{1}{2}ml\dot{\varphi}^2\sin\varphi \end{pmatrix} = \begin{pmatrix} 0 \\ Q(\varphi,\dot{\varphi}) \end{pmatrix} , \tag{6.24}$$

where g stands for the gravitational acceleration. The displacement x is a cyclic coordinate that can be eliminated from the equation. The essential motion φ is then governed by

$$\left(\frac{1}{3}ml^2 - \frac{1}{4}ml^2\cos^2\varphi\right)\ddot{\varphi} + \frac{1}{8}ml^2\dot{\varphi}^2\sin(2\varphi) - \frac{1}{2}mgl\sin\varphi = -\frac{1}{2}lQ(\varphi,\dot{\varphi})\cos\varphi \ . \tag{6.25}$$

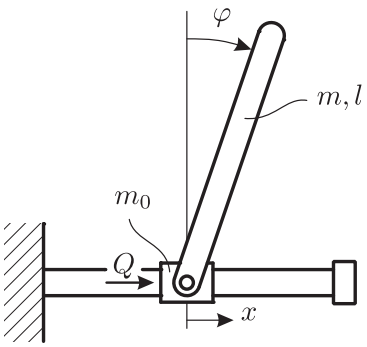

Figure 6.2: Mechanical model of stick-balancing.

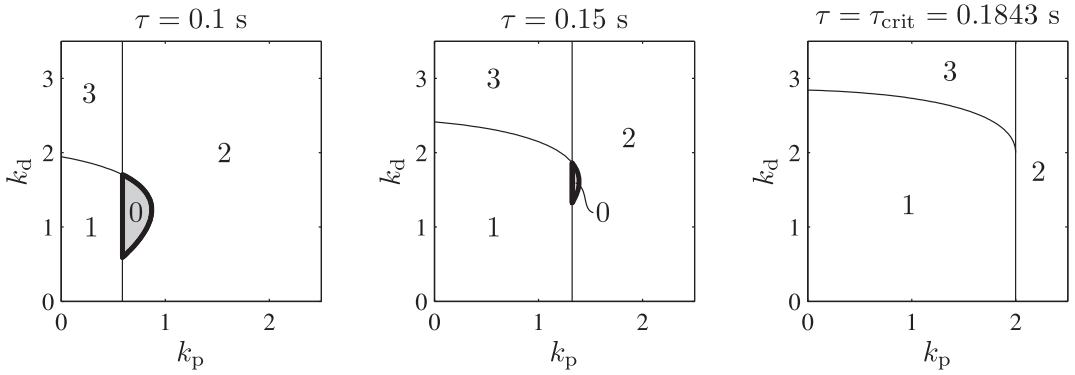

Figure 6.3: Number of unstable characteristic exponents for (6.28) with length $l = 1\,\text{m}$ and with different feedback delays τ.

The control force Q is assumed to be a locally linear function of the angular position φ and the angular velocity $\dot{\varphi}$ in the form

$$Q(\varphi, \dot{\varphi}) = K_{\text{p}}\varphi + K_{\text{d}}\dot{\varphi} + \text{h.o.t.}\,, \tag{6.26}$$

where K_{p} is the proportional gain, K_{d} is the derivative gain, and h.o.t. stands for the higher-order terms not modeled here.

Linearization around the upright position $\varphi = 0$ and modeling the delay τ in the feedback loop gives

$$\frac{1}{12}ml^2\ddot{\varphi}(t) - \frac{1}{2}mgl\varphi(t) = -\frac{1}{2}l\left(K_{\text{p}}\varphi(t-\tau) + K_{\text{d}}\dot{\varphi}(t-\tau)\right)\,. \tag{6.27}$$

Introducing new parameters, the system can be transformed into the form

$$\ddot{\varphi}(t) + a_0\varphi(t) = -k_{\text{p}}\varphi(t-\tau) - k_{\text{d}}\dot{\varphi}(t-\tau)\,, \tag{6.28}$$

where

$$a_0 = -\frac{6g}{l} < 0\,, \qquad k_{\text{p}} = \frac{6K_{\text{p}}}{ml}\,, \qquad k_{\text{d}} = \frac{6K_{\text{d}}}{ml}\,. \tag{6.29}$$

Stability charts for this system can be determined based on the D-subdivision method (see [167], [206]). Some stability charts are shown in Figure 6.3 for pendulum length $l = 1\,\text{m}$ and for different feedback delays τ. As can be seen, the stable domain shrinks with increasing feedback delay τ, and it disappears if $\tau > \tau_{\text{crit}}$. It is know (see, e.g., [206, 214]) that the value of the critical delay can be given as

$$\tau_{\text{crit}} = \sqrt{\frac{-2}{a_0}} = \sqrt{\frac{l}{3g}} = \frac{T_{\text{p}}}{\pi\sqrt{2}}\,, \tag{6.30}$$

where $T_{\text{p}} = \pi\sqrt{2l/(3g)}$ is the period of the small oscillations of the pendulum about its downward equilibrium. For a pendulum of length $l = 1\,\text{m}$, PD controllers with feedback delays larger than $\tau_{\text{crit}} = 0.1843\,\text{s}$ cannot stabilize the upward position.

Consider now the same system subjected to the act-and-wait controller in the form

$$\ddot{\varphi}(t) + a_0\varphi(t) = -g(t)\left(k_\mathrm{p}\varphi(t-\tau) + k_\mathrm{d}\dot{\varphi}(t-\tau)\right) \ , \tag{6.31}$$

where

$$g(t) = \begin{cases} 0 & \text{if } \ 0 \le (t \bmod T) < t_\mathrm{w} \ , \\ 1 & \text{if } \ t_\mathrm{w} \le (t \bmod T) < t_\mathrm{w} + t_\mathrm{a} = T \ , \end{cases} \tag{6.32}$$

is the act-and-wait switching function. Here, the feedback is zero for the waiting period, and constant proportional and derivative gains are applied in the acting period. The system can be written in the form

$$\dot{\mathbf{x}}(t) = \mathbf{A}\mathbf{x}(t) + g(t)\mathbf{B}\mathbf{u}(t-\tau) \ , \tag{6.33}$$

$$\mathbf{u}(t) = \mathbf{D}\mathbf{x}(t) \ , \tag{6.34}$$

where

$$\mathbf{x}(t) = \begin{pmatrix} \varphi(t) \\ \dot{\varphi}(t) \end{pmatrix} \ , \quad \mathbf{A} = \begin{pmatrix} 0 & 1 \\ -a_0 & 0 \end{pmatrix} \ , \quad \mathbf{B} = \begin{pmatrix} 0 \\ 1 \end{pmatrix} \ , \quad \mathbf{D} = \begin{pmatrix} -k_\mathrm{p} & -k_\mathrm{d} \end{pmatrix} \ . \tag{6.35}$$

Stability charts for (6.33)–(6.34) can be determined by the semi-discretization method, as shown in Chapter 3.

For the special case $t_\mathrm{w} \ge \tau$, the monodromy matrix can also be given in closed form, as shown in Section 6.2. For this purpose, the system should first be written in the form of (6.6), where $\mathbf{C}$ is the 2×2 identity matrix and $\mathbf{G}(t) = g(t)\mathbf{D}$. Then, the recurrence (6.16) with (6.13) can be used to obtain the closed-form representation of the monodromy matrix (see, e.g., (6.22) or (6.23) for the cases $0 < t_\mathrm{a} \le \tau$ or $\tau < t_\mathrm{a} \le 2\tau$, respectively).

A measure for the decay of the oscillations around the upper equilibrium is characterized by the magnitude of the critical (largest in modulus) characteristic multiplier μ_1, i.e., $\|\mathbf{x}_{t+T}\| \le |\mu_1| \, \|\mathbf{x}_t\|$. In order to compare cases with different act-and-wait periods $T = t_\mathrm{w} + t_\mathrm{a}$, introduce the decay ratio such that $\rho = |\mu_1|^{1/T}$. This decay ratio characterizes the decay over a unit time step, i.e., $\|\mathbf{x}_{t+1}\| \le \rho \, \|\mathbf{x}_t\|$.

Figure 6.4 shows a series of stability charts in the plane $(k_\mathrm{p}, k_\mathrm{d})$ for a pendulum of length $l = 1\,\mathrm{m}$ with feedback delay $\tau = 0.1\,\mathrm{s}$ for different acting and waiting periods. These diagrams can be considered projections of the 4 dimensional stability chart in the parameter space $(k_\mathrm{p}, k_\mathrm{d}, t_\mathrm{a}, t_\mathrm{w})$. The contour lines where the decay ratio ρ is equal to $1, 1.5, 2, \ldots$ are also presented. The stability boundaries, where $\rho = 1$, are indicated by thick lines. It can be seen that there is a qualitative change in the structure of the stable domains if the waiting period t_w becomes larger than the feedback delay τ. The reason is that in this case, the dynamics changes radically: the dimension of the

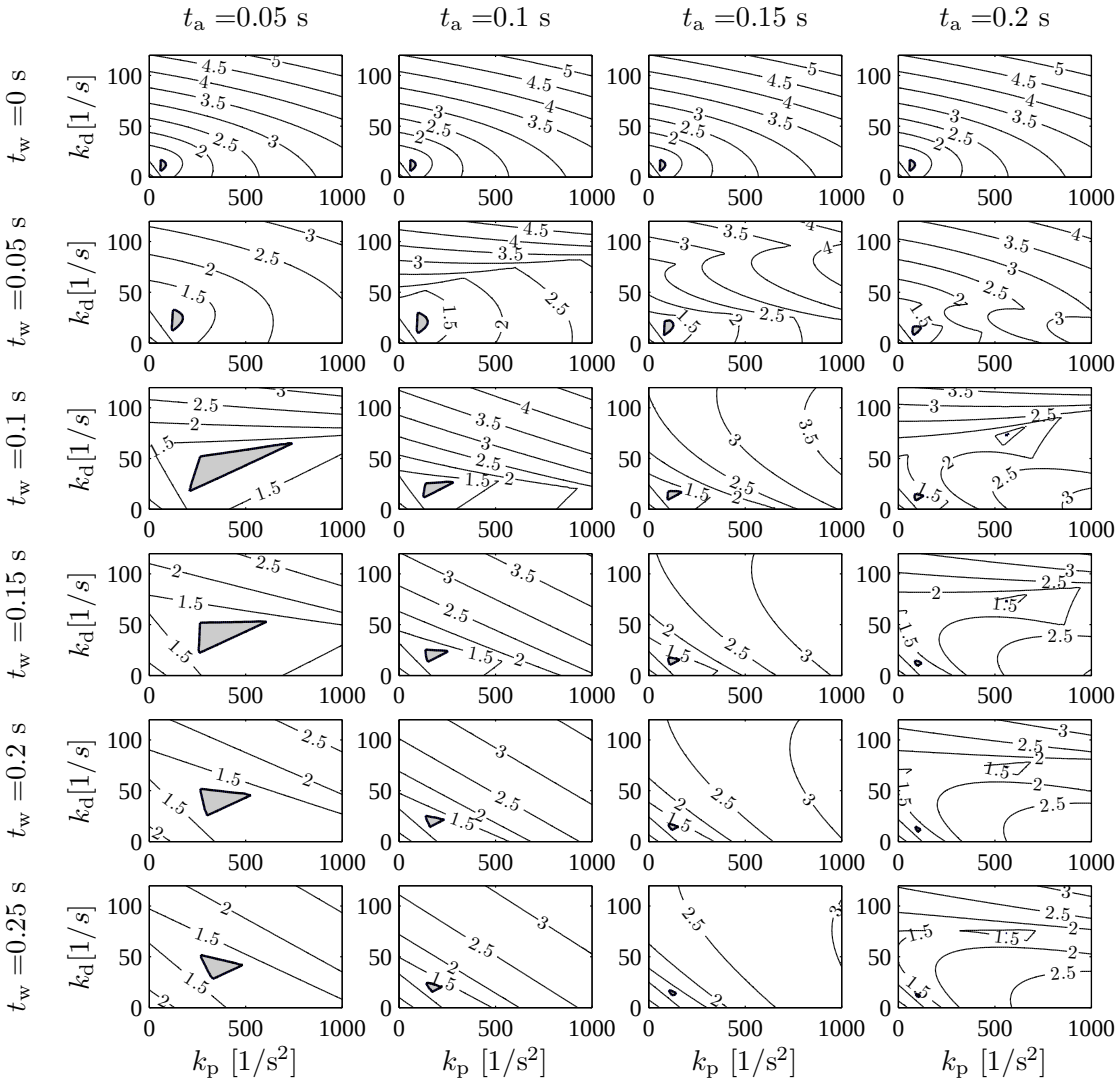

Figure 6.4: Stability charts and contour curves of the decay ratio $\rho = |\mu_1|^{1/T}$ for different acting and waiting periods for a pendulum of length $l = 1\,\mathrm{m}$ with feedback delay $\tau = 0.1\,\mathrm{s}$. Stable domains are indicated by gray shading.

system is reduced to $n = 2$, and the system is described by the corresponding 2×2 monodromy matrix. Consequently, the stability diagrams for the case $t_w \geq \tau = 0.1\,\mathrm{s}$ can also be obtained by analyzing the 2×2 matrix $\mathbf{\Phi}^{(2)}(T)$ or $\mathbf{\Phi}^{(3)}(T)$ in (6.22) or (6.23) depending on whether $0 < t_a \leq \tau$ or $\tau < t_a \leq 2\tau$.

In Figure 6.4, the feedback delay ($\tau = 0.1\,\mathrm{s}$) is smaller than the critical delay $\tau_{\mathrm{crit}} = 0.1843\,\mathrm{s}$; consequently, the system can be stabilized by the traditional (constant gain) controller as well. The diagrams for the case $t_w = 0$ correspond in fact to the stability chart in the left panel of Figure 6.3.

The same diagrams are presented in Figure 6.5 for a pendulum of length $l = 1\,\mathrm{m}$

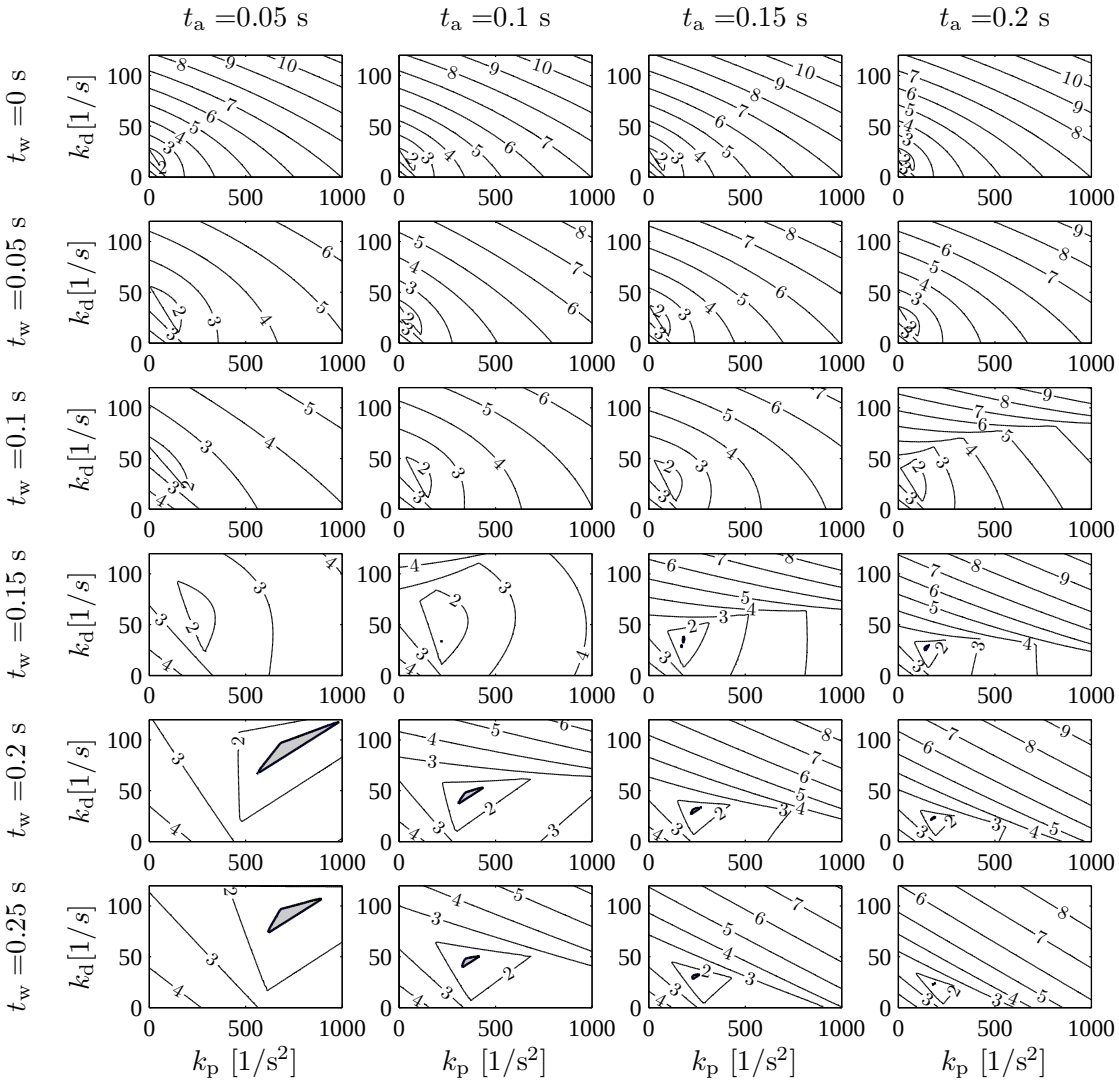

Figure 6.5: Stability charts and contour curves of the decay ratio $\rho = |\mu_1|^{1/T}$ for different acting and waiting periods for a pendulum of length $l = 1\,\mathrm{m}$ with feedback delay $\tau = 0.2\,\mathrm{s}$. Stable domains are indicated by gray shading.

with feedback delay $\tau = 0.2\,\mathrm{s}$. In this case, the feedback delay is larger than the critical value; consequently, the system cannot be stabilized by constant control gains. Periodic switching of the control gains according to the act-and-wait concept may, however, result in a stabilizing control. As can be seen, large triangular stable domains appear for $t_w \geq \tau = 0.2$, but small stable domains can also be observed in some plots with $t_w = 0.15\,\mathrm{s}$.

The act-and-wait concept provides an alternative for control systems with feedback delays. The traditional approach is the continuous use of constant control gains, when a cautious, slow feedback is applied with small gains, resulting in slow convergence (if

such a controller can stabilize the system at all). The act-and-wait control concept is a special case of periodic controllers, where time-varying control gains are used in the acting phase and zero gains are used in the waiting intervals. Several (actually, infinitely many) periodic functions could be chosen as time-periodic controllers. The main idea behind choosing the one that involves waiting intervals just longer than the feedback delay is that this kills the memory effect by waiting for the system's response induced by the previous action. Although it might seem unnatural not to actuate during the waiting interval at all, the act-and-wait concept is still a natural control logic for time-delayed systems. This is how, for example, one would adjust the shower temperature considering the delay between the controller (tap) and the sensed output (water temperature at skin).

6.4 New results

Thesis 4 *The act-and-wait control concept was introduced for continuous-time systems with feedback delay such that the feedback control is periodically switched off and on. It was shown that if the switch-off (or waiting) period is larger than the feedback delay, then the system is described by an n-dimensional discrete map with n being the order of the delay-free system. Consequently, only n characteristic multipliers should be monitored during the control design as opposed to the infinitely many characteristic exponents of the continuous-feedback controller.*

As a case study, a stick balancing problem was considered with reflex delay. The corresponding model was a PD controller with feedback delay. It was shown that by using the act-and-wait control concept, the stick can be balanced in the vertical position for such large reflex delays, for which the time-invariant PD controller cannot provide a stable control process.

The results composed in the thesis were published in Insperger [106] and also in the book Insperger and Stépán [115].

Chapter 7

Increasing the accuracy of force control process using the act-and-wait concept

Force control is an essential mechanical controlling problem in robotics, since most robotic applications involve interactions with other objects. The first publications on the basics of force-control approaches appeared in the early 1980s, starting with the pioneering work of Whitney [236], Mason [149], and Raibert and Craig [183]. Since then, several comprehensive textbooks have been published summarizing different methods of force-control processes in the field of robotics [40, 9, 139, 36, 205]. The aim of force control is to provide a desired force between the actuator and the environment (or workpiece). In order to achieve high accuracy in maintaining the prescribed contact force against Coulomb friction, high proportional control gains are to be used [40, 9]. However, in practical realizations of force-control processes with high proportional gains, the robot often loses stability, and starts to oscillate at a relatively low frequency. These oscillations are mainly caused by digital effects [236, 207, 211, 132, 131] and by time delays in the feedback loop [206, 69]. In spite of efforts to minimize time delays, they cannot be eliminated totally, even with today's advanced technology due to physical limits. Teleoperation is a typical example in which communication delay plays a crucial role [126, 7, 163, 130, 180], but similar delays may arise in haptic interfaces as well [37, 62].

In this chapter, a force control process is considered in the presence of feedback delay. The error in the contact force between the actuator and the environment is analyzed for a time-invariant proportional (P) controller and for the act-and-wait controller. In order to minimize the contact force error, the proportional gain in the controller should be increased. But on the other hand, for large proportional gains,

the system looses stability due to the feedback delay. Here, it is shown that the proportional gain and, consequently, the accuracy of the contact force can be increased by the application of the act-and-wait control concept. The theoretical results were confirmed by tendentious experiments for a range of feedback delays. The results are composed in Thesis 5 and have been published in Insperger et al. [111] and also in the book Insperger and Stépán [115].

7.1 Mechanical model and stability analysis for the continuous controller

The single-degree-of-freedom mechanical model of the force-control process is shown in Figure 7.1. The modal mass m_b and the equivalent stiffness k represent the inertia and the stiffness of the robot and the environment, while equivalent damping c models the viscous damping due to the servo motor characteristics and the environment. The force Q represents the controller's action, and C is the magnitude of the effective Coulomb friction. Considering a proportional force controller, the control force can be given as

$$Q(t) = F_\mathrm{d} - k_\mathrm{p}\left(F_\mathrm{m}(t) - F_\mathrm{d}\right) \ , \tag{7.1}$$

where k_p is the proportional gain, F_d is the desired force, and F_m is the measured force. The equation of motion reads

$$m_\mathrm{b}\ddot{q}(t) + c\dot{q}(t) + kq(t) = F_\mathrm{d} - k_\mathrm{p}\left(F_\mathrm{m}(t) - F_\mathrm{d}\right) - C\mathrm{sgn}\big(\dot{q}(t)\big) \ . \tag{7.2}$$

Assuming a steady-state condition by setting all the time derivatives to zero, considering a constant Coulomb friction force, and using that $F_\mathrm{m} = kq(t)$, the maximum force error can be given as

$$F_\mathrm{e}^\mathrm{max} = \frac{C}{1+k_\mathrm{p}} \ . \tag{7.3}$$

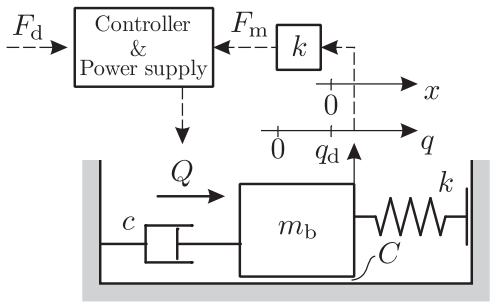

Figure 7.1: Single-degree-of-freedom mechanical model of force-control process.

Thus, the higher the gain k_p, the less the force error. Theoretically, there is no upper limit for the gain k_p, since the constant solution $q(t) \equiv q_\mathrm{d}$ of (7.2) is always asymptotically stable when $C = 0$. Experiments show, however, that the real system with feedback delay is not stable for large gain k_p [207]. Here, the goal is to decrease the force error by increasing the proportional gain k_p, but note that there exist other methods to compensate friction-caused stick-slip phenomena (see., e.g,. [140, 148]).

In practical realizations, the control force can be written in the form

$$Q(t) = F_\mathrm{d} - k_\mathrm{p}(F_\mathrm{m}(t-\tau) - F_\mathrm{d}) = kq_\mathrm{d} - k_\mathrm{p}\left(kq(t-\tau) - kq_\mathrm{d}\right) \ , \tag{7.4}$$

where τ is the time delay in the feedback loop. Thus, the equation of motion reads

$$m_\mathrm{b}\ddot{q}(t) + c\dot{q}(t) + kq(t) = kq_\mathrm{d} - k_\mathrm{p}\left(kq(t-\tau) - kq_\mathrm{d}\right) - C\mathrm{sgn}\big(\dot{q}(t)\big) \ . \tag{7.5}$$

Stability properties of the system can be determined by analyzing the variational system of (7.5) around the desired position q_d. For this calculation, the dry friction is neglected in the model. Considering that $q(t) = q_\mathrm{d} + x(t)$, the variational system reads

$$\ddot{x}(t) + 2\zeta\omega_\mathrm{n}\dot{x}(t) + \omega_\mathrm{n}^2 x(t) = -\omega_\mathrm{n}^2 k_\mathrm{p} x(t-\tau) \ , \tag{7.6}$$

where $\omega_\mathrm{n} = \sqrt{k/m_\mathrm{b}}$ is the natural angular frequency of the uncontrolled undamped system and $\zeta = c/(2m_\mathrm{b}\,\omega_\mathrm{n})$ is the damping ratio. The stability analysis can be performed by the D-subdivision method (see [167], [206]). The stability boundaries in the plane (τ, k_p) can be given as

$$\text{if } \omega = 0 \ : \quad k_\mathrm{p} = -1 \ , \tag{7.7}$$

$$\text{if } \omega \neq 0 \ : \quad \tau = \frac{1}{\omega}\left(j\pi - \arctan\left(\frac{2\zeta\omega_\mathrm{n}\omega}{\omega_\mathrm{n}^2 - \omega^2}\right)\right) \ , \quad j \in \mathbb{Z} \ , \tag{7.8}$$

$$k_\mathrm{p} = \frac{(-1)^j \mathrm{sgn}(\omega - \omega_n)}{\omega_n^2}\sqrt{\left(\omega_n^2 - \omega^2\right)^2 + 4\zeta^2\omega_n^2\omega^2} \ . \tag{7.9}$$

Stability charts for different damping parameters c are shown in Figure 7.2. The mass and the stiffness parameters are $m_\mathrm{b} = 29.57\,\mathrm{kg}$ and $k = 16414\,\mathrm{N/m}$. Stable domains with different gray shades are associated with different damping parameters c. If the feedback delay is zero, then the system is asymptotically stable for any $k_\mathrm{p} > -1$. Note that the system without control (i.e., if $k_\mathrm{p} = 0$) is stable itself, and the goal of the control is to ensure an accurate contact force.

7.2 Application of the act-and-wait control concept

Consider now the same system with an act-and-wait controller. In this case, the control force can be given as

$$Q_\mathrm{a\&w}(t) = F_\mathrm{d} - g(t)k_\mathrm{p}(F_\mathrm{m}(t-\tau) - F_\mathrm{d}) \ , \tag{7.10}$$

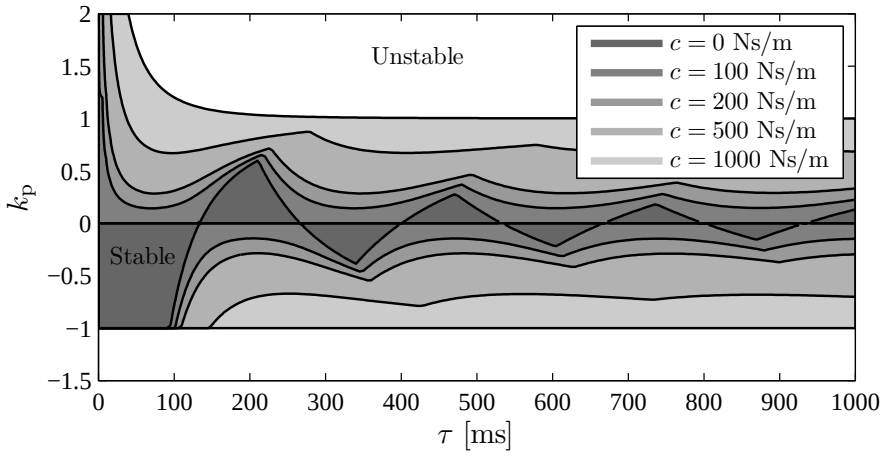

Figure 7.2: Stability charts for (7.6) with different damping parameters.

where $g(t)$ is the T-periodic act-and-wait switching function defined in (6.32). Thus,

$$Q_{\mathrm{a\&w}} = \begin{cases} F_\mathrm{d} & \text{if } \ 0 \le (t \bmod T) < t_\mathrm{w} \ , \\ F_\mathrm{d} - k_\mathrm{p}(F_\mathrm{m}(t-\tau) - F_\mathrm{d}) & \text{if } \ t_\mathrm{w} \le (t \bmod T) < t_\mathrm{w} + t_\mathrm{a} = T \ . \end{cases} \tag{7.11}$$

This means that the control force is equal to the desired force for period of length t_w, and the feedback is switched on only for periods of length t_a. The corresponding variational system reads

$$\ddot{x}(t) + 2\zeta\omega_\mathrm{n}\dot{x}(t) + \omega_\mathrm{n}^2 x(t) = -g(t)\omega_\mathrm{n}^2 k_\mathrm{p} x(t-\tau) \ , \tag{7.12}$$

where

$$g(t) = \begin{cases} 0 & \text{if } \ 0 \le (t \bmod T) < t_\mathrm{w} \ , \\ 1 & \text{if } \ t_\mathrm{w} \le (t \bmod T) < t_\mathrm{w} + t_\mathrm{a} = T \ , \end{cases} \tag{7.13}$$

is the act-and-wait switching function. Transformation into first-order form gives

$$\dot{\mathbf{x}}(t) = \mathbf{A}\mathbf{x}(t) + g(t)\mathbf{B}\mathbf{u}(t-\tau) \ , \tag{7.14}$$

$$\mathbf{u}(t) = \mathbf{D}\mathbf{x}(t) \ , \tag{7.15}$$

with

$$\mathbf{x}(t) = \begin{pmatrix} x(t) \\ \dot{x}(t) \end{pmatrix} \ , \quad \mathbf{A} = \begin{pmatrix} 0 & 1 \\ -\omega_\mathrm{n}^2 & -2\zeta\omega_\mathrm{n} \end{pmatrix} \ , \quad \mathbf{B} = \begin{pmatrix} 0 \\ -\omega_\mathrm{n}^2 \end{pmatrix} \ , \quad \mathbf{D} = \begin{pmatrix} k_\mathrm{p} & 0 \end{pmatrix} \ . \tag{7.16}$$

Stability charts for (7.14)–(7.15) can be determined by the semi-discretization method. Alternatively, if $t_\mathrm{w} \ge \tau$ and $0 < t_\mathrm{a} \le \tau$, then the monodromy matrix of the system can also be determined in closed form according to (6.22).

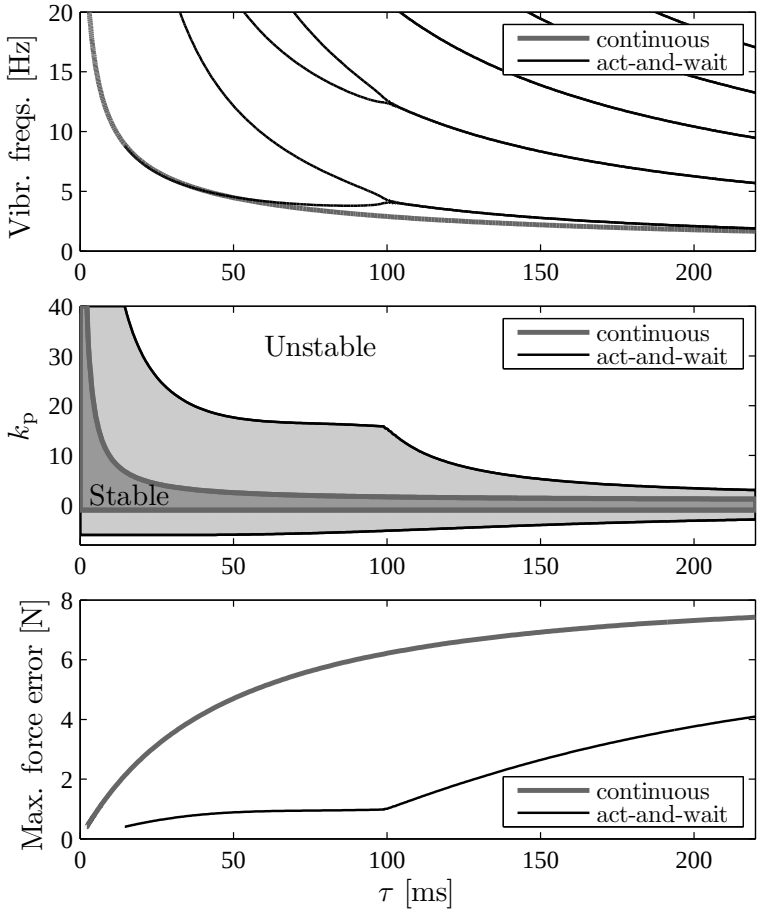

Figure 7.3: Theoretically predicted stability charts, frequency diagrams and the maximum force error for the continuous and for the act-and-wait control concept.

Let μ_1 denote the critical (maximum in modulus) eigenvalue. The system is asymptotically stable if $|\mu_1| < 1$. The frequency of the resulting self-excited vibrations at the loss of stability is related to the phase angle

$$\omega_1 = \frac{1}{T}\mathrm{Im}\ (\ln(\mu_1)) = \frac{1}{T}\arctan\left(\frac{\mathrm{Im}\,\mu_1}{\mathrm{Re}\,\mu_1}\right) \tag{7.17}$$

with $-\pi < \omega_1 T \leq \pi$. The vibration frequencies are the positive values of

$$f = \pm\frac{\omega_1}{2\pi} + \frac{j}{T} \quad [\mathrm{Hz}], \quad j = 0, \pm 1, \pm 2, \ldots . \tag{7.18}$$

Figure 7.3 presents the stability charts (middle panel), the vibration frequencies along the stability boundaries (top panel), and the maximum force error (bottom panel) for the continuous controller described by (7.4) and for the act-and-wait controller given by (7.11). The parameters are $m_\mathrm{b} = 29.57\,\mathrm{kg}$, $k = 16414\,\mathrm{N/m}$, $c = 1447\,\mathrm{Ns/m}$, and the Coulomb friction force is $C = 16.5\,\mathrm{N}$. The length of the waiting period is equal to the feedback delay, i.e., $t_\mathrm{w} = \tau$, while the ratio of the acting period length and

the delay is set to a fixed number $t_a/\tau = 0.2$. It can be seen that the maximum achievable stable proportional gain k_p is larger for the act-and-wait controller than for the continuous one. The maximum force error is determined by the maximum stable gain k_p (see equation (7.3)). Consequently, the act-and-wait controller results in a smaller force error than the continuous controller. The frequency diagram shows that while the continuous control case is associated with a single vibration frequency, for the act-and-wait control case, a series of vibration frequencies arises according to equation (7.18).

7.3 Experimental verification

For the experimental validation of the theoretical results, a HIRATA (MB-H180-500) DC drive robot was used (see Fig. 7.4). The axis of the robot was connected to the base of the robot (environment) by a helical spring of stiffness $k = 16414\,\mathrm{N/m}$. The contact force was measured by a Tedea-Huntleight Model 355 load cell mounted between the spring and the robot's flange. The driving system of the moving axis consisted of a HIRATA HRM-020-100-A DC servo motor connected directly to a ballscrew with a 20 mm pitch thread. The robot was controlled by a micro-controller based control unit providing the maximum sampling frequency 1 kHz for the overall force control loop. This controller made it also possible to vary the time delay as integer multiples of 1 ms, and to set the control force by the pulse width modulation (PWM) of supply voltage of the DC motor. Time delay was varied between 20 and 200 ms, which are significantly larger than the sampling period 1 ms; therefore, the system can be considered a continuous-time system. The modal mass and the damping ratio were experimentally determined: $m_b = 29.57\,\mathrm{kg}$ and $c = 1447\,\mathrm{Ns/m}$. The Coulomb friction was measured to be $C = 16.5\,\mathrm{N}$. The desired force was $F_d = 50\,\mathrm{N}$.

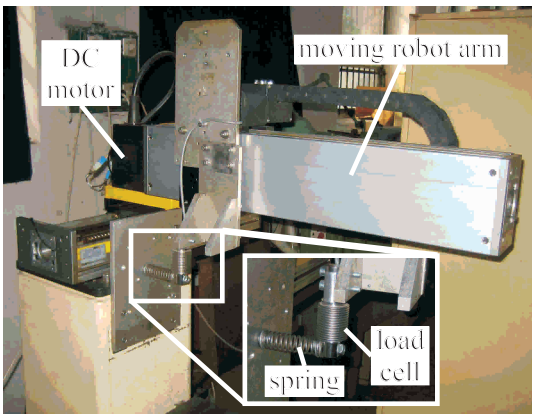

Figure 7.4: Experimental setup.

The measurements were performed at the Department of Manufacturing Sciences and Technology (BME) with my colleague, Dr. László Kovács. The programming of the robot arm was provided by Péter Galambos and András Juhász. Their help is gratefully acknowledged.

During the measurements, the time delay was fixed and the proportional gain was increased slowly until the process lost stability for perturbations larger than 50 N. The displacement of the force sensor was recorded during the loss of stability in order to analyze the frequency content of the motion. Then, the gain k_{p} was set to 90% of the critical value to obtain a stable process, the system was perturbed three times, and the resulting force errors were documented (three for each fixed time delay).

Figures 7.5 and 7.6 show a comparison of the theoretical predictions with some experimental results for the continuous controller and for the act-and-wait controller, respectively. The figures present the stability charts (left middle panel), the associated frequency diagrams (left top panel), the maximum force error (left bottom panel), and series of power spectrum density (PSD) diagrams for the test points with different feedback delays (right panels). The experimental stability boundaries and the measured maximum force errors are represented by crosses. The theoretically predicted vibration frequencies are also shown in the experimental PSD diagrams by black dots for reference. It can clearly be seen that the experimental results show good agreement with the theoretical predictions. The critical proportional gains for the act-and-wait controller are 2-3-times larger than those for the the continuous controller. The theoretically predicted vibration frequencies coincide with the measured frequencies. Regarding the remaining force error, there are some discrepancies between the theoretical predictions and the measurements, but the tendency can clearly be seen: the measured force errors are significantly smaller for the act-and-wait controller than those for the the continuous controller.

A similar analysis for a digital force control process with sampling effect, see Insperger et al. [114].

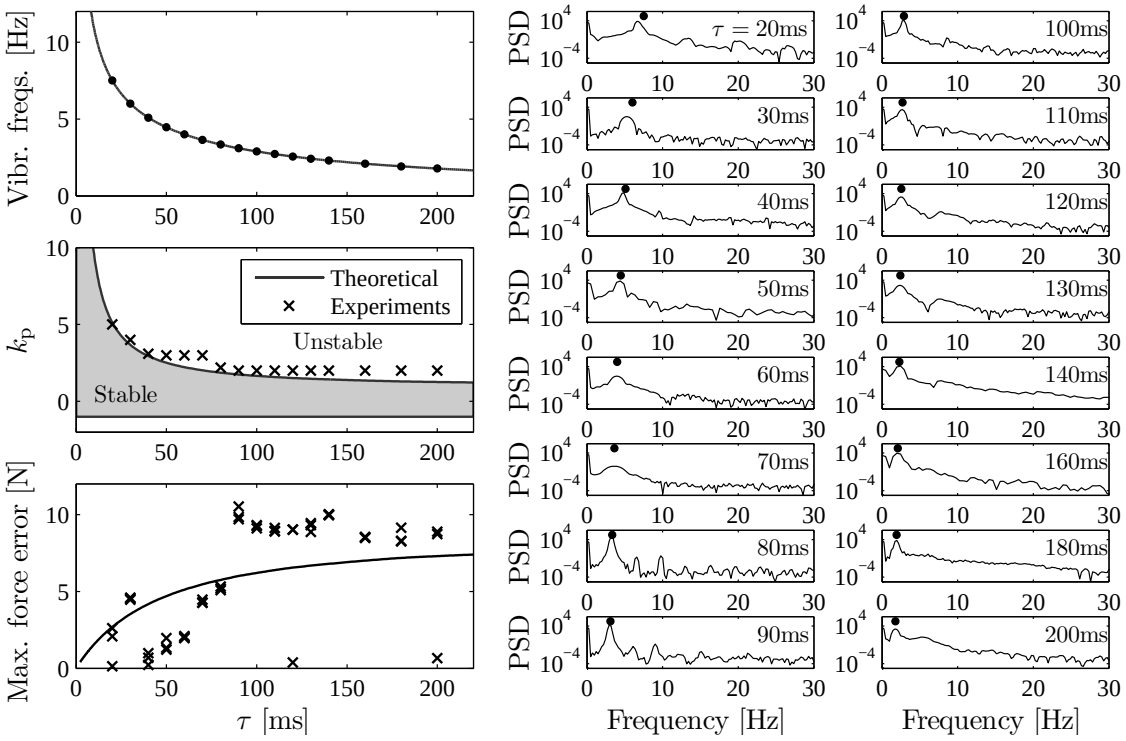

Figure 7.5: Comparison of the theoretical stability chart, vibration frequencies, and force errors to the experimental results for the continuous controller.

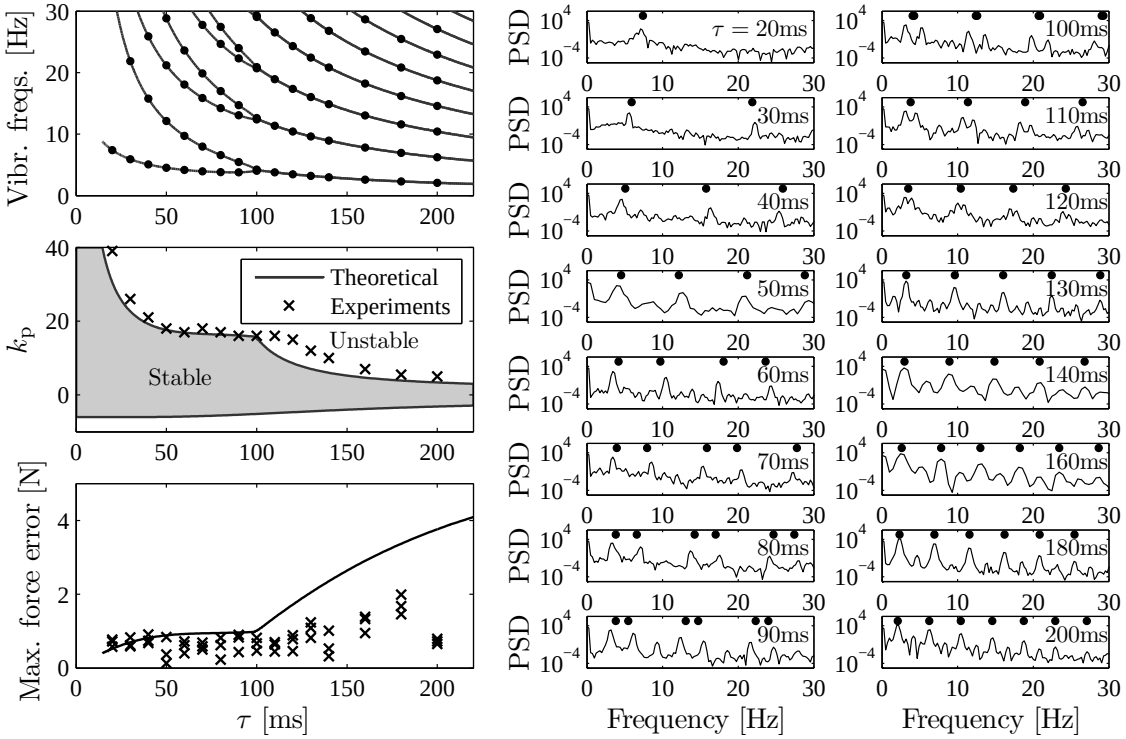

Figure 7.6: Comparison of the theoretical stability chart, vibration frequencies, and force errors to the experimental results for the act-and-wait controller.

7.4 New results

Thesis 5 *The act-and-wait control concept was applied to a single-degree-of-freedom force control problem with feedback delay and compared to the traditional, continuous-feedback controller. Stability charts were constructed that plots the critical proportional gains, where the process looses stability, as function of the feedback delay. It was shown that the application of the act-and-wait concept allows the use of larger proportional gains without loosing stability. Since the force error decreases with increasing proportional gain, the accuracy of the force control process can significantly be increased if the act-and-wait concept is used.*

The theoretical results were confirmed by experiments for a range of feedback delays. Vibration frequencies at the stability boundaries were used to verify the model. The theoretically predicted frequencies agreed well with the measured frequencies. The experiments confirmed that the application of the act-and-wait concept allows the use of 2-3-times larger proportional gains without losing stability. It was also confirmed that the force error can significantly be decreased by the application of the act-and-wait control concept.

The results composed in the thesis were published in Insperger et al. [111] and also in the book Insperger and Stépán [115].

Chapter 8

Summary

In this dissertation, engineering problems were considered where the governing equations involve terms with varying time delays in their arguments. The early engineering models in the 1940s where time delay played crucial role, like the wheel shimmy problem [190], the ship stabilization model [157] or the feedback control systems [228]), were all associated with constant delays. The corresponding mathematical theorems, like existence, uniqueness or continuous dependence were established only later for different classes of functional differential equations by Myshkis [164], Bellman and Cooke [19], Èl'sgol'c [54], Halanay [77], Hale [78], Driver [51], Kolmanovskii and Nosov [127], just to mention a few. This knowledge were then continuously transferred to different engineering applications resulting in more and more sophisticated mechanical models including distributed delays [209, 210, 220], time-varying delays [175, 103, 241] or state-dependent delays [108, 14].

The theses presented in Chapters 3–7 are all related to DDEs with varying time delays. In Chapter 3, higher-order versions of the numerical semi-discretization method was presented for linear periodic DDEs including cases with periodically varying delays. This method was then applied to problems from different field of engineering in the next chapters. In Chapter 4, a two-degrees-of-freedom model of orthogonal turning process was analyzed considering the relative vibrations between the tool and the workpiece, which resulted in a state-dependent delay in the governing equation. The associated linear system and the corresponding stability charts were determined in an analytic way. In Chapter 5, single-degree-of-freedom milling process with spindle speed modulation was consider with some special parameter combination such that the governing equation is a periodic DDE with periodic delay. Stability charts for this system were constructed using the first-order semi-discretization method presented in Chapter 3. In Chapter 6, a special periodic controller was introduced for systems with feedback delay. The point of the so-called act-and-wait control concept is that the feedback control is periodically switched off and on. This can also be considered as a kind of time-varying delay:

during the acting (switch-on) period, the time delay in the governing equation is the feedback delay, while for the waiting (switch-off) period, there is no time delay in the system. Finally, in Chapter 7, an application of the act-and-wait concept is presented for a force control process.

Overall, it can be stated that varying time delay has a kind of stabilizing effect in all the engineering models analyzed in Chapters 4–7. For the turning model with state-dependent delay in Chapter 4, it was obtained that the domains of stability are slightly larger for the state-dependent-delay model than for the constant delay model. This difference is due to the explicit dependence of the cutting force on the state-dependent delay. In this case, the state-dependency of the delay can be considered as a kind of compliance compared to the "stiff" constant delay that is capable to stabilize the system. For the varying-spindle speed milling, the time delay is varying periodically in time according to a prescribed function. The idea behind this technique is to disturb the regenerative effect such that each flute experiences a different regenerative delay. For low spindle speeds this technique has a stabilizing effect. For high spindle speeds, spindle speed variation may either stabilize or destabilize the milling process depending on the spindle speed–depth of cut combination. For the act-and-wait control concept in Chapters 6 and 7, the time delay is switched off and on periodically. If the waiting period is larger than the feedback delay, then the delay can be eliminated, which results in a finite dimensional system instead of the infinite dimensional one. The corresponding stability charts showed that the stability domains for the act-and-wait controller are larger compared to the case of continuously active controller. In some cases, the act-and-wait controller provides a stable process even for such large feedback delays, for which the continuous-feedback controller cannot provide a stable control process.

Appendix A

Solution of Linear Inhomogeneous ODEs

In this appendix, the solutions for linear homogeneous and inhomogeneous ODEs are given.

Consider first the linear homogeneous ODE

$$\dot{\mathbf{y}}(t) = \mathbf{A}\mathbf{y}(t) \,, \tag{A.1}$$

where $\mathbf{y}(t) \in \mathbb{R}^n$ and $\mathbf{A}$ is an $n \times n$ matrix. The solution for this system associated with the initial state $\mathbf{y}(t_0) = \mathbf{y}_0$ can be given as

$$\mathbf{y}(t) = \mathrm{e}^{\mathbf{A}t}\mathbf{y}_0 \,, \tag{A.2}$$

where the matrix exponential is defined by the Taylor series of the exponential function as

$$\mathrm{e}^{\mathbf{A}t} = \exp(\mathbf{A}t) := \sum_{k=0}^{\infty} \frac{1}{k!}\mathbf{A}^k t^k \,, \tag{A.3}$$

with $\mathbf{A}^0 = \mathbf{I}$ being the identity matrix (see, for instance, [90, 179]). The following properties hold:

$$\frac{\mathrm{d}}{\mathrm{d}t}\,\mathrm{e}^{\mathbf{A}t} = \mathbf{A}\,\mathrm{e}^{\mathbf{A}t} = \mathrm{e}^{\mathbf{A}t}\mathbf{A} \,, \qquad \mathrm{e}^{\mathbf{A}0} = \mathbf{I} \,, \qquad \det\left(\mathrm{e}^{\mathbf{A}t}\right) \neq 0 \,, \qquad \left(\mathrm{e}^{\mathbf{A}t}\right)^{-1} = \mathrm{e}^{-\mathbf{A}t} \,. \tag{A.4}$$

The matrix exponential $\mathrm{e}^{\mathbf{A}t}$ can be calculated in terms of the eigenvalues and eigenvectors of $\mathbf{A}$. For instance, if $\mathbf{A}$ is a 2×2 matrix, then there exists an invertible transformation matrix $\mathbf{P}$ (whose columns consist of the generalized eigenvectors of $\mathbf{A}$) such that $\mathbf{J} = \mathbf{P}^{-1}\mathbf{A}\mathbf{P}$ has one of the following forms:

$$\mathbf{J} = \begin{pmatrix} \lambda & 0 \\ 0 & \mu \end{pmatrix} \,, \qquad \mathbf{J} = \begin{pmatrix} \lambda & 1 \\ 0 & \lambda \end{pmatrix} \,, \qquad \mathbf{J} = \begin{pmatrix} a & -b \\ b & a \end{pmatrix} \,, \tag{A.5}$$

where $\lambda, \mu, a, b \in \mathbb{R}$. The corresponding matrix exponentials read

$$\mathrm{e}^{\mathbf{J}t} = \begin{pmatrix} \mathrm{e}^{\lambda t} & 0 \\ 0 & \mathrm{e}^{\mu t} \end{pmatrix}, \qquad \mathrm{e}^{\mathbf{J}t} = \begin{pmatrix} \mathrm{e}^{\lambda t} & t\,\mathrm{e}^{\lambda t} \\ 0 & \mathrm{e}^{\lambda t} \end{pmatrix}, \qquad \mathrm{e}^{\mathbf{J}t} = \mathrm{e}^{at} \begin{pmatrix} \cos(bt) & -\sin(bt) \\ \sin(bt) & \cos(bt) \end{pmatrix}, \tag{A.6}$$

respectively. The matrix exponential $\mathrm{e}^{\mathbf{A}t}$ can then be given by

$$\mathrm{e}^{\mathbf{A}t} = \mathrm{e}^{\mathbf{P}\mathbf{J}\mathbf{P}^{-1}t} = \mathbf{P}\,\mathrm{e}^{\mathbf{J}t}\mathbf{P}^{-1}\,. \tag{A.7}$$

For $n \times n$ matrices with $n > 2$, the matrix exponential can be determined in a similar way using the Jordan form transformation of the matrix (see, for instance, [90, 179]). Matrix exponentials can be calculated by most of the numerical and symbolic software packages, as well.

Consider now the linear inhomogeneous ODE

$$\dot{\mathbf{y}}(t) = \mathbf{A}\mathbf{y}(t) + \mathbf{b}(t)\,, \tag{A.8}$$

where $\mathbf{y}(t) \in \mathbb{R}^n$, $\mathbf{A}$ is an $n \times n$ matrix, and $\mathbf{b}(t) \in \mathbb{R}^n$ is a continuous function. The solution is determined by the method called variation of constants. The solution is searched for in the form

$$\mathbf{y}(t) = \mathrm{e}^{\mathbf{A}t}\mathbf{g}(t)\,, \tag{A.9}$$

where $\mathbf{g}(t) \in \mathbb{R}^n$ is a differentiable function. Every solution can be written in this form, since $\mathrm{e}^{\mathbf{A}t}$ is invertible. Differentiation of (A.9) yields

$$\dot{\mathbf{y}}(t) = \mathbf{A}\,\mathrm{e}^{\mathbf{A}t}g(t) + \mathrm{e}^{\mathbf{A}t}\dot{\mathbf{g}}(t)\,. \tag{A.10}$$

Substitution into (A.8) gives

$$\mathrm{e}^{\mathbf{A}t}\dot{\mathbf{g}}(t) = \mathbf{b}(t)\,, \tag{A.11}$$

which implies

$$\mathbf{g}(t) = \int_{t_0}^{t} \mathrm{e}^{-\mathbf{A}s}\mathbf{b}(s)\,\mathrm{d}s + \mathbf{K}\,, \tag{A.12}$$

where $\mathbf{K}$ is a constant vector. The solution reads

$$\mathbf{y}(t) = \mathrm{e}^{\mathbf{A}t}\int_{t_0}^{t} \mathrm{e}^{-\mathbf{A}s}\mathbf{b}(s)\,\mathrm{d}s + \mathrm{e}^{\mathbf{A}t}\mathbf{K}\,. \tag{A.13}$$

The initial condition $\mathbf{y}(t_0) = \mathbf{y}_0$ is satisfied if

$$\mathbf{K} = \mathrm{e}^{-\mathbf{A}t_0}\mathbf{y}_0\,. \tag{A.14}$$

Thus, the solution of (A.8) for the initial condition $\mathbf{y}(t_0) = \mathbf{y}_0$ reads

$$\mathbf{y}(t) = \mathrm{e}^{\mathbf{A}(t-t_0)}\mathbf{y}_0 + \int_{t_0}^{t} \mathrm{e}^{\mathbf{A}(t-s)}\mathbf{b}(s)\,\mathrm{d}s\,. \tag{A.15}$$

This formula is called the variation of constants formula or the Duhamel–Neumann formula for linear inhomogeneous ODEs.

An Example: the Forced Oscillator

Consider the linear forced oscillator

$$\ddot{x}(t) + ax(t) = b\cos(\omega t)\ , \tag{A.16}$$

with $a = \alpha^2 > 0$, $\omega > 0$. This system can be written in the form of (A.8) with

$$\mathbf{y}(t) = \begin{pmatrix} x(t) \\ \dot{x}(t) \end{pmatrix}\ , \quad \mathbf{A} = \begin{pmatrix} 0 & 1 \\ -a & 0 \end{pmatrix}\ , \quad \mathbf{b}(t) = \begin{pmatrix} 0 \\ b\cos(\omega t) \end{pmatrix}\ . \tag{A.17}$$

If $a = \alpha^2 > 0$, then the matrix exponential can be given as

$$\mathrm{e}^{\mathbf{A}t} = \begin{pmatrix} \cos(\alpha t) & \frac{1}{\alpha}\sin(\alpha t) \\ -\alpha\sin(\alpha t) & \cos(\alpha t) \end{pmatrix}\ . \tag{A.18}$$

Application of the variation of constants formula (A.15) with the initial state $\mathbf{y}(0) = \mathbf{y}_0 = (x_0,\ v_0)^T$ gives the solution

$$\begin{aligned} \mathbf{y}(t) &= \begin{pmatrix} \cos(\alpha t) & \frac{1}{\alpha}\sin(\alpha t) \\ -\alpha\sin(\alpha t) & \cos(\alpha t) \end{pmatrix} \begin{pmatrix} x_0 \\ v_0 \end{pmatrix} + \int_0^t \begin{pmatrix} \frac{b}{\alpha}\sin(\alpha(t-s))\cos(\omega s) \\ b\cos(\alpha(t-s))\cos(\omega s) \end{pmatrix} \mathrm{d}s \\ &= \begin{pmatrix} \left(x_0 + \frac{b}{\omega^2-\alpha^2}\right)\cos(\alpha t) + \frac{v_0}{\alpha}\sin(\alpha t) - \frac{b}{\omega^2-\alpha^2}\cos(\omega t) \\ v_0\cos(\alpha t) + \left(-\alpha x_0 - \frac{b\alpha}{\omega^2-\alpha^2}\right)\sin(\alpha t) + \frac{b\omega}{\omega^2-\alpha^2}\sin(\omega t) \end{pmatrix}\ . \end{aligned} \tag{A.19}$$

Alternatively, according to the theory of forced oscillators, the solution of (A.16) is searched for in the form

$$x(t) = C_1\cos(\alpha t) + C_2\sin(\alpha t) + x_{\mathrm{p}}(t)\ , \tag{A.20}$$

where $x_{\mathrm{p}}(t)$ is the particular solution of the form

$$x_{\mathrm{p}}(t) = K\cos(\omega t) + L\sin(\omega t)\ . \tag{A.21}$$

Substitution of (A.21) into (A.16) gives

$$K = -\frac{b}{\omega^2 - \alpha^2}\ , \qquad L = 0\ . \tag{A.22}$$

The parameters C_1 and C_2 are obtained by the substitution of the initial conditions $x(0) = x_0$, $\dot{x}(0) = v_0$, which gives

$$C_1 = x_0 + \frac{b}{\omega^2 - \alpha^2}\ , \qquad C_2 = \frac{v_0}{\alpha}\ . \tag{A.23}$$

Thus, the solution and its derivative read

$$x(t) = \left(x_0 + \frac{b}{\omega^2 - \alpha^2}\right)\cos(\alpha t) + \frac{v_0}{\alpha}\sin(\alpha t) - \frac{b}{\omega^2 - \alpha^2}\cos(\omega t)\ , \tag{A.24}$$

$$\dot{x}(t) = \left(-x_0\alpha - \frac{b\alpha}{\omega^2 - \alpha^2}\right)\sin(\alpha t) + v_0\cos(\alpha t) - \frac{b\omega}{\omega^2 - \alpha^2}\cos(\omega t)\ , \tag{A.25}$$

which are equivalent to (A.19).

Appendix B

Rate of convergence estimates for the semi-discretization method

In this appendix, the terms

$$\mathbf{J}_0(h) = \int_0^h \mathbf{A}(s)\mathbf{x}(s) - \mathbf{A}_0\mathbf{x}(s)\,\mathrm{d}s\,, \tag{B.1}$$

$$\mathbf{J}_{j,1}(h) = \int_0^h \mathbf{B}_j(s)\mathbf{u}(s-\tau_j(s)) - \mathbf{B}_{j,0}\mathbf{u}(s-\tau_j(s))\,\mathrm{d}s\,, \tag{B.2}$$

$$\mathbf{J}_{j,2}(h) = \int_0^h \mathbf{B}_{j,0}\mathbf{u}(s-\tau_j(s)) - \mathbf{B}_{j,0}\mathbf{u}(s-\tau_{j,0})\,\mathrm{d}s\,, \tag{B.3}$$

$$\mathbf{J}_{j,4}(h) = \int_0^h \mathbf{B}_{j,0}\mathbf{D}\mathbf{y}(s-\tau_{j,0}) - \mathbf{B}_{j,0}\mathbf{\Gamma}_{j,0}^{(q)}(s-\tau_{j,0})\,\mathrm{d}s \tag{B.4}$$

in (3.38) are determined as power series of the discretization step h. For this analysis, consider the Taylor expansions

$$\mathbf{x}(t) = \tilde{\mathbf{x}}_0 + \tilde{\mathbf{x}}_1 t + \tilde{\mathbf{x}}_2 t^2 + \cdots\,, \tag{B.5}$$

$$\mathbf{y}(t) = \tilde{\mathbf{y}}_0 + \tilde{\mathbf{y}}_1 t + \tilde{\mathbf{y}}_2 t^2 + \cdots\,, \tag{B.6}$$

$$\mathbf{A}(t) = \tilde{\mathbf{A}}_0 + \tilde{\mathbf{A}}_1 t + \tilde{\mathbf{A}}_2 t^2 + \cdots\,, \tag{B.7}$$

$$\mathbf{B}_j(t) = \tilde{\mathbf{B}}_{j,0} + \tilde{\mathbf{B}}_{j,1} t + \tilde{\mathbf{B}}_{j,2} t^2 + \cdots\,, \qquad j = 1,2,\ldots,g\,, \tag{B.8}$$

$$\tau_j(t) = \tilde{\tau}_{j,0} + \tilde{\tau}_{j,1} t + \tilde{\tau}_{j,2} t^2 + \cdots\,, \qquad j = 1,2,\ldots,g\,. \tag{B.9}$$

Note that the initial assumption $\mathbf{x}_t(0) \equiv \mathbf{y}_t(0)$ implies $\tilde{\mathbf{x}}_0 = \tilde{\mathbf{y}}_0$. Equations (3.7), (3.8) and (3.9) give

$$\mathbf{A}_0 = \frac{1}{h}\int_0^h \mathbf{A}(s)\mathrm{d}t = \tilde{\mathbf{A}}_0 + \frac{1}{2}\tilde{\mathbf{A}}_1 h + \frac{1}{3}\tilde{\mathbf{A}}_2 h^2 + \cdots\,, \tag{B.10}$$

$$\mathbf{B}_{j,0} = \frac{1}{h}\int_0^h \mathbf{B}_j(t)\,\mathrm{d}t = \tilde{\mathbf{B}}_0 + \frac{1}{2}\tilde{\mathbf{B}}_1 h + \frac{1}{3}\tilde{\mathbf{B}}_2 h^2\,, \qquad j = 1,2,\ldots,g\,, \tag{B.11}$$

$$\tau_{j,0} = \frac{1}{h}\int_0^h \tau_j(t)\,\mathrm{d}t = \tilde{\tau}_{j,0} + \frac{1}{2}\tilde{\tau}_{j,1} h + \frac{1}{3}\tilde{\tau}_{j,2} h^2 + \cdots\,, \qquad j = 1,2,\ldots,g\,. \tag{B.12}$$

Furthermore, we will also use the equations

$$\mathbf{u}(t) = \mathbf{D}\mathbf{x}(t) \ , \tag{B.13}$$

$$\mathbf{v}(t_i) = \mathbf{D}\mathbf{y}(t_i), \tag{B.14}$$

(see equations (3.2) and (3.6)).

Using the above Taylor expansions and taking into account (B.13) and (B.14), the magnitude of the terms $\mathbf{J}_0(h)$, $\mathbf{J}_{j,1}(h)$ and $\mathbf{J}_{j,2}(h)$ can be estimated with respect to the discretization step h. Substitution of the Taylor expansions (B.5) and (B.7) with (B.10) into (B.1) gives

$$\mathbf{J}_0(h) = \frac{1}{12}\tilde{\mathbf{A}}_1\tilde{\mathbf{x}}_1 h^3 + \mathcal{O}(h^4) \ . \tag{B.15}$$

Substitution of the Taylor expansions (B.5), (B.8) and (B.9) with (B.13) and (B.11) into (B.2) give

$$\mathbf{J}_{j,1}(h) = -\frac{1}{12}\tilde{\mathbf{B}}_1\mathbf{D}(\tilde{\tau}_{j,1}-1)(\tilde{\mathbf{x}}_1 - 2\tilde{\mathbf{x}}_2\tilde{\tau}_{j,0} + 3\tilde{\mathbf{x}}_3\tilde{\tau}_{j,0}^2)h^3 + \mathcal{O}(h^4) \ , \tag{B.16}$$

Substitution of the Taylor expansions (B.5) and (B.9) with (B.13), (B.11) and (B.12) into (B.3) give

$$\mathbf{J}_{j,2}(h) = \frac{1}{12}\tilde{\mathbf{B}}_0\mathbf{D}\tilde{\tau}_{j,1}(\tilde{\tau}_{j,1}-2)(\tilde{\mathbf{x}}_2 - 3\tilde{\mathbf{x}}_3\tilde{\tau}_{j,0})h^3 + \mathcal{O}(h^4) \ . \tag{B.17}$$

Note that $\mathbf{J}_0(h)$, $\mathbf{J}_{j,1}(h)$ and $\mathbf{J}_{j,2}(h)$ do not depend on the approximation order q, i.e., these terms remain of order $\mathcal{O}(h^3)$ for any q.

The term $\mathbf{J}_{j,4}(h)$ is analyzed separately for the cases $q = 0$ and $q = 1$. If $q = 0$ (zeroth-order semi-discretization), then

$$\mathbf{\Gamma}_{j,i}^{(q)}(t-\tau_{j,i}) = \mathbf{v}(t_{i-r_{j,i}}) = \mathbf{D}\mathbf{y}(t_{i-r_{j,i}}) \ , \tag{B.18}$$

where $r_{j,i} = \mathrm{int}\big(\tau_{j,i}/h\big)$. In this case,

$$\mathbf{J}_{j,4}(h) = \int_0^h \mathbf{B}_{j,0}\mathbf{D}\mathbf{y}(s-\tau_{j,0}) - \mathbf{B}_{j,0}\mathbf{D}\mathbf{y}(t_{0-r_{j,0}})\,\mathrm{d}s = \mathbf{B}_{j,0}\mathbf{D}\int_0^h \mathbf{y}(s-\tau_{j,0}) - \mathbf{y}(-r_{j,0}h)\,\mathrm{d}s \ . \tag{B.19}$$

Substitution of the Taylor expansion (B.6) with (B.13), (B.11) and (B.12) gives

$$\mathbf{J}_{j,4}(h) = \tilde{\mathbf{B}}_0\mathbf{D}(\tilde{\tau}_{j,0} - r_{j,0}h)\Big(-\tilde{\mathbf{y}}_1 + (r_{j,0}h + \tilde{\tau}_{j,0})\tilde{\mathbf{y}}_2 - (r_{j,0}^2h^2 + \tilde{\tau}_{j,0}r_{j,0}h + \tilde{\tau}_{j,0}^2)\tilde{\mathbf{y}}_3\Big)h + \mathcal{O}(h^2) \ . \tag{B.20}$$

The difference $|\tilde{\tau}_{j,0} - r_{j,0}h|$ can be estimated as function of the discretization step h. The relation $r_{j,i} = \mathrm{int}\big(\tau_{j,i}/h\big)$ implies $|\tau_{j,0} - r_{j,0}h| \leq h$. Using (B.12), this gives

$$|\tilde{\tau}_{j,0} - r_{j,0}h| \leq \left(1 + \frac{1}{2}|\tilde{\tau}_{j,1}|\right)h + \mathcal{O}(h^2) \ , \tag{B.21}$$

that is,

$$|\tilde{\tau}_{j,0} - r_{j,0}h| = \mathcal{O}(h) \; . \tag{B.22}$$

Equation (B.20) with (B.22) gives

$$\mathbf{J}_{j,4}(h) = \mathcal{O}(h^2) \; . \tag{B.23}$$

If $q = 1$ (first-order semi-discretization), then

$$\begin{aligned}\mathbf{\Gamma}^{(1)}_{j,i}(t-\tau_{j,i}) &= \beta_{j,i,0}(t)\mathbf{v}(t_{i-r_{j,i}}) + \beta_{j,i,1}(t)\mathbf{v}(t_{i-r_{j,i}+1}) \\ &= \frac{\tau_{j,i} + (i - r_{j,i} + 1)h - t}{h}\mathbf{D}\mathbf{y}(t_{i-r_{j,i}}) + \frac{t - (i - r_{j,i})h - \tau_{j,i}}{h}\mathbf{D}\mathbf{y}(t_{i-r_{j,i}+1}) \; ,\end{aligned} \tag{B.24}$$

where $r_{j,i} = \mathrm{int}\big(\tau_{j,i}/h + 1/2\big)$. In this case,

$$\begin{aligned}\mathbf{J}_{j,4}(h) &= \int_0^h \mathbf{B}_{j,0}\mathbf{D}\mathbf{y}(s - \tau_{j,0}) \\ &- \mathbf{B}_{j,0}\left(\frac{\tau_{j,0} + (0 - r_{j,0} + 1)h - s}{h}\mathbf{D}\mathbf{y}(t_{0-r_{j,0}}) + \frac{s - (0 - r_{j,0})h - \tau_{j,0}}{h}\mathbf{D}\mathbf{y}(t_{0-r_{j,0}+1})\right) \mathrm{d}s \\ &= \mathbf{B}_{j,0}\mathbf{D}\int_0^h \mathbf{y}(s-\tau_{j,0}) - \left(\frac{\tau_{j,0} + (1 - r_{j,0})h - s}{h}\mathbf{y}(-r_{j,0}h) + \frac{s + r_{j,0}h - \tau_{j,0}}{h}\mathbf{y}((1 - r_{j,0})h)\right) \mathrm{d}s \; .\end{aligned} \tag{B.25}$$

Substitution of the Taylor expansion (B.6) with (B.13), (B.11) and (B.12) gives

$$\begin{aligned}\mathbf{J}_{j,4}(h) &= -\tilde{\mathbf{B}}_0\mathbf{D}(\tilde{\tau}_{j,0} - r_{j,0}h)^2((\tilde{\tau}_{j,0} + 2r_{j,0}h)\tilde{\mathbf{y}}_3 - \tilde{\mathbf{y}}_2)h \\ &\quad - \frac{1}{2}(\tilde{\tau}_{j,0} - r_{j,0}h)\Big(\tilde{\mathbf{B}}_1\mathbf{D}\Big((\tilde{\tau}^2_{j,0} + \tilde{\tau}_{j,0}r_{j,0}h - 2r^2_{j,0}h^2)\tilde{\mathbf{y}}_3 - (\tilde{\tau}_{j,0} - r_{j,0}h)\tilde{\mathbf{y}}_2\Big) + \\ &\quad \tilde{\mathbf{B}}_0\mathbf{D}\Big((3r_{j,0}h - 3\tilde{\tau}_{j,0} + 3\tilde{\tau}_{j,0}\tilde{\tau}_{j,1} + 3\tilde{\tau}_{j,1}r_{j,0}h)\tilde{\mathbf{y}}_3 - 2\tilde{\tau}_{j,1}\tilde{\mathbf{y}}_2\Big)\Big)h^2 + \mathcal{O}(h^3) \; .\end{aligned} \tag{B.26}$$

Here, $r_{j,i} = \mathrm{int}\big(\tau_{j,i}/h + 1/2\big)$, which implies $|\tau_{j,0} - r_{j,0}h| \leq h/2$. Using (B.12), this give

$$|\tilde{\tau}_{j,0} - r_{j,0}h| \leq \frac{1}{2}\left(1 + |\tilde{\tau}_{j,1}|\right)h + \mathcal{O}(h^2) \; , \tag{B.27}$$

that is, again,

$$|\tilde{\tau}_{j,0} - r_{j,0}h| = \mathcal{O}(h) \; . \tag{B.28}$$

Equation (B.26) with (B.28) gives

$$\mathbf{J}_{j,4}(h) = \mathcal{O}(h^3) \; . \tag{B.29}$$

Concluding the results, it was found that $\mathbf{J}_0(h) = \mathcal{O}(h^3)$, $\mathbf{J}_1(h) = \mathcal{O}(h^3)$ and $\mathbf{J}_2(h) = \mathcal{O}(h^3)$ and these terms do not depend on q. The term $\mathbf{J}_4(h)$, however, do depend on q: if $q = 0$ then $\mathbf{J}_{j,4}(h) = \mathcal{O}(h^2)$, if $q = 1$ then $\mathbf{J}_{j,4}(h) = \mathcal{O}(h^3)$.

Bibliography

[1] Ackermann J (1983) Abtastregelung – Band1: Analyse und Synthese. Springer-Verlag, Berlin.

[2] Alexander ME, Bowman CS, Feng Zh, Gardam M, Moghadas SM, Röst G, Wu J, Yan P (2007) Emergence of drug-resistance: implications for antiviral control of influenza pandemic. P Roy Soc B–Biol Sci 274:1675–1684.

[3] Allwright JC, Astolfi A, Wong HP (2005) A note on asymptotic stabilization of linear systems by periodic, piecewise constant output feedback. Automatica 41:339–344.

[4] Altintas Y, Budak E (1995) Analytical prediction of stability lobes in milling. CIRP Ann–Manuf Techn 44:357–362.

[5] Altintas Y (2000) Manufacturing automation: metal cutting mechanics, machine tool vibrations, and CNC design. Cambridge University Press, New York.

[6] Altintas Y, Weck M (2004) Chatter stability of metal cutting and grinding. CIRP Ann 53(3):1–24.

[7] Anderson RJ, Spong MW (1989) Bilateral control of teleoperators with time delay. IEEE T Automat Contr 34:494–501.

[8] Andronov AA, Leontovich EA (1937) Some cases of dependence of limit cycles on a parameters. Uchenye Zapiski Gorkovskogo Universiteta 6:3–24.

[9] Asada H, Slotine JJE (1986) Robot Analysis and Control. Wiley, New York.

[10] Asai Y, Tasaka Y, Nomura K, Nomura T, Casadio M, Morasso P (2009) A model of postural control in quiet standing: Robust compensation of delay-induced instability using intermittent activation of feedback control. PLoS ONE 4:e6169.

[11] Asl FM, Ulsoy AG (2004) Analysis of a system of linear delay differential equations. J Dyn Syst–T ASME 125:215–223.

[12] Åström KJ, Wittenmark B (1984) Computer controlled systems: Theory and design. Prentice-Hall, Englewood Cliffs, NJ.

[13] Bachrathy D, Insperger T, Stépán G (2009) Surface properties of the machined workpiece for helical mills. Mach Sci Technol 13:227-245.

[14] Bachrathy D, Turi J, Stépán G (2011) State dependent regenerative effect in milling processes. J Comput Nonlin Dyn–T ASME, 6:041002.

[15] Balachandran B, Kalmar-Nagy T, Gilsinn D (2009) Delay differential equations: Recent advances and new directions. Springer Verlag, New York.

[16] Baldi P, Atiya AF (1994) How delays affect neural dynamics and learning. IEEE T Neural Networ 5:612–621.

[17] Bayly PV, Halley JE, Mann BP, Davies MA (2003) Stability of interrupted cutting by temporal finite element analysis. J Manuf Sci E–T ASME 125:220–225.

[18] Bellen A, Zennaro M (2003) Numerical methods for delay differential equations, Oxford University Press, Oxford.

[19] Bellman R, Cooke K (1963) Differential-difference equations. Academic Press, New York.

[20] Bhatt SJ, Hsu CS (1966) Stability criteria for second-order dynamical systems with time lag. J Appl Mech-T ASME 33E:113–118.

[21] Boikov IV (2005) The Brockett stabilization problem. Automat Rem Contr 66:746–751.

[22] Bolotin VV (1964) The dynamic stability of elastic systems. Holden-Day, San Francisco.

[23] Breda D, Maset S, Vermiglio R (2005) Pseudospectral differencing methods for characteristic roots of delay differential equations. SIAM J Sci Comput 27:482–495.

[24] Breda D, Maset S, Vermiglio R (2006) Pseudospectral approximation of eigenvalues of derivative operators with non-local boundary conditions. Appl Numer Math 56:318–331.

[25] Brockett RW (1999) A stabilization problem. In: Blondel VD, Sontag ED, Vidyasagar M, Willems JC (eds) Open problems in mathematical systems and control theory, Springer, London.

[26] Budak E, Altintas Y (1998) Analytical prediction of chatter stability in milling, Part I: General formulation. J Dyn Syst–T ASME 120:22–30.

[27] Budak E, Altintas Y (1998) Analytical prediction of chatter stability in milling, Part II: Application of the general formulation to common milling systems. J Dyn Syst–T ASME 120:31–36.

[28] Burns TJ, Davies MA (1997) Nonlinear dynamics model for chip segmentation in machining. Phys Rev Lett 79:447–450.

[29] Burns TJ, Davies MA (2002) On repeated adiabatic shear band formation during high-speed machining. Int J Plasticity 8:487–506.

[30] Butcher EA, Ma H, Bueler E, Averina V, Szabó Zs (2004) Stability of time-periodic delay-differential equations via Chebyshev polynomials. Int J Numer Meth Eng 59:895–922.

[31] Butcher EA, Bobrenkov OA, Bueler E, Nindujarla P (2009) Analysis of milling stability by the Chebyshev collocation method: algorithm and optimal stable immersion levels. J Comput Nonlin Dyn–T ASME 4:031003.

[32] Butcher EA, Sari M, Bueler E, Carlson T (2009) Magnuséxpansion for time-periodic systems: Parameter-dependent approximations. Commun Nonlinear Sci 14:4226–4245.

[33] Butcher EA, Bobrenkov OA (2011) On the Chebyshev spectral continuous time approximation for constant and periodic delay differential equations. Commun Nonlinear Sci 16:1541–1554.

[34] Cabrera JL, Milton JG (2004) Stick balancing: On-off intermittency and survival times. Nonlinear Studies 11:305–317.

[35] Campbell SA, Ncube I, Wu J (2006) Multistability and stable asynchronous periodic oscillations in a multiple-delayed neural system, Physica D 214: 101–119.

[36] Canudas C, Siciliano B, Bastin G (1996) Theory of robot control. Springer, New York.

[37] Cho C, Song J-B, Kim M (2008) Stable haptic display of slowly updated virtual environment with multirate wave transform. IEEE-ASME T Mech 13:566–575.

[38] Corpus WT, Endres WJ (2004) Added stability lobes in machining processes that exhibit periodic time variation - Part 1: An analytical solution. J Manuf Sci E–T ASME 126:467–474.

[39] Corpus WT, Endres WJ (2004) Added stability lobes in machining processes that exhibit periodic time variation - Part 2: Experimental validation. J Manuf Sci E–T ASME 126:475–480.

[40] Craig JJ (1986) Introduction to robotics mechanics and control. Addison-Wesley, Reading.

[41] Csernák G, Pálmai Z (2007) Exploration of the chaotic phenomena induced by fast plastic deformation of metals. Int J Adv Manuf Tech 40:270–276.

[42] Davies MA, Pratt JR, Dutterer B, Burns TJ (2000) The stability of low radial immersion milling. CIRP Ann–Manuf Techn 49:37–40.

[43] Davies MA, Pratt JR, Dutterer B, Burns TJ (2002) Stability prediction for low radial immersion milling. J Manuf Sci E–T ASME 124:217–225.

[44] Diekmann O, van Gils SA, Lunel SMV, Walther H-O (1995) Delay equations. Springer-Verlag, New York.

[45] Ding Y, Zhu LM, Zhang XJ, Ding H (2010) A full-discretization method for prediction of milling stability. Int J Mach Tool Manu 50:502–509.

[46] Ding Y, Zhu LM, Zhang XJ, Ding H (2010) Second-order full-discretization method for milling stability prediction. Int J Mach Tool Manu 50:927–932.

[47] Dombovari Z, Wilson RE, Stépán G (2008) Estimates of the bistable region in metal cutting. P Roy Soc A–Math Phy 464:3255–3271.

[48] Dombovari Z, Altintas Y, Stépán G (2010) The effect of serration on mechanics and stability of milling cutters. Int J Mach Tool Manu 50:511–520.

[49] Dombovari Z, Iglesias A, Zatarain M, Insperger T (2011) Prediction of multiple dominant chatter frequencies in milling processes, Int J Mach Tool Manu 51:457–464.

[50] Driver RD (1963) A two-body problem of classical electrodynamics: the one-dimensional case. Ann Phys 21:122–142.

[51] Driver RD (1977) Ordinary and delay differential equations. Applied Mathematical Sciences 20, Springer-Verlag, New York.

[52] Dudás I, Bakondi K, Szabó A, Kodácsy J (2001) A forgácsolás technológiájának fejlesztési irányai. In: (Prohászka J ed) A technológia helyzete és jövője. Budapest: MTA Társadalomkutató Központ, pp. 89-110.

[53] Elbeyli O, Sun JQ (2004) On the semi-discretization method for feedback control design of linear systems with time delay. J Sound Vib 273:429–440.

[54] Èl'sgol'c LÈ (1964) Qualitative methods in mathematical analysis. AMS, Providence.

[55] Engelborghs K, Dambrine M, Roose D (2001) Limitations of a class of stabilization methods for delay systems. IEEE T Automat Contr 46:336–339.

[56] Engelborghs K, Luzyanina T, Samaey G (2001) DDE-BIFTOOL v.2.00: A Matlab package for bifurcation analysis of delay differential equations. Technical Report TW-330, Department of Computer Science, K.U.Leuven, Belgium.

[57] Engelborghs K, Luzyanina T, Roose D (2002) Numerical bifurcation analysis of delay differential equations using DDE-BIFTOOL. ACM T Math Software 28:1–21.

[58] Erneux T (2009) Applied delay differential equations, Springer, New York.

[59] Faassen RPH, van de Wouw N, Nijmeijer H, Oosterling JAJ (2007) An improved tool path model including periodic delay for chatter prediction in milling. J Comput Nonlin Dyn–T ASME 2:167–179.

[60] Farkas M (1994) Periodic motions. Springer-Verlag, New York.

[61] Floquet MG (1883) Équations différentielles linéaires à coefficients périodiques. Ann Sci Ecole Norm S 12:47–89.

[62] Galambos P, Baranyi P, Korondi P (2010) Extended TP model transformation for polytopic representation of impedance model with feedback delay. WSEAS T Sys Control 5(9):701–710.

[63] Garay B (2005) A brief survey on the numerical dynamics of functional differential equations. Int J Bifurcat Chaos 15:729–742.

[64] Gawthrop PJ, Wang L (2007) Intermittent model predictive control. P I Mech Eng I-J Sys 221:1007–1018.

[65] Gawthrop PJ, Wang L (2009) Event-driven intermittent control. Int J Control 82:2235–2248.

[66] Gawthrop P (2010) Act-and-wait and intermittent control: Some comments. IEEE T Contr Syst T 18:1195–1198.

[67] Germay C, Denoel V, Detournay E (2009) Multiple mode analysis of the self-excited vibrations of rotary drilling systems. Journal of Sound and Vibration, 325(1-2):362-381.

[68] Gianone L, Palkovics L, Bokor J (1995) Design of an active 4ws system with physical uncertainties. Control Eng Pract 3(8): 1075-1083.

[69] Gorinevsky DM, Formalsky AM, Schneider AY (1997) Force control of robotics systems, CRC Press LLC, Boca Raton.

[70] Gradišek J, Kalveram M, Insperger T, Weinert K, Stépán G, Govekar E, Grabec I (2005) On stability prediction for milling. Int J Mach Tool Manu 45:741–991.

[71] Gu K, Kharitonov V, Chen J (2003) Stability of time-delay systems. Birkhäuser, Boston.

[72] Guckenheimer J, Holmes P (1983) Nonlinear oscillations, dynamical systems, and bifurcations of vector fields. Springer-Verlag, New York.

[73] Győri I, Hartung F, Turi J (1993) Approximation of functional differential equations with time- and state-dependent delays by equations with piecewise constant arguments. IMA Preprint Series # 1130.

[74] Győri I, Hartung F, Turi J (1995) Numerical approximations for a class of differential equations with time- and state-dependent delays. Appl Math Lett 8:19–24.

[75] Győri I, Hartung F, Turi J (1998) Preservation of stability in delay equations under delay perturbations. J Math Anal Appl 220:290–312.

[76] Halanay A (1961) Stability theory of linear periodic systems with delay (in Russian). Rev Roum Math Pure A, 6(4):633–653.

[77] Halanay A (1966) Differential equations: Stability, oscillations, time lags. Academic Press, New York.

[78] Hale JK (1977) Theory of functional differential equations. Springer-Verlag, New York.

[79] Hale JK, Lunel SMV (1993) Introduction to functional differential equations. Springer-Verlag, New York.

[80] Hartung F, Turi J (1995) On the asymptotic behavior of the solutions of a state-dependent delay equation. Diff Integ Equ 8(7):1867–1872.

[81] Hartung F, Turi J (1997) On differentiability of solutions with respect to parameters in state-dependent delay equations. Journal of Differential Equations, 135(2):192–237.

[82] Hartung F, Turi J (2000) Linearized stability in functional-differential equations with state-dependent delays. Proceedings of the conference Dynamical Systems and Differential Equations, added volume of Discrete and Continuous Dynamical Systems, pp. 416–425.

[83] Hartung F (2005) Linearized stability in periodic functional differential equations with state-dependent delays. Journal of Computational and Applied Mathematics, 174:201–211.

[84] Hartung F, Insperger T, Stépán G, Turi J (2006) Approximate stability charts for milling processes using semi-discretization. Appl Math Comput 174:51–73.

[85] Hartung F, Krisztin T, Walther H-O, Wu J (2006) Functional differential equations with state-dependent delays: theory and applications. In: Cañada A, Drábek P, Fonda A (eds) Handbook of Differential Equations, Ordinary Differential Equations, vol. 3, Elsevier, North-Holland.

[86] Hassard BD (1997) Counting roots of the characteristic equation for linear delay-differential systems. J Differ Equations 136:222–235.

[87] Henninger C, Eberhard P (2007) A new curve tracking algorithm for efficient computation of stability boundaries of cutting processes. J Comput Nonlin Dyn–T ASME 2:360–365.

[88] Henninger C, Eberhard P (2008) Improving the computational efficiency and accuracy of the semi-discretization method for periodic delay-differential equations. Eur J Mech A-Solid 27:975–985.

[89] Hill GW (1886) On the part of the motion of the lunar perigee which is a function of the mean motions of the sun and moon. Acta Math 8:1–36.

[90] Hirsch MW, Smale S (1974) Differential equations, dynamical systems and linear algebra. Academic Press, Berkeley.

[91] Hocken RD, Salehi SV, Marshall JE (1983) Time-delay mismatch and the performance of predictor control schemes. Int J Control 38(2):433–47.

[92] Hopf E (1942) Abzweigung einer periodischen Lösung von einer stationären Lösung eines Differentialsystems. Ber Verh Sach Akad Wiss Leipzig, Math–Nat 95:3–22.

[93] Horváth M, Somló J (1979) A forgácsolási folyamatok optimalizálása és adaptív irányítása. Műszaki Könyvkiadó.

[94] Hsu CS (1974) On approximating a general linear periodic system. J Math Anal Appl 45:234–251.

[95] Hurwitz A (1895) Über die Bedingungen unter welchen eine Gleichung nur Wurzeln mit negativen reellen Theilen besitzt. Math Ann 46:74–81.

[96] Inamura T, Sata T (1974) Stability analysis of cutting under varying spindle speed. Ann CIRP 23:119–120.

[97] Insperger T, Stépán G (2000) Stability of high-speed milling. In: Proc. of the ASME 2000 International Mechanical Engineering Congress & Exposition, AMD-241:119–123.

[98] Insperger T, Stépán G (2000) Stability of the milling process. Period Polytech Mech 44:47–57.

[99] Insperger T (2002) Stability analysis of periodic delay-differential equations modeling. PhD dissertation, Budapest University of Technology and Economics, Budapest, Hungary.

[100] Insperger T, Stépán G (2002) Semi-discretization method for delayed systems. Int J Numer Meth Eng 55:503–518.

[101] Insperger T, Stepan G (2002) Stability chart for the delayed Mathieu equation. Proc R Soc Lond A–Math Phy 458:1989–1998.

[102] Insperger T, Mann BP, Stépán G, Bayly PV (2003) Stability of up-milling and down-milling, Part 1: Alternative analytical methods. Int J Mach Tool Manu 43:25–34.

[103] Insperger T, Stépán G (2004) Stability analysis of turning with periodic spindle speed modulation via semi-discretization. J Vib Control 10:1835–1855.

[104] Insperger T, Stépán G (2004) Updated semi-discretization method for periodic delay-differential equations with discrete delay. Int J Numer Meth Eng 61:117–141.

[105] Insperger T, Stépán G, Hartung F, Turi J (2005) State-dependent regenerative delay in milling processes. in: Proc. of the ASME 2005 International Design Engineering Technical Conferences, DETC2005-85282.

[106] Insperger T (2006) Act and wait concept for time-continuous control systems with feedback delay. IEEE T Contr Syst T 14:974–977.

[107] Insperger T, Stépán G (2007) Act-and-wait control concept for discrete-time systems with feedback delay. IET Control Theory A 1:553–557.

[108] Insperger T, Stépán G, Turi J (2007) State-dependent delay in regenerative turning processes. Nonlinear Dynam 47:275–283.

[109] Insperger T, Barton DAW, Stépán G (2008) Criticality of Hopf bifurcation in state-dependent delay model of turning processes. Int J Nonlin Mech 43:140–149.

[110] Insperger T, Stépán G, Turi J (2008) On the higher-order semi-discretizations for periodic delayed systems. J Sound Vib 313:334–341.

[111] Insperger T, Kovacs LL, Galambos P, Stépán G (2009) Act-and-wait control concept for a force control process with delayed feedback. In: Ulbrich H, Ginzinger L (eds) Motion and vibration control, Selected papers from MOVIC 2008, Springer, Garching.

[112] Insperger T (2010) Full-discretization and semi-discretization for milling stability prediction: Some comments. Int J Mach Tool Manu 50:658–662.

[113] Insperger T, Stépán G (2010) On the dimension reduction of systems with feedback delay by act-and-wait control. IMA J Math Control I 27, 457–473.

[114] Insperger T, Kovacs LL, Galambos P, Stépán G (2010) Increasing the accuracy of digital force control process using the act-and-wait concept. IEEE-ASME T Mech 15:291–298.

[115] Insperger T, Stépán G (2011) Semi-discretization for time-delay systems. Springer, New York.

[116] Iserles A (1984) Solving linear ordinary differential equations by exponentials of iterated commutators. Numer Math 45:183–199.

[117] Iserles A, Nørsett SP (1999) On the solution of linear differential equation in Lie groups. Philos T R Soc Lond A 357:983–1019.

[118] Jayaram S, Kapoor SG, DeVor RE (2000) Analytical stability analysis of variable spindle speed machining. J Manuf Sci E–T ASME 122:391–397.

[119] Kabamba P (1987) Control of linear systems using generalized sampled-data hold functions. IEEE T Automat Contr 32:772–783.

[120] Kalmár-Nagy T, Stépán G, Moon FC (2001) Subcritical Hopf bifurcation in the delay equation model for machine tool vibrations. Nonlinear Dynam 26:121–142.

[121] Khasawneh FA, Mann BP (2011) A spectral element approach for the stability of delay systems. Int J Numer Meth Eng, 87(6):566–592.

[122] Khasawneh FA, Mann BP (2011) Stability of delay integro-differential equations using a spectral element method. Math Comput Model 54(9-10):2493–2503.

[123] Keviczky L, Bányász Cs (2002) On the reachable robustness limits for time delay control systems. Kybernetes 31(9-10): 1429–1441.

[124] Keviczky L, Bányász Cs (2007) Robust stability and performance of time-delay control systems. ISA T 46:233–237.

[125] Kienzle O (1957) Spezifische Schnittkräfte bei der Metallbearbeitung. Werkstattstechnik und Maschinenbau 47:224–225.

[126] Kim WS, Bejczy AK (1993) Demonstration of a high-fidelity predictive preview display technique for telerobotic servicing in space. IEEE T Robotic Autom, 9(5):698–704.

[127] Kolmanovskii VB, Nosov VR (1986) Stability of functional differential equations. Academic Press, London.

[128] Konishi K, Hara N (2011) Stabilization of unstable fixed points with queue-based delay feedback control, Dynam Cont Dis Ser B, in press.

[129] Konishi K, Kokame H, Hara N (2011) Delayed feedback control based on the act-and-wait concept. Nonlinear Dynam 63:513–519.

[130] Korondi P, Szemes P, Hashimoto H (2004) Internet based telemanipulation. In: Zurawski (ed) The industrial information technology handbook, CRC Press LLC.

[131] Kovacs LL, Kövecses J, Stépán G (2008) Analysis of effects of differential gain on dynamic stability of digital force control. Int J Nonlin Mech 43:514–520.

[132] Kövecses J, Kovacs LL, Stépán G (2007) Dynamics modeling and stability of robotic systems with discrete-time force control. Arch Appl Mech 77:293–299.

[133] Krisztin T, Arino O (2001) The 2-dimensional attractor of a differential equation with state-dependent delay. J Dyn Differ Equ 13:453–522.

[134] Krisztin T (2003) A local unstable manifold for differential equations with state-dependent delay. Discrete Cont Dyn S 9:993–1028.

[135] Kuang Y (1993) Delay differential equations with applications in population dynamics. Academic Press, New York.

[136] Kudinov VA (1967) Dynamics of Tool-Lathe (in Russian), Mashinostroenie, Moscow.

[137] Kuo BC (1977) Digital Control Systems. SRL Publishing Company, Champaign.

[138] Kundrák J, Mamalis AG, Gyáni K, Markopoulos A (2006) Environmentally friendly precision machining, Mater Manuf Process 21(1): 29-37.

[139] Lantos B (1991) Robotok irányítása, Akadémiai Kiadó, Budapest.

[140] Lantos B, Márton L (2005) Friction modelling and adaptive compensation for intelligent DC servo systems. In: Elmenreich W, Tenreiro Machado JA, Rudas IJ (eds) Intelligent Systems at the Service of Mankind - Volume II, Augsburg: U Books.

[141] Landry M, Campbell SA, Morris K, Aguilar CO (2005) Dynamics of an inverted pendulum with delayed feedback control. SIAM J Appl Dyn Syst 4:333–351.

[142] Leonov GA (2002) Brockett's problem in the theory of stability of linear differential equations. St. Petersburg Math J 13:613–628.

[143] Liu L, Kalmár-Nagy T (2010) High dimensional harmonic balance analysis for second-order delay-differential equations. J Vib Control 16:1189–1208.

[144] Long X-H, Balachandran B, Mann BP (2007) Dynamics of milling processes with variable time delays. Nonlinear Dynam 47:49–63.

[145] Magnus W (1954) On the exponential solution of differential equations for a linear operator. Comm Pure Appl Math 7:649–673.

[146] Manitius AZ, Olbrot AW (1979) Finite spectrum assignment problem for systems with delays. IEEE T Automat Contr 24:541–553.

[147] Mann BP, Patel BR (2010) Stability of delay equations written as state space models. J Vib Control 16:1067–1085.

[148] Márton L, Lantos B (2007) Modelling, identification and compensation of stick slip friction. IEEE T Ind Electron 54(1):511–521.

[149] Mason MT (1981) Compliance and force control for computer controlled manipulators. IEEE T Syst Man Cy 11:418–432.

[150] Merdol SD, Altintas Y (2004) Multi frequency solution of chatter stability for low immersion milling. J Manuf Sci E–T ASME 126:459–466.

[151] Michiels W, Engelborghs K, Vansevenant P, Roose D (2002) Continuous pole placement for delay equations. Automatica, 38:747–761.

[152] Michiels W, Niculescu S-I (2007) Stability and stabilization of time-delay systems: an eigenvalue-based approach. SIAM Publications, Philadelphia.

[153] Michiels W, Vyhlidal T, Zitek P (2010) Control design for time-delay systems based on quasi-direct pole placement. J Process Contr 20:337–343.

[154] Milton JG, Ohira T, Cabrera JL, Fraiser RM, Gyorffy JB, Ruiz FK, Strauss MA, Balch EC, Marin RJ, Alexander JL (2009) Balancing with vibration: A prelude for "drift and act" balance control. PLoS ONE 4:e7427.

[155] Milton J, Townsend JL, King MA, Ohira T (2009) Balancing with positive feedback: the case for discontinuous control. Philos T R Soc A 367:1181–1193.

[156] Minis I, Yanushevsky R (1993) A new theoretical approach for the prediction of machine tool chatter in milling. J Eng Ind–T ASME 115:1–8.

[157] Minorsky N (1942) Self-excited oscillations in dynamical systems possessing retarded actions. J Appl Mech–T ASME 9:65–71.

[158] Mondié S, Dambrine M, Santos O (2002) Approximation of control laws with distributed delays: a necessary condition for stability. Kybernetika 38:541–551.

[159] Mondié S, Michiels W (2003) Finite spectrum assignment of unstable time-delay systems with a safe implementation. IEEE T Automat Contr 48:2207–2212.

[160] Monostori L (1993) A step towards intelligent manufacturing: Modeling and monitoring of manufacturing processes through artificial neural networks. CIRP Ann–Manuf Techn 42(1):485–488.

[161] Monostori L, Váncza J, Kumara SRT(2006) Agent-based systems for manufacturing. CIRP Ann–Manuf Techn 55(2):697–720.

[162] Moreau L, Aeyels D (2004) Periodic output feedback stabilization of single-input single-output continuous-time systems with odd relative degree. Syst Control Lett 51:395–406.

[163] Munir S, Book WJ (2002) Internet-based teleoperation using wave variables with prediction. IEEE-ASME T Mech 7:124–133.

[164] Myshkis AD (1955) Lineare Differentialgleichungen mit nacheilendem Argument. Deutscher Verlag der Wissenschaften, Berlin.

[165] Namachchivaya NS, Beddini R (2003) Spindle speed variation for the suppression of regenerative chatter. J Nonlinear Sci 13:265–288.

[166] Nayfeh AH, Mook DT (1979) Nonlinear oscillations. John Wiley and Sons, New York.

[167] Neimark Ju I (1949) D-subdivision and spaces of quasi-polynomials (in Russian). Prikl Mat Mekh 13:349–380.

[168] Niculescu S-I (2001) Delay effects on stability – A robust control approach. Springer-Verlag, London.

[169] Nisbet RM, Gurney WSC (1983) The systematic formulation of population models for insects with dynamically varying instar duration. Theor Popul Biol 23:114–135.

[170] Ogata K (1995) Discrete-time control systems. Prentice-Hall, Englewood Cliffs.

[171] Olgac N, Sipahi R (2002) An exact method for the stability analysis of time delayed LTI systems. IEEE T Automat Contr 47:793–797.

[172] Olgac N, Sipahi R (2005) The cluster treatment of characteristic roots and the neutral type time-delayed systems. J Dyn Syst–T ASME 127:88–97.

[173] Orosz G, Stépán G (2006) Subcritical Hopf bifurcations in a car-following model with reaction-time delay. P Roy Soc A–Math Phy 462:2643–2670.

[174] Orosz G, Moehlis J, Murray RM (2010) Controlling biological networks by time-delayed signals. Philos T R Soc A 368:439–454.

[175] Pakdemirli M, Ulsoy AG (1997) Perturbation analysis of spindle speed variation in machine tool chatter. J Vib Control 3:261–278.

[176] Palkovics L, Venhovens PJT (1992) Investigation on stability and possible chaotic motions in the controlled wheel suspension system. Vehicle Syst Dyn 21:269–296.

[177] Palkovics L, Bokor J, Venhovens P (1994) Design problems of the semi-active wheel suspension system and a possible way of their elimination. XXV. FISITA congress. Automobile in harmony with human society. Vehicle dynamics. Technical papers. Beijing, pp. 30–40.

[178] Pálmai Z, Csernák G (2009) Chip formation as an oscillator during the turning process. J Sound Vib 326:809–820.

[179] Perko L (1996) Differential equations and dynamical systems. Springer-Verlag, New York.

[180] Polushin IG, Liu PX, Lung C-H (2007) A force-reflection algorithm for improved transparency in bilateral teleoperation with communication delay. IEEE-ASME T Mech 12:361–374.

[181] Pontryagin LS (1942) On the zeros of some elementary transcendental functions (in Russian). Izv Akad Nauk SSSR 6:115–134.

[182] Quintana G, Ciurana J (2011) Chatter in machining processes: A review. Int J Mach Tool Manu 51(5):363–376.

[183] Raibert MH, Craig JJ (1981) Hybrid position/force control of manipulators, J Dyn Syst–T ASME 102:126–133.

[184] Richard T, Germay C, Detournay E (2007) A simplified model to explore the root cause of stick-slip vibrations in drilling systems with drag bits. Journal of Sound and Vibration, 305:432–456.

[185] Ronco E, Arsan T, Gawthrop PJ (1999) Open-loop intermittent feedback control: Practical continuous-time GPC. IEE P–Contr Theor Ap 146:426–434.

[186] Röst G, Wu J (2008) SEIR epidemiological model with varying infectivity and infinite delay. Math Biosci Eng 5:389–402.

[187] Routh EJ (1877) A treatise on the stability of a given state of motion. Macmillan, London.

[188] Sastry S, Kapoor SG, DeVor RE, Dullerud GE (2001) Chatter stability analysis of the variable speed face-milling process. J Manuf Sci E–T ASME 123:537–546.

[189] Sastry S, Kapoor SG, DeVor RE (2002) Floquet theory based approach for stability analysis of the variable speed face-milling process. J Manuf Sci E–T ASME 124:10–17.

[190] von Schlippe B, Dietrich R (1941) Shimmying of a pneumatic wheel. Lilienthal-Gesellschaft für Luftfahrtforschung, Bericht, 140:125–160, translated for the AAF in 1947 by Meyer & Company.

[191] Schmitz TL, Smith KS (2009) Machining dynamics - Frequency response to improved productivity. Springer, New York.

[192] Seguy S, (2008) From the spindle speed selection to the spindle speed variation for chatter control in thin wall milling: modelling and experiments, PhD Thesis, École Nationale d'Ingénieurs de Tarbes, France.

[193] Seguy S, Insperger T, Arnaud L, Dessein G, Peigné G (2010) On the stability of high-speed milling with spindle speed variation. Int J Adv Manuf Tech 48:883–895.

[194] Seguy S, Insperger T, Arnaud L, Dessein G, Peigné G (2011) Suppression of period doubling chatter in high-speed milling by spindle speed variation. Mach Sci Technol 15(2):153–171.

[195] Sellmeier V, Denkena B (2011) Stable islands in the stability chart of milling processes due to unequal tooth pitch, Int J Mach Tool Manu 51:152–164.

[196] Sexton JS, Milne RD, Stone BJ (1977) A stability analysis of single point machining with varying spindle speed. Appl Math Model 1:310–318.

[197] Sheng J, Elbeyli O, Sun JQ (2004) Stability and optimal feedback controls for time-delayed linear periodic systems. AIAA J 42:908–911.

[198] Shi HM, Tobias SA (1984) Theory of finite amplitude machine tool instability. Int J Mach Tool D R 24:45–69.

[199] Sieber J, Krauskopf B (2004) Complex balancing motions of an inverted pendulum subject to delayed feedback control. Physica D 197:332–345.

[200] Sieber J, Szalai R (2011) Characteristic matrices for linear periodic delay differential equations. SIAM J Appl Dyn Syst 10:129–147.

[201] Sinha SC, Wu DH (1991) An efficient computational scheme for the analysis of periodic systems. J Sound Vib 151:91–117.

[202] Sinha SC, Butcher EA (1997) Symbolic computation of fundamental solution matrices for linear time-periodic dynamical systems. J Sound Vib 206:61–85.

[203] Sims ND, Mann B, Huyanan S (2008) Analytical prediction of chatter stability for variable pitch and variable helix milling tools. J Sound Vib 317:664–686.

[204] Smith OJM (1958) Feedback control systems, McGraw-Hill Series in Control Systems Engineering. McGraw-Hill, New York.

[205] Somló J, Lantos B, Cat PH (1997) Advanced robot control. Akadémiai Kiadó, Budapest.

[206] Stépán G (1989) Retarded dynamical systems. Longman, Harlow.

[207] Stépán G, Steven A, Maunder L (1990) Design principles of digitally controlled robots. Mech Mach Theory 25:515–527.

[208] Stépán G, Kalmár-Nagy T (1997) Nonlinear regenerative machine tool vibrations. In: Proc. of the 1997 ASME Design Engineering Technical Conferences, DETC97/VIB-4021.

[209] Stépán G (1998) Delay-differential equation models for machine tool chatter. In: Moon FC (ed) Dynamics and chaos in manufacturing processes, Wiley, New York.

[210] Stepan G (1998) Delay, nonlinear oscillations and shimmying wheels. In: Moon FC (ed) Applications of nonlinear and chaotic dynamics in mechanics, Kluwer Academic Publisher, Dordrecht.

[211] Stépán G (2001) Vibrations of machines subjected to digital force control. Int J Solids Struct 38:2149–2159.

[212] Stépán G, Insperger T (2006) Stability of time-periodic and delayed systems – a route to act-and-wait control. Annu Rev Control 30:159–168.

[213] Stépán G (2009) Introduction to delay effects in brain dynamics. Philos T R Soc A 367:1059–1062.

[214] Stépán G (2009) Delay effects in the human sensory system during balancing. Philos T R Soc A 367:1195–1212.

[215] Strutt JW (Lord Rayleigh) (1887) On the maintenance of vibrations by forces of double frequency, and on the propagation of waves through a medium endowed with a periodic structure. Philosophical Magazine and Journal of Science 24:145–159.

[216] Sun JQ (2009) A method of continuous time approximation of delayed dynamical systems. Commun Nonlinear Sci 14:998–1007.

[217] Sun JQ, Song B (2009) Control studies of time-delayed dynamical systems with the method of continuous time approximation. Commun Nonlinear Sci 14:3933–3944.

[218] Szalai R, Stépán G (2006) Lobes and lenses in the stability chart of interrupted turning. J Comput Nonlin Dyn–T ASME 1:205–211.

[219] Szalai R, Stépán G, Hogan SJ (2006) Continuation of bifurcations in periodic delay-differential equations using characteristic matrices. SIAM J Sci Comput 28:1301–1317.

[220] Takacs D, Orosz G, Stepan G (2009) Delay effects in shimmy dynamics of wheels with stretched-string like tyres. Eur J Mech A-Solid 28:516–525.

[221] Takemura T, Kitamura T, Hoshi T, Okushima K (1974) Active suppression of chatter by programmed variation of spindle speed. Ann CIRP 23:121–122.

[222] Taylor FW (1907) On the art of cutting metals. Transactions of ASME, 28:31–350.

[223] Tlusty J, Polacek A, Danek C, Spacek J (1962) Selbsterregte Schwingungen an Werkzeugmaschinen. VEB Verlag Technik, Berlin.

[224] Tlusty J (2000) Manufacturing processes and equipment, Prentice Hall, New Jersey.

[225] Tobias SA, Fishwick, W (1958) Theory of regenerative machine tool chatter. The Engineer, Feb. 199–203, 238–239.

[226] Tobias SA (1965) Machine tool vibration. Blackie, London.

[227] Tsao TC, McCarthy MW, Kapoor SG (1993) A new approach to stability analysis of variable speed machining systems. Int J Mach Tool Manu 33:791–808.

[228] Tsypkin YaZ (1946) The systems with delayed feedback. Avtomatika i Telemekhanika 7:107–129.

[229] Vyhlídal T, Zítek P (2009) Mapping based algorithm for large-scale computation of quasi-polynomial zeros. IEEE T Automat Contr 54:171–177.

[230] Volterra V (1928) Sur la théorie mathématique des phénomènes héréditaires. J Math Pure Appl 7:149–192.

[231] Wahi P (2005) A study of delay Differential equations with applications to machine tool vibrations, PhD thesis, Indian Institute of Science, Bangalore, India.

[232] Wahi P, Chatterjee A (2005) Galerkin projections for delay differential equations. J Dyn Syst–T ASME 127:80–87.

[233] Walther HO (2002) Stable periodic motion of a system with state-dependent delay. Differential and Integral Equations 15:923–944.

[234] Wan M, Zhang WH, Dang JW, Yang Y (2010) A unified stability prediction method for milling process with multiple delays. Int J Mach Tool Manu 50:29–41.

[235] Wang Q-G, Lee TH, Tan KK (1998) Finite spectrum assignment for time-delay systems. In: Lecture Notes in Control and Information Sciences, 239, Springer.

[236] Whitney DE (1977) Force feedback control of manipulator fine motion. J Dyn Syst–T ASME 98:91–97.

[237] Wu D, Chen K, Wang X (2009) An investigation of practical application of variable spindle speed machining to noncircular turning process. Int J Adv Manuf Tech 44:1094–1105.

[238] Yi S, Nelson PW, Ulsoy AG (2010) Eigenvalue assignment via the Lambert W function for control for time-delay systems. J Vib Control 16:961–982.

[239] Yi S, Nelson PW, Ulsoy, AG (2010) Time-delay systems: Analysis and control using the Lambert W function. World Scientific, New Jersey.

[240] Yilmaz A, AL-Regib E, Ni J (2002) Machine tool chatter suppression by multi-level random spindle speed variation. J Manuf Sci E–T ASME 124:208–216.

[241] Zatarain M, Bediaga I, Munoa J, Lizarralde R (2008) Stability of milling processes with continuous spindle speed variation: Analysis in the frequency and time domains, and experimental correlation. CIRP Ann–Manuf Techn 57:379–384.

[242] Zhao MX, Balachandran B (2001) Dynamics and stability of milling process. Int J Solids Struct 38:2233–2248.

[243] Zhong Q-C (2006) Robust control of time-delay systems. Springer-Velag, London.